UNITED STATES DEPARTMENT OF THE INTERIOR

GEOLOGICAL SURVEY

Delineation of Lenticular-type Sand Bodies by the Vertical Seismic Profiling Method

by M. W. Lee[1]

Open-File Report 84-265

[1]U.S. Geological Survey, Box 25046, Denver Federal Center, Denver, Colorado 80225

1984

CONTENTS

ILLUSTRATIONS

DELINEATION OF LENTICULAR SAND BODIES BY THE VERTICAL SEISMIC PROFILING METHOD

By Myung W. Lee

ABSTRACT

This study focuses on the feasibility of detection and delineation of small lenticular-type bodies within the Mesaverde Group in western Colorado using a vertical seismic profiling (VSP) method. A series of three-dimensional diffraction VSP models were generated by the Kirchhoff wave theory and the amplitude characteristics of the seismic response from the lenticular-type sand bodies were analyzed. This investigation showed that the VSP method is a viable technique in delineating the spatial extent of lenticular sands in certain conditions. Also, this study includes the advantages of VSP methods over conventional surface profiling methods and limitations of the VSP technique in locating spatial extent of small bodies.

INTRODUCTION

The vertical seismic profiling (VSP) method is a powerful investigative technique (Gal'perin, 1973) and has been used for a variety of seismic exploration problems (Balch and others, 1982). One of the primary objectives in using the VSP technique is to make a highly reliable tie between a well log and a surface seismic profile run across the well. For this purpose, a set of VSP data was acquired at the Department of Energy Multi-well Experiment (MWX) site, Garfield County, Colorado, in order to tie the high-resolution, three-dimensional surface seismic data with the available well-log data.

The purpose of the surface seismic data acquisition was to delineate the lateral extent of tight-gas sand bodies within the Mesaverde Group at the MWX site and to determine the extent to which stimulation and production of gas from the lenticular sands can be achieved (Searls and others, 1983). However, analysis of the 3-dimensional surface seismic profile indicated that it is very difficult to delineate the lateral extent of the lenticular sands, primarily due to the low-frequency content of the section. Analysis of the VSP data showed that there are some possibilities for delineating lenticular sand bodies in this area. Based on this observation, a detailed study of delineating lenticular sands by the VSP method was performed.

A series of 3-dimensional VSP modeling was performed using the Kirchhoff wave theory. Seismic responses from lenticular sand bodies were analyzed to see how the lenticular sand body manifests itself on the VSP section.

Three-dimensional diffraction theory for arbitrary source-receiver pairs was developed by Trorey (1977) and Berryhill (1977). Hilterman (1982) investigated the amplitude characteristics of certain geologic surfaces using the 3-dimensional diffraction theory. His investigation is suitable for conventional surface profile data. In this study, the lenticular-type sand body was modeled by a rectangular-type body using Trorey's (1977) method.

This study consists of five main parts:

1. Development of a 3-dimensional VSP modeling technique in order to investigate the seismic response of the lenticular-type sand body with respect to the well-phone location, model parameters, and field configuration.

2. Study of detailed seismic response for a particular type of sand body in the coastal, paludal, and coal zones at the MWX site; and determination of which zone has the higher potential to be detected and delineated by the VSP method.
3. Development of processing techniques which utilize the difference in seismic responses with respect to the areal extent of the lenticular-type sand bodies.
4. Simulation of the field VSP experiment in an ideal condition and investigation of the feasibility of the VSP method and its limitations in mapping the spatial distribution of the lenticular-type sand body.
5. Investigation of optimum VSP field configuration in order to delineate the lenticular-type sand bodies at the MWX well site.

This study indicates that in certain cases, when the approximate orientation of the lenticular body is known, the VSP method is a viable technique in delineating spatial extent of the body. It was also determined that lenticular sands within the paludal zone at the MWX well site have the highest potential for being detected seismically.

ACKNOWLEDGMENTS

Sincere appreciation is expressed to Keith Westhusing, U.S. Department of Energy, for his encouragement during this study and providing the model parameters for the sand bodies at the MWX well site. I wish to thank J. J. Miller and C. A. Searls for their review. The U.S. Department of Energy and Sandia National Laboratories funded this study.

THREE-DIMENSIONAL VSP MODELING

Theory

The general diffraction theory for arbitrary source-receiver locations was developed by Trorey (1977) and Berryhill (1977). In this report, Trorey's formula was adopted to investigate seismic responses of the 3-dimensional lenticular bodies. This is a scalar wave-equation solution, so only compressional waves are considered.

The Kirchhoff-Helmholtz diffraction equation is given by

$$4\pi\phi_d(p) = \iint_s e^{-pR_d/v}\left[\frac{1}{R_d}\frac{\partial\phi_s}{\partial n} - \frac{\partial}{\partial n}\left(\frac{\phi_s}{R_d}\right) + \frac{p\phi_s}{vR_d}\frac{\partial R_d}{\partial n}\right]ds$$

where ϕ_s is the potential on the reflecting surface s, R_d is the distance from the detector to the element of reflecting surface ds, v is the medium velocity, n is the normal to ds in the direction away from the detector, and $\phi_d(p)$ is the Laplace-transformed potential at the detector location and p is the transform variable.

The source potential on the surface of the reflecting surface can be approximated by the following formula:

$$\phi_s(p) = rf(p)\frac{e^{-pR_s/v}}{R_s}$$

where r is the reflection coefficient, R_s is the distance from the source to the reflecting surface, and f(p) is the Laplace-transformed, source-time function.

Assuming that the reflecting surface is a plane reflector located in the X-Y plane, the source and detector are located in the X-Z plane (fig. 1), and the reflection coefficient is independent of the angle of incidence. Let $(0, 0, Z_d)$ be the coordinate of the detector location, $(X_s, 0, Z_s)$ be the coordinate of the source location, and $(X_r, Y_r, 0)$ be the coordinate of the boundary of the reflecting surface.

Then, from Trorey (1977), the seismic response can be written as:

$$\phi_d(t) = \frac{rf(t) * \delta(t-t_1)}{vt_1} - \frac{rf(t)}{4\pi v} * \int_\theta b(t,\theta)\,\delta[t - t_2(\theta)]d\theta \qquad (1a)$$

when the least-time origin $(X_i, 0, 0)$ falls on the reflecting surface s, and

$$\phi_d(t) = \frac{rf(t)}{4\pi v} * \int_\theta b(t,\theta)\,\delta[t - t_2(\theta)]d\theta \qquad (1b)$$

when the least-time origin is not on the reflecting surface s.

In Equation (1), $b(t, \theta)$ is defined by the following formula:

$$b(t,\theta) = \frac{\rho\left(\frac{Z_d}{R_d} + \frac{Z_s}{R_s}\right)}{\left[\rho t + \frac{X_s(Z_dR_s - Z_sR_d)\cos\theta}{v(Z_s + Z_d)}\right]} \qquad (2)$$

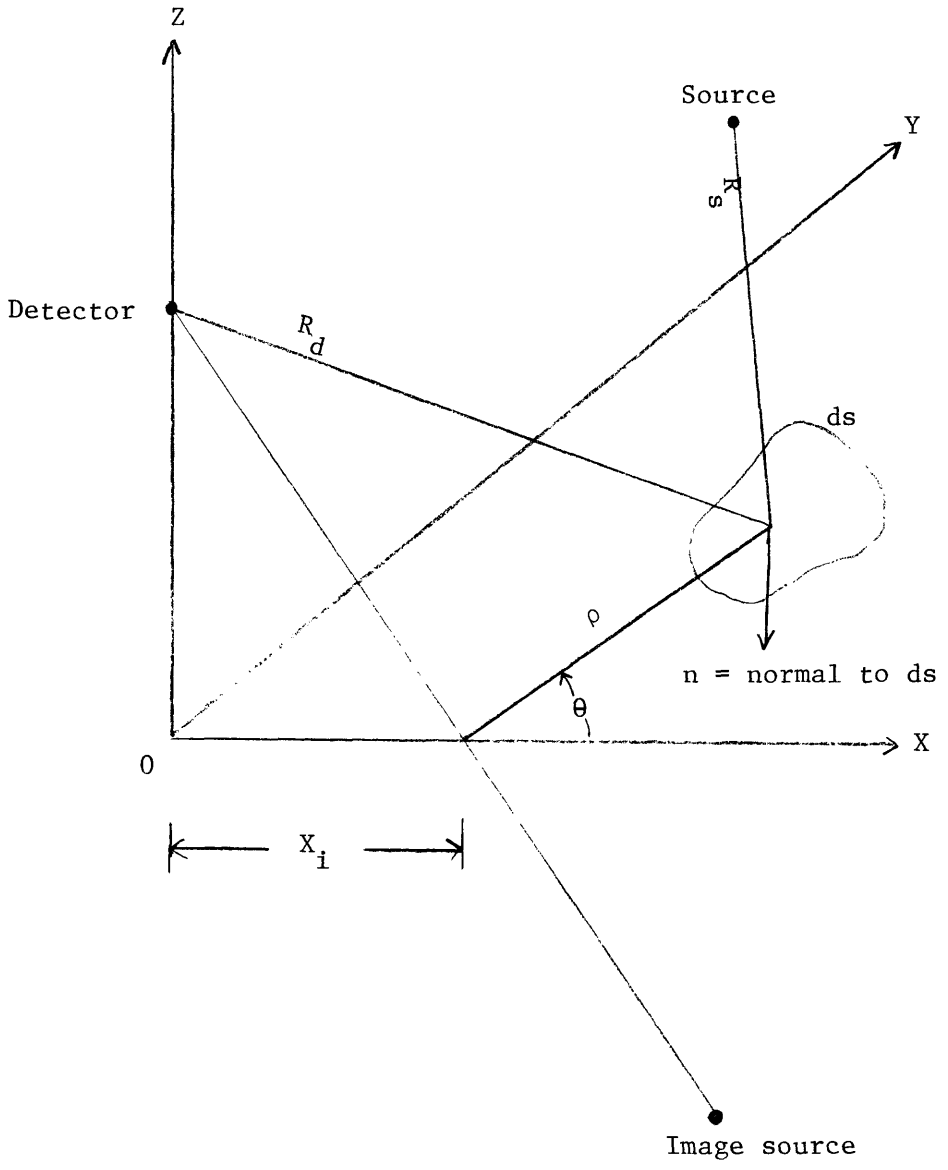

Figure 1.--Geometrical relation among source, receiver, and an elementary area ds in the X-Y plane. Detector is located in the Z-axis and source is in the X-Z plane.

where

$$\rho = \sqrt{(X_i - X_r)^2 + Y_r^2}$$

The integration with respect to Θ, appearing in Equation (1), can be written as:

$$\int_{\Theta} b(t,\Theta)\,\delta\,[t-t_z(\Theta)]d\Theta = b(t_1, \Theta)\frac{d\Theta}{dt_1} \tag{3}$$

where t_1 is the time from the source to the boundary of the reflecting surface plus time from the boundary to the detector.

Application of Equation (1) is very simple when a circular disc with a radius D is located in the center of a borehole, and a source is on the borehole axis (fig. 2). In this case, the seismic response can be written as:

$$\phi_d(t) = \frac{\delta\,(t-t_1)}{vt_1} * rf(t) - \frac{rf(t)}{4\pi v} * \int_{\Theta} b(t,\Theta)\,\delta\,[t-t_2(\Theta)]d\Theta \tag{4}$$

where

$$t_1 = \frac{(Z_s + Z_d)}{v}$$

$$t_2 = \frac{1}{v}\left(\sqrt{Z_d^2 + D^2} + \sqrt{Z_s^2 + D^2}\right.$$

$$b(t_2) = \frac{\dfrac{Z_s}{\sqrt{Z_s^2 + D^2}} + \dfrac{Z_d}{\sqrt{Z_d^2 + D^2}}}{t_2}$$

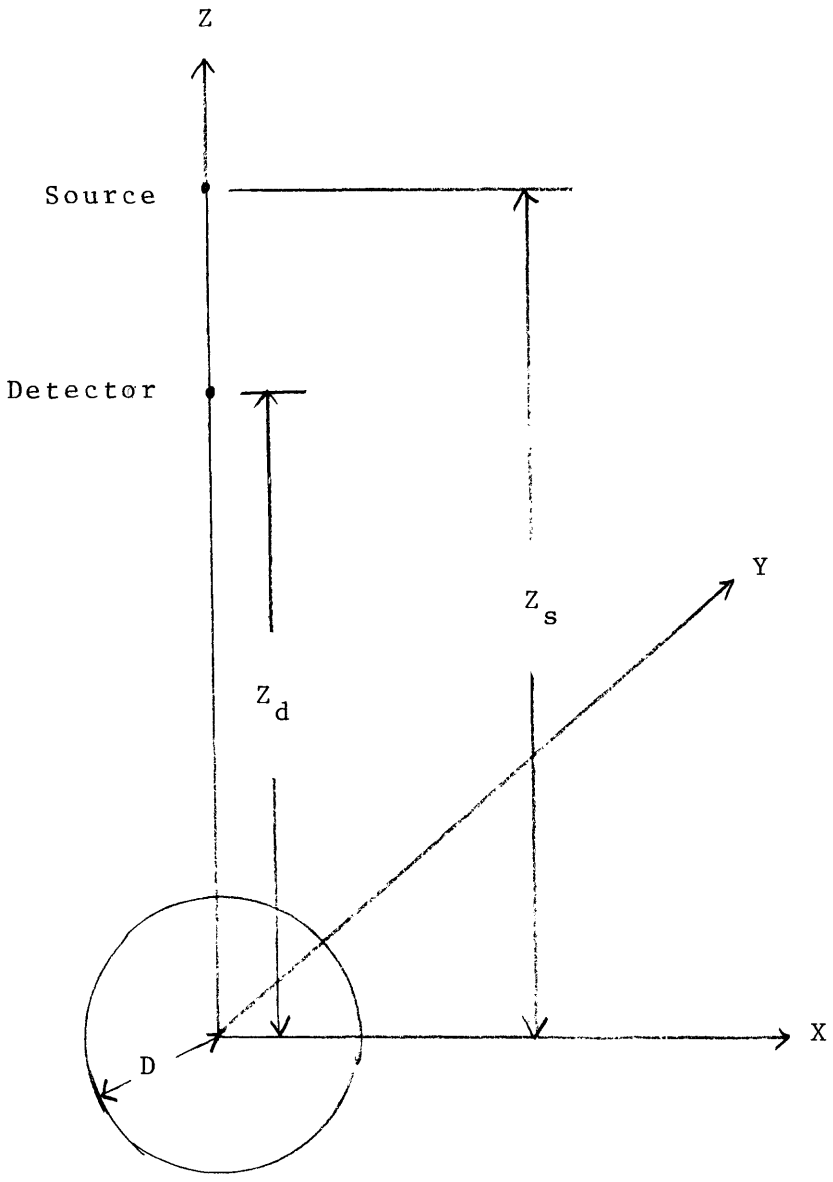

Figure 2.--Zero-offset VSP configuration for a circular disc with a radius D lying in the X-Y plane.

The lenticular-type sand body is modeled as a rectangular-type body. Because the boundary of the rectangular body is a straight line, if the seismic response from a line element is known, the total seismic responses can be derived by superposition of the 4-linear elements. Figure 3 shows the geometrical relation of a line segment in the X-Y plane. In figure 3, H is the perpendicular distance from the least-time point, X_i, to the line element. Angle Θ is positive when measured in the clockwise direction, and negative when measured in the counter-clockwise direction.

From this geometry, it is shown that:

$$R_d^2 = Z_d^2 + X_i^2 + H^2\sec^2\Theta - 2X_i H\sec\Theta\cos(\pm\Theta) \triangleq \rho_d^2 + Z_d^2 \tag{5}$$

$$R_s^2 = Z_s^2 + (X_s - X_i)^2 + H^2\sec^2\Theta + 2(X_s - X_i)H\sec\Theta\cos(\alpha \pm \Theta) = \rho_s^2 + Z_s^2$$

Using $t = \dfrac{R_s + R_d}{v}$, the following equations can be derived:

$$\frac{d\Theta}{dt} = \frac{vR_sR_d}{\rho_d R_s\left(\frac{d\rho_d}{d\Theta}\right) + \rho_s R_d\left(\frac{d\rho_s}{d\Theta}\right)} \tag{6}$$

where

$$\rho_d\frac{d\rho_d}{d\Theta} = H^2\sec^2\Theta\tan\Theta - X_i H\sec\Theta\tan\Theta\cos(\alpha \pm \Theta) \pm X_i H\sec\Theta\sin(\alpha \pm \Theta)$$

$$\rho_s\frac{d\rho_s}{d\Theta} = H^2\sec^2\Theta\tan\Theta + (X_s - X_i)H\sec\Theta\tan\Theta\cos(\alpha \pm \Theta) \pm (X_s - X_i)H\sec\Theta\sin(\alpha \pm \Theta)$$

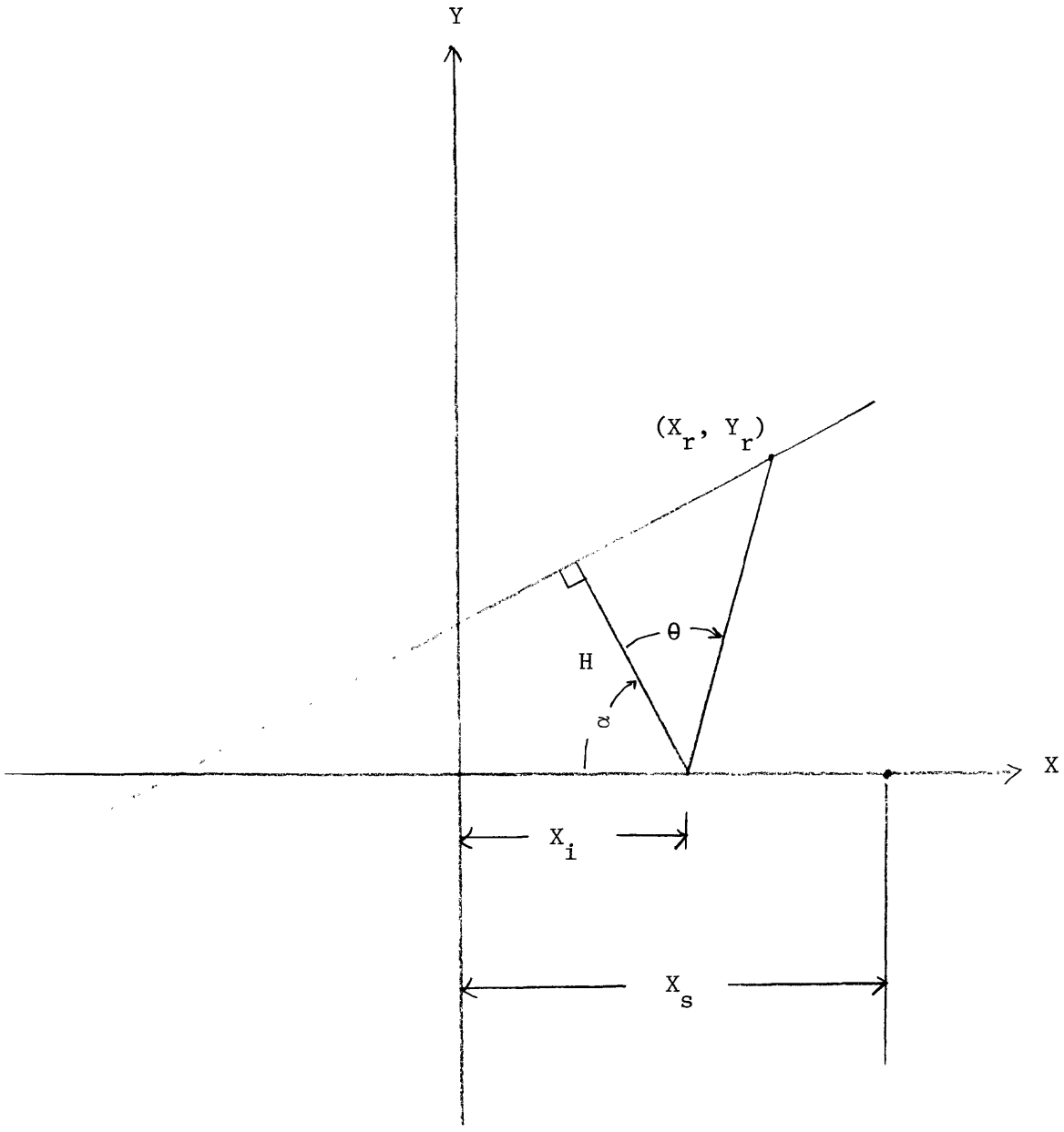

Figure 3.--Geometrical relation between the line element and source in the X-Y plane. X_i is the X-coordinate where the ray path from the image source to the receiver intersects the X-axis and H is the perpendicular distance from X_i to the line element.

When $\alpha = 0^{o}$, $X_s = 0.0$, and $Z_s = Z_d$, which is the case of the coincident source and receiver for a half-space, then:

$$\frac{d\theta}{dt} = \frac{vR_d}{2H^2\sec^2\theta\tan\theta} \tag{7}$$

and

$$b(t,\theta) = \frac{vZ_d}{R_d^2}$$

Substituting Equation (7) into Equation (1), the diffraction response for the half-space for the normal incidence can be written as:

$$\phi_d(t) = \frac{rf(t)}{4\pi v} * \frac{v^2 Z_s Z_d}{R_d^2 H^2 \sec^2\theta\tan\theta} \tag{8}$$

$$= f(t) * \frac{vZ_s\cos^2\theta}{4\pi R_d H^2\tan\theta}$$

Equation (8) is equivalent to Trorey's (1970) Equation (A-311).

Amplitude Analysis

The amplitude analysis of a finitely extended body, such as a circular disc or a rectangular body, is appropriate for the problem of detecting a small target using VSP configuration. The amplitude variation with respect to a detector location is very similar to a thin-bed amplitude variation with respect to a bed thickness. To illustrate this concept, a circular disc model is used, as shown in figure 2. Figure 4 shows the seismic response of a circular disc with respect to detector locations using 40 Hz Ricker wavelet. A seismic velocity of 10,000 ft/sec was used throughout this section. In this figure, and for all the following figures, heavy horizontal lines represent the impulse response of a body; light dotted and continuous lines represent each individual response for the input wavelet; and heavy continuous lines represent the total seismic response. The first spike of each plot shown in figure 4 represents the response from the center

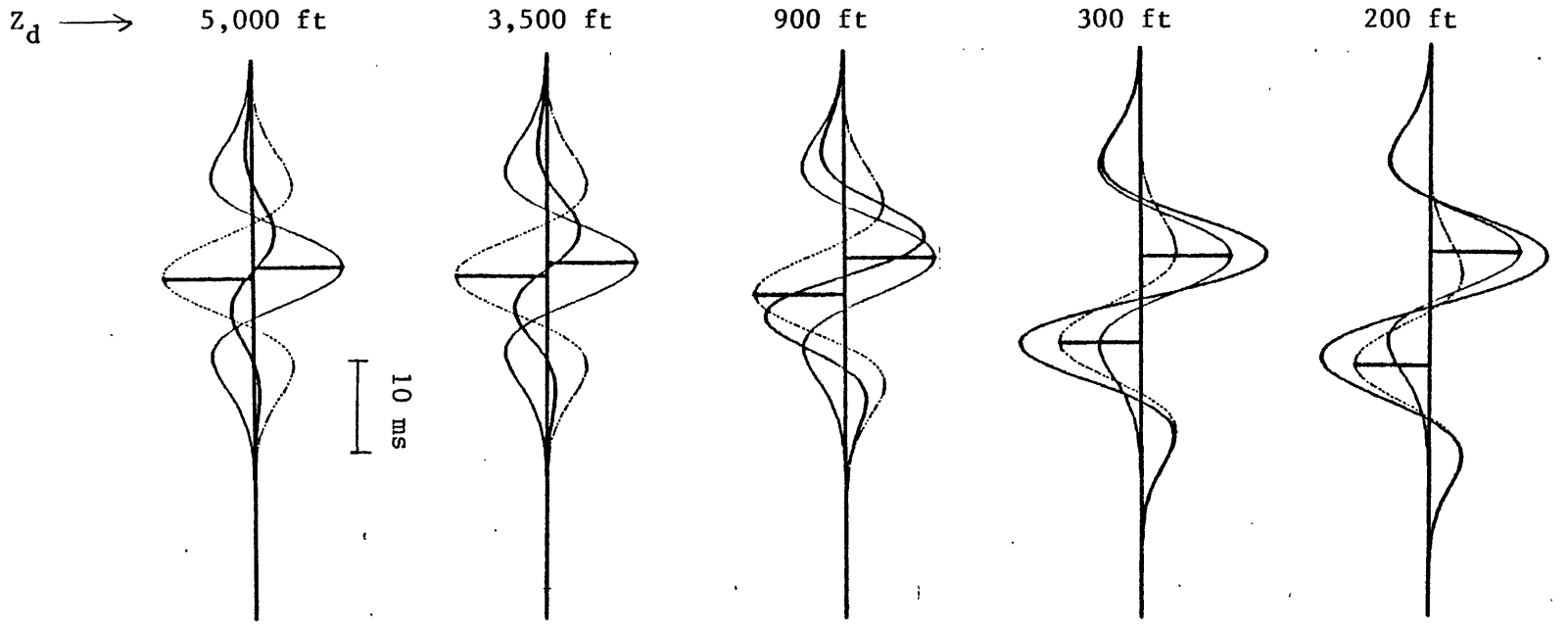

Figure 4.--Diffraction model response for a circular disc with a radius D = 250 ft (see fig. 2). The model parameters are: V = 10,000 ft/sec and Z_s = 5,000 ft. Each spike is convolved with 40 Hz Ricker wavelet which appears as a light-weight solid or dashed line. The composite waveform appears as a heavy solid line.

of a disc and the following spike represents the response from the edge of the circular disc. When a detector is very close to the reflecting body, the amplitude of a seismic response is greater than the individual responses due to a tuning effect. When the detector is very far away from the reflector, the total amplitude is much smaller than the individual response due to a destructive interference. From this figure, the advantage of VSP configuration over surface seismic profiling in detecting small bodies is evident.

Figure 5 shows the one-dimensional models demonstrating the interference pattern for a thin bed. As far as the peak amplitude is concerned, the overall seismic response of a thin bed is very similar to the diffraction response of a circular disc model. In the case of a thin bed, the two-way travel time of a thin bed is a controlling factor for the amplitude variation. In the diffraction case, the time difference between the least-reflection time (center of the disc) and the diffraction time from the edge of the circular disc are controlling factors.

Figure 6 shows the peak amplitude variation of a thin-bed response with respect to the two-way travel time ΔT using Ricker wavelets. From this plot, the approximate amplitude variation of a diffraction response from a circular disc for the zero-offset VSP configuration can be estimated.

Define

$$\tilde{Z}_s = \frac{Z_s}{\lambda}$$

$$\tilde{Z}_d = \frac{Z_d}{\lambda}$$

$$\tilde{D} = \frac{D}{\lambda}$$

where λ is source wavelength. Then the following equation can be derived from Equation (4) with correction of the spreading effect.

$$f\Delta T = \sqrt{\tilde{Z}_d^2 + \tilde{D}^2} - \sqrt{\tilde{Z}_s^2 + \tilde{D}^2} - (\tilde{Z}_D + \tilde{Z}_s) \qquad (9)$$

In Equation (9), f is the source-dominant frequency and ΔT is the time difference between the least-reflection time and arrival time from the edge of a circular disc.

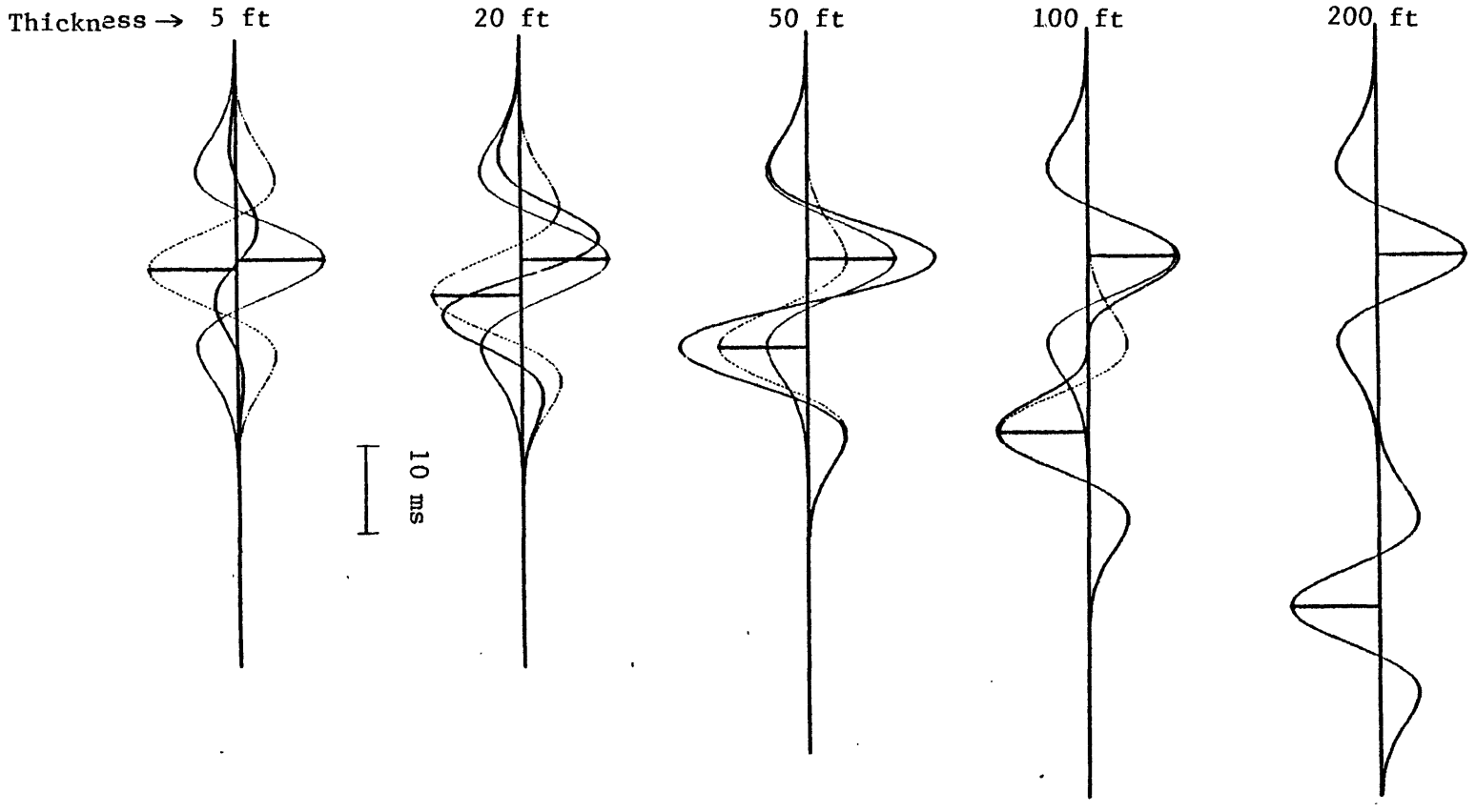

Figure 5.--One-dimensional model response for a thin bed showing the interference effect due to the bed thickness with V = 10,000 ft/sec, and 40 Hz Ricker wavelet.

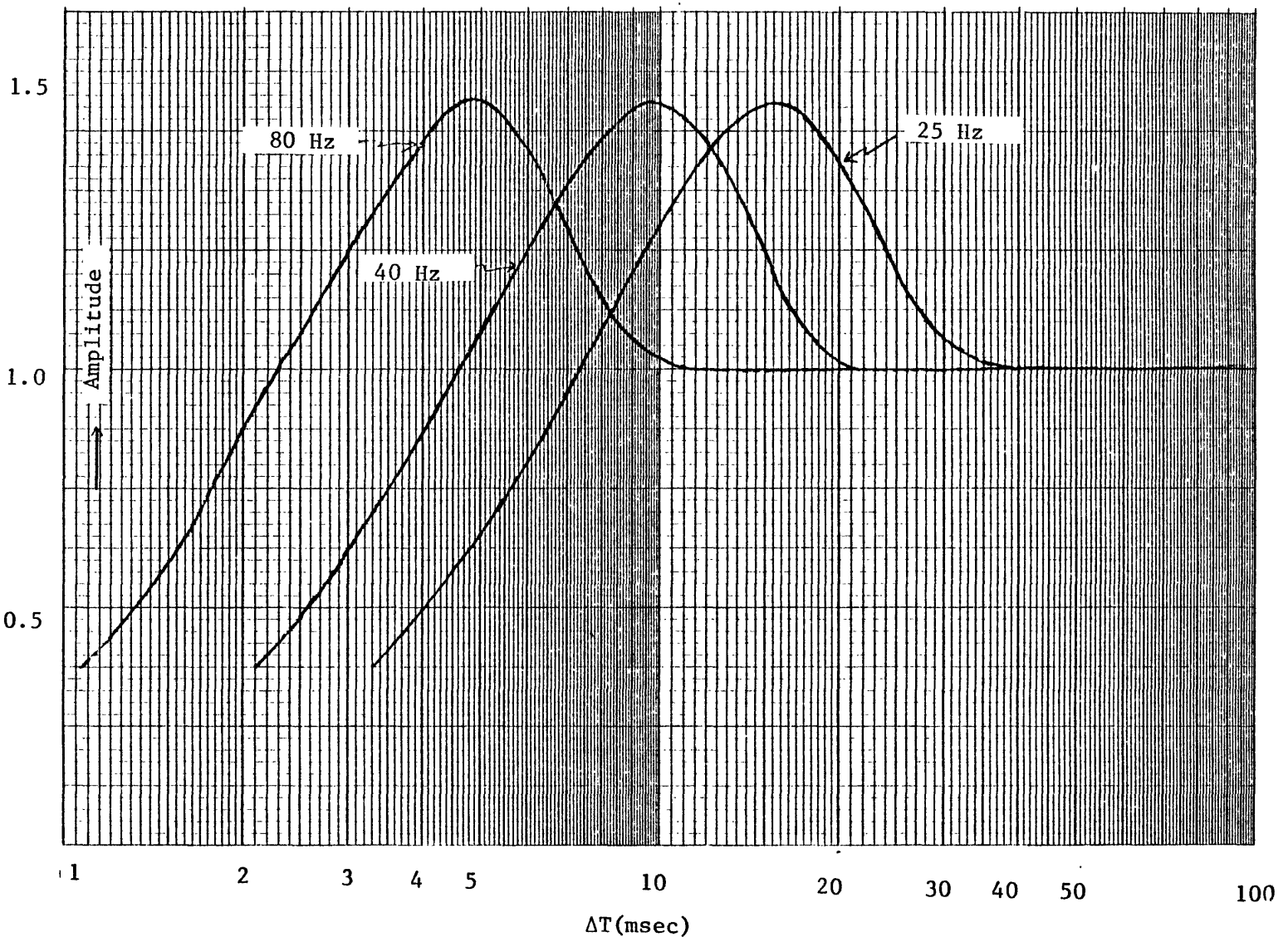

Figure 6.--Amplitude variation with respect to the two-way travel time ΔT (in msec) of the thin bed and the peak frequency of the Ricker wavelet.

Figure 7 shows the plot of Equation (9) for selected disc sizes with $\tilde{Z}_s$ = 30. In this figure, the amplitude variation of the thin bed with respect to $f\Delta T$ using Ricker wavelet is also shown. For example, A_T in figure 7 means that when $f\Delta T$ is approximately 0.38, the amplitude of a thin bed response is tuned and $A_{1/2}$ means that when $f\Delta T$ is about 0.085, the total amplitude due to the thin bed interference is about 1/2 amplitude of an infinitely thick layer.

From this figure, it is observed that the peak amplitude of a seismic response from a circular disc with $\tilde{D}$ = 1.0 is less than 1/4 the amplitude of an infinitely extended disc when the detector is located more than 20 wavelengths away from the circular disc.

To perform the amplitude analysis of seismic response from a rectangular-type body, the following definitions were used throughout this report (fig. 8).

W: Width of a rectangular body.

L: Length of a rectangular body.

(X_o, Y_o): X and Y coordinate of the center of the body.

Ø: Rotation of the axis of the body with respect to the X-axis.

X_e: X-coordinate of the edge of the body in the direction of the source.

Z_e: Z-coordinate where the raypath passing through the edge of the model intersects the borehole axis.

H_r: Depth of the rectangular-type body from the surface.

H_e: $H_r - Z_e$.

X_s: Source-offset distance.

In generating 3-dimensional diffraction models for the rectangular-type bodies, the following assumptions were made.

1. The thicknesses of most of the models are very thin compared with the source wavelength, so the response from the vertical face is assumed to be small. Thus, the seismic responses from the vertical faces of the body is excluded.
2. The reflection coefficient is independent of the angle of incidence.

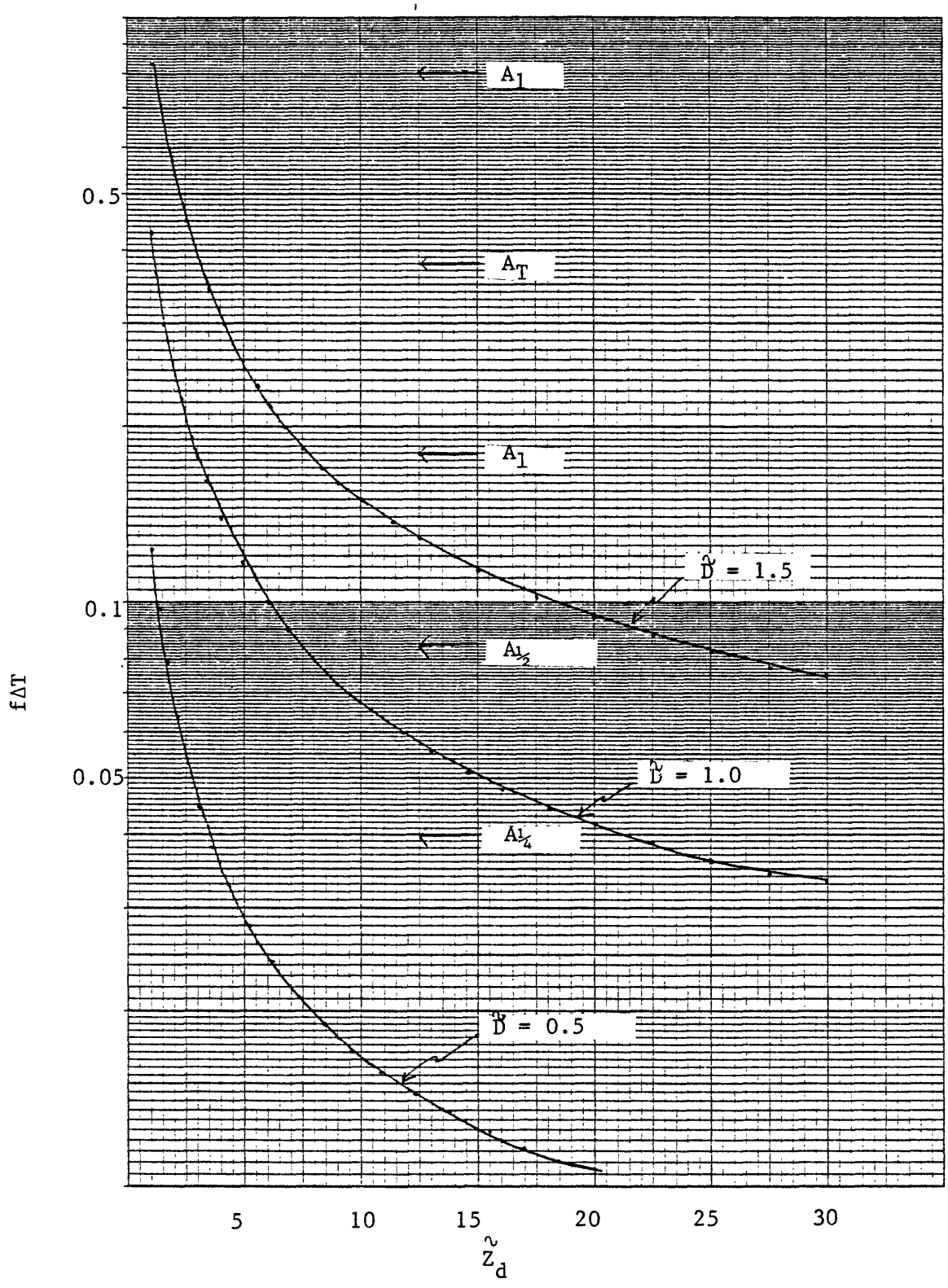

Figure 7.--The amplitude variation of a circular disc model with respect to the receiver location ($\tilde{Z}_d$) and size ($\tilde{D}$) for a fixed target depth ($\tilde{Z}_s = 30$). ΔT (in msec) is the arrival time difference between the least reflection (from the center of the disc) and the diffraction from the boundary of the disc.

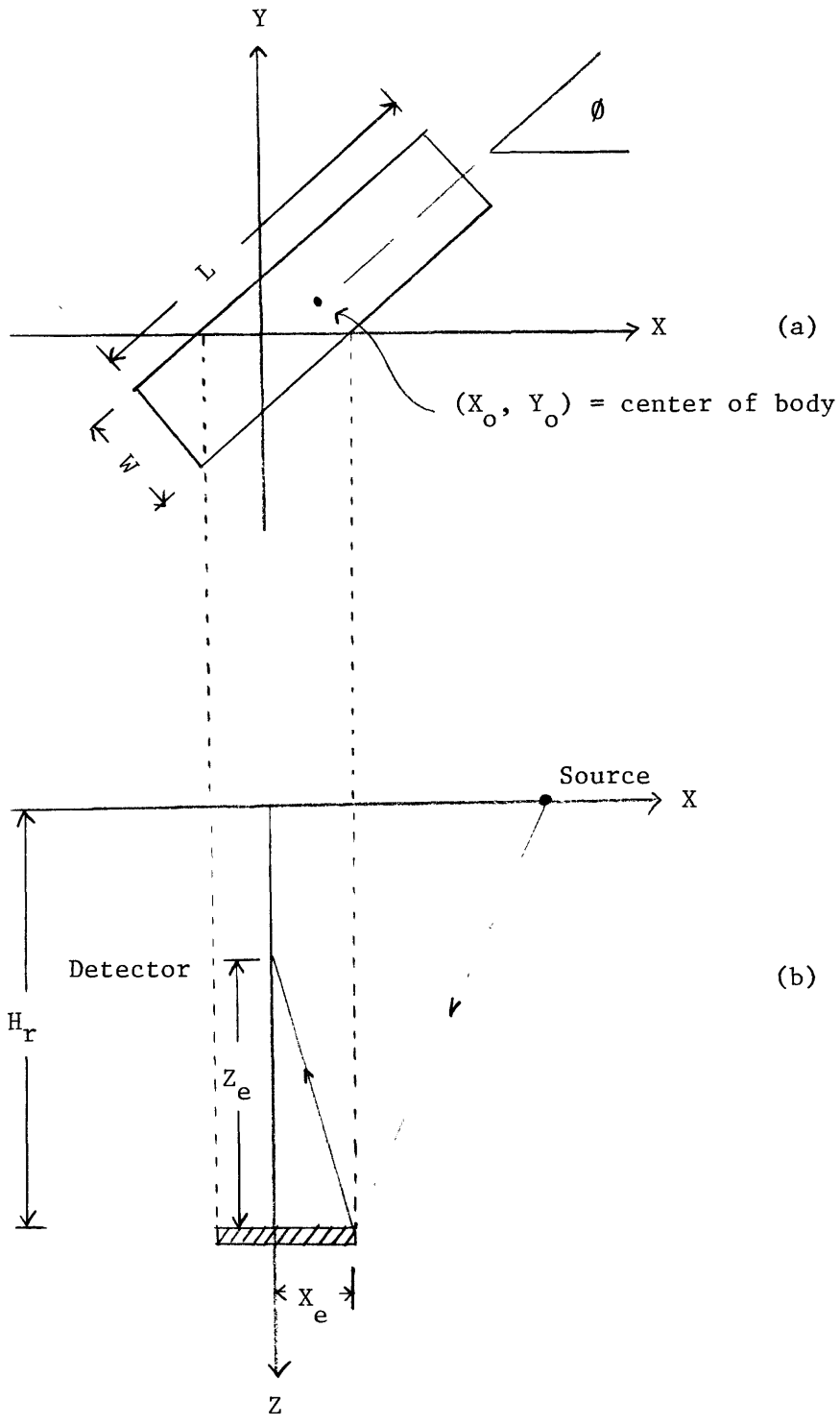

Figure 8.--Geometrical relation of a rectangular-type body. (a) Plan view in the X-Y plane. (X_o, Y_o) is the X- and Y-coordinate of the center of the body, L and N are the length and width of the rectangular body, and Ø is the angle between X-axis and the axis of the body. (b) Cross-sectional view in X-Z plane. X_e is the X-coordinate of the edge of the rectangular-type body in the X-Z plane, and Z_e is the Z-coordinate where the ray path from the image source to the X_e intersects the borehole axis.

3. The velocity of the media is constant. Therefore, the thickness of the rectangular-type model and depth of the models are scaled by the constant velocity.

4. Transmission effect is ignored.

Diffraction responses for rectangular-type bodies are shown in figure 9. This figure was generated in order to see the amplitude variation with respect to the width of the body. The model parameters are: L = 1,000 ft, $X_o = Y_o = 0$, H_r = 5,000 ft, $\emptyset = 0^o$, and X_s = 1,500 ft. Figure 9a shows the VSP model result with W = 250 ft with 40 Hz Ricker wavelet. The reference amplitude is defined as the seismic response of the infinitely extended body. When W = 250 ft, the half amplitude point with respect to the reference amplitude occurs about 800 ft above the body, and the 1/4 amplitude point is located about 1,300 ft above the body. At the geometrical edge, which is defined as Z_e in figure 8, the peak amplitude is almost negligible compared to the reference amplitude.

Figure 9b shows the VSP models with W = 500 ft. When the well-phone location is very close to the body, for example, 100 ft above the body, the seismic response from the rectangular-type body is very similar to the infinitely extended body in amplitude and shape. Generally the wave shape of the seismic response from the rectangular-type body is the derivative form of the input wavelet. At the geometrical edge, which is Z_e = 2,400 ft, the amplitude is about 1/4 of the reference amplitude.

Figure 9c shows the modeling result with W = 1,000 ft. In this case, the edge amplitude, which is defined as the amplitude at Z_e, is about 1/2 of the reference amplitude.

These models show that the edge amplitude varies with respect to the size of the body.

Figure 10 was generated in order to analyze the effect of the thickness and lateral extent of a rectangular-type body on the seismic response. The model parameters are: W = 400 ft, L = 4,000 ft, X_s = 3,000 ft, $X_o = Y_o = 0$, $\emptyset = 0^o$, H_r = 5,000 ft. Figure 10a shows the seismic response with a thickness of 10 ft and 40 Hz Ricker wavelet. Compared with the reference amplitude, the amplitudes of the total response are very small, partly because of the destructive interference due to the thickness of the body, and partly because of the size of the body.

Figure 10b shows the result when the bed thickness is 50 ft. This bed thickness is the tuning thickness for the 40 Hz Ricker wavelet. The

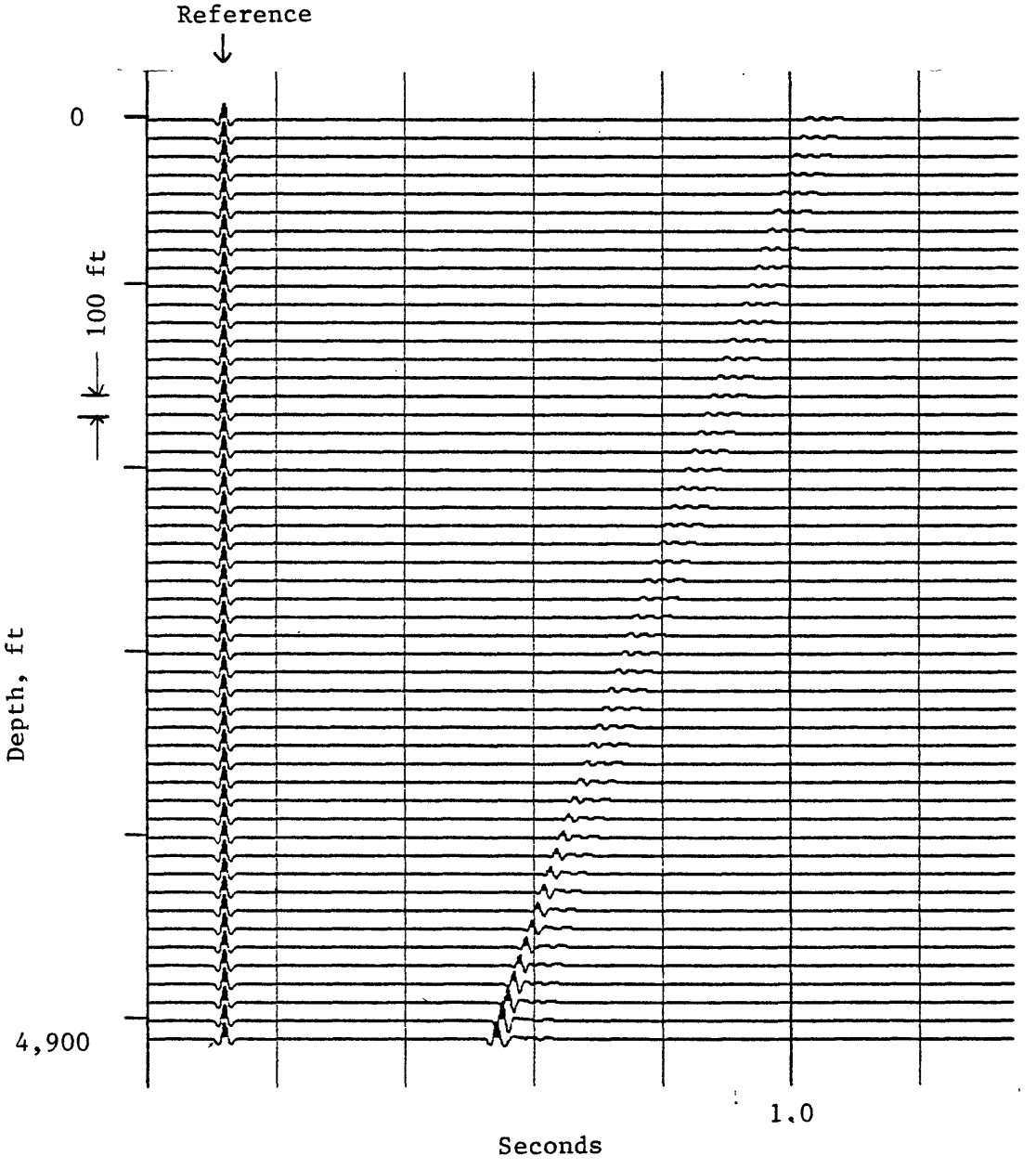

Figure 9a.--Three-dimensional VSP model showing the effect of the width of the rectangular body. Model parameters are: L = 1,000 ft, Z_S = 5,000 ft, X_O = Y_O = 0, $\emptyset$ = 0^O, X_S = 1,500 ft, V = 10,000 ft/sec, and 40 Hz Ricker wavelet. W = 250 ft.

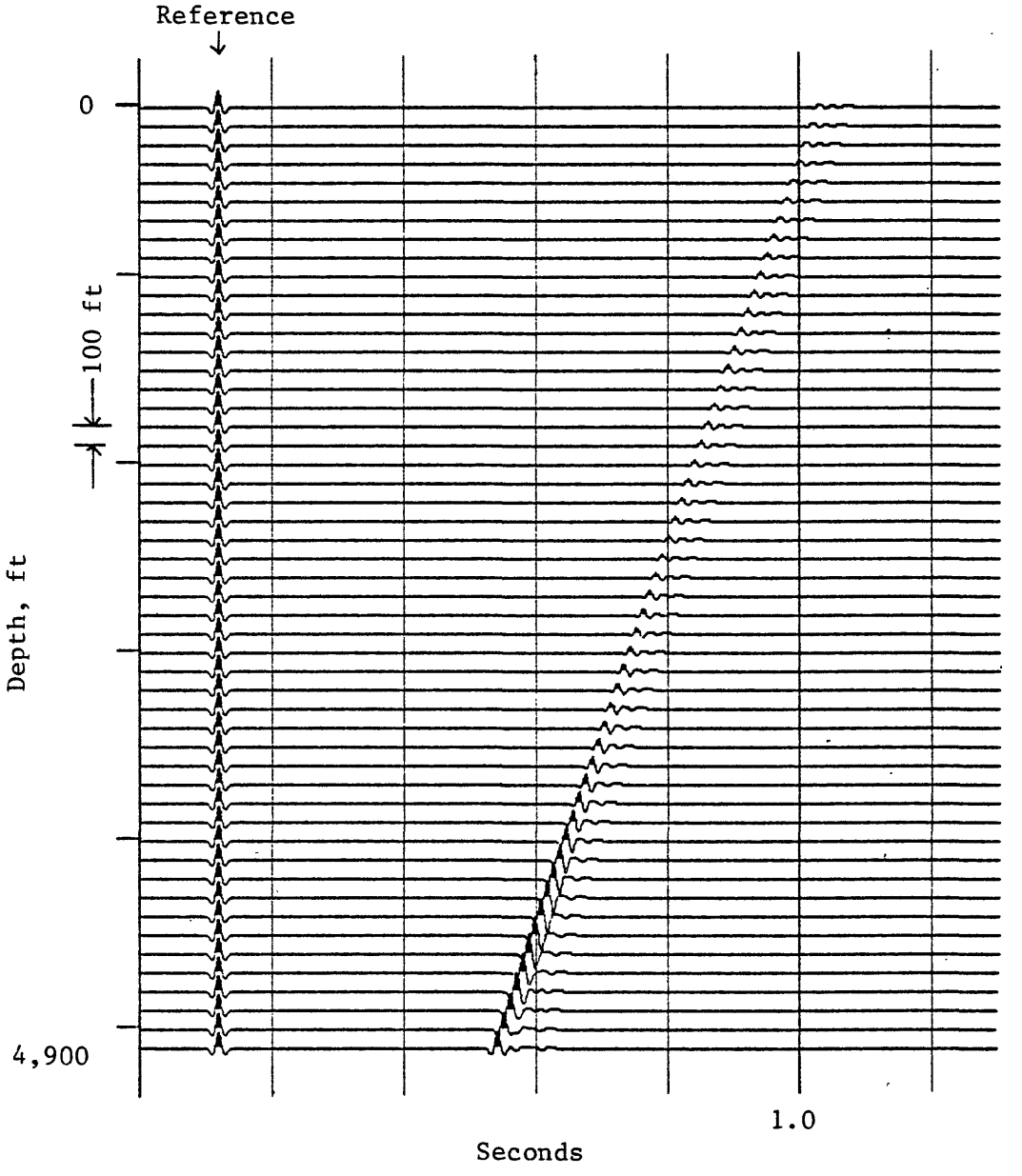

Figure 9b.--Same as figure 9a. W = 500 ft.

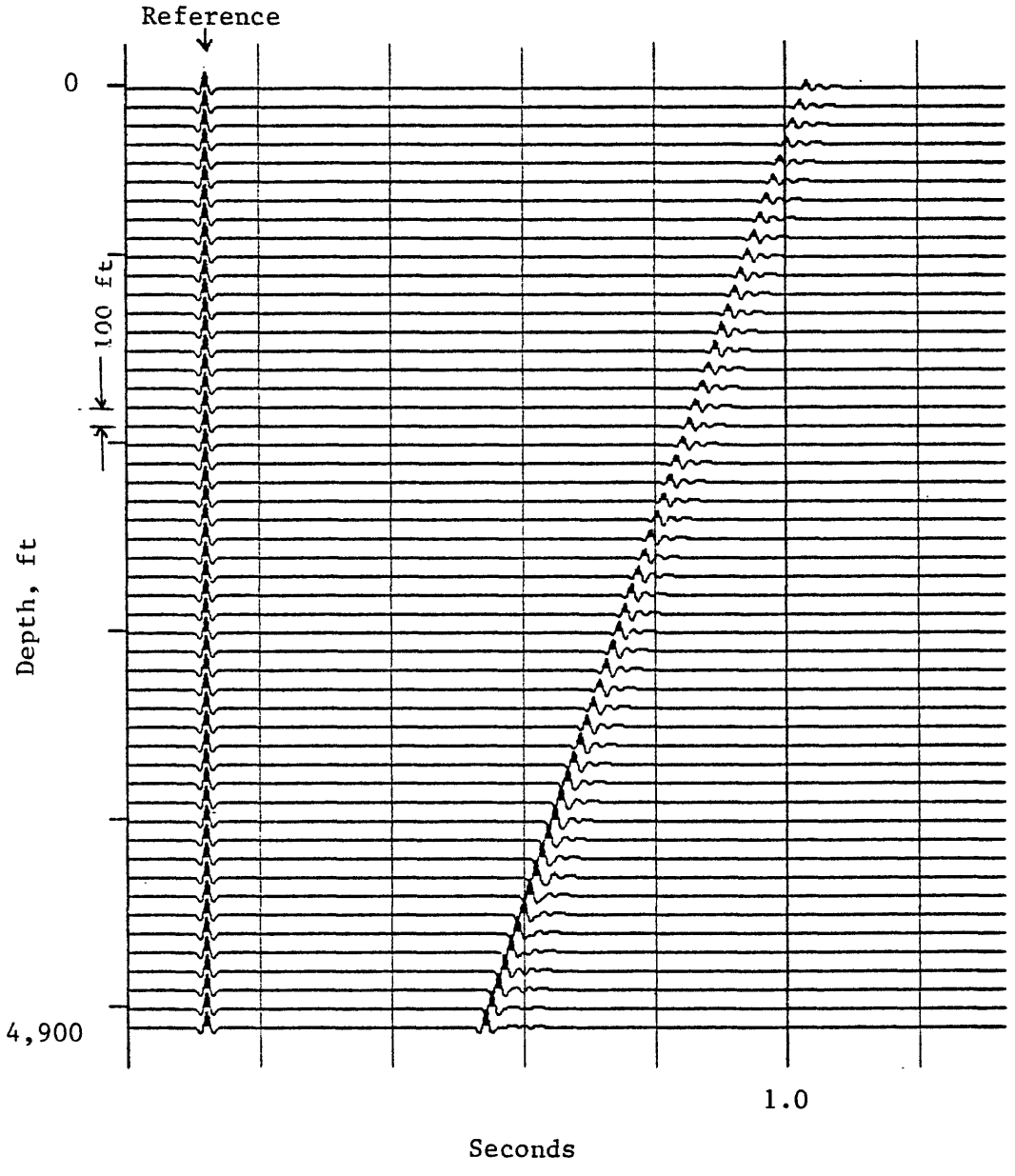

Figure 9c.--Same as figure 9a. W = 1,000 ft.

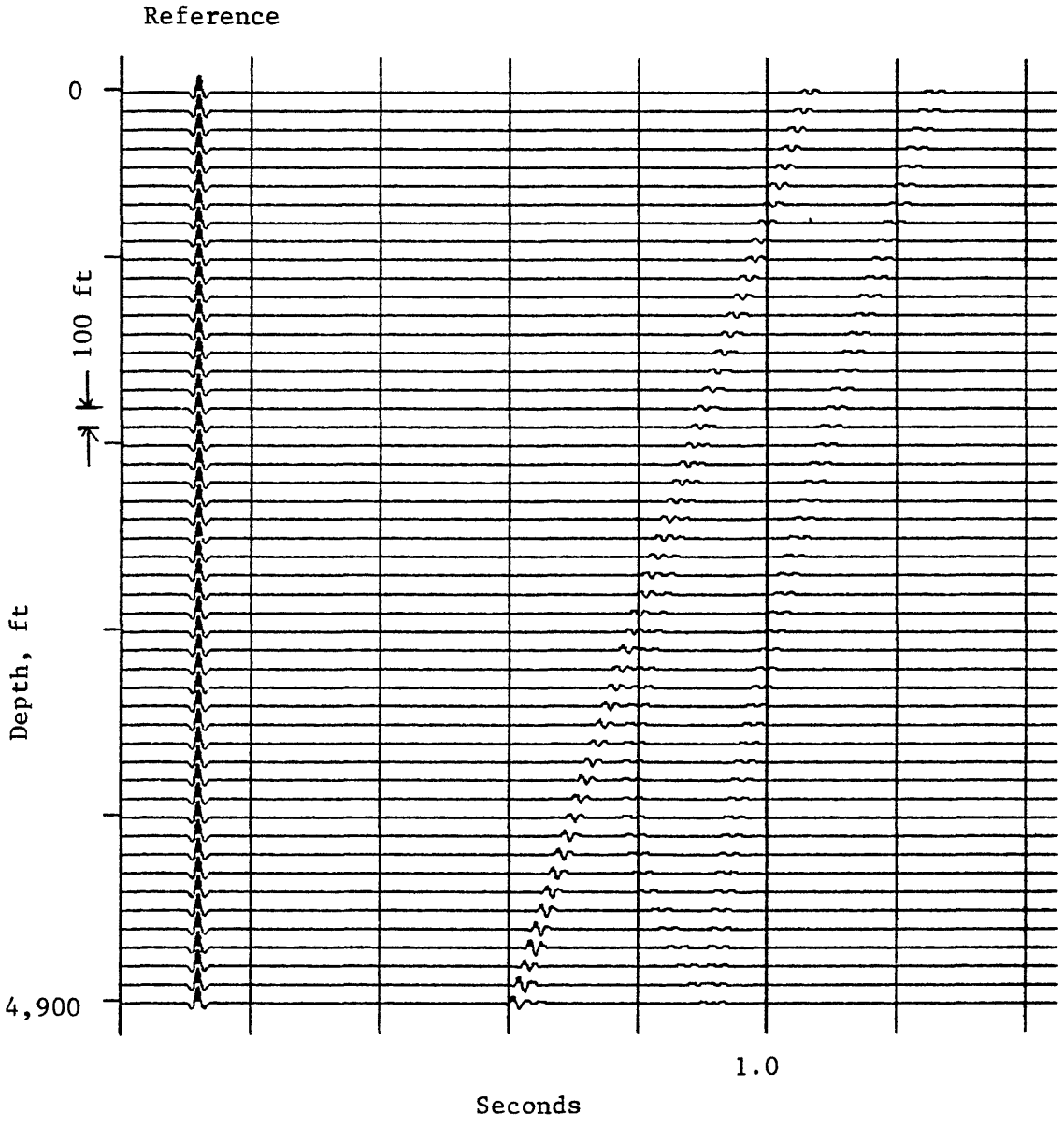

Figure 10a.--Three-dimensional VSP model showing the effect of the thickness of the rectangular body. Model parameters are: L = 4,000 ft, W = 400 ft, $X_o = Y_o = 0$, $\emptyset = 0^o$, X_s = 3,000 ft, V = 10,000 ft/sec, and 40 Hz Ricker wavelet. Thickness = 10 ft.

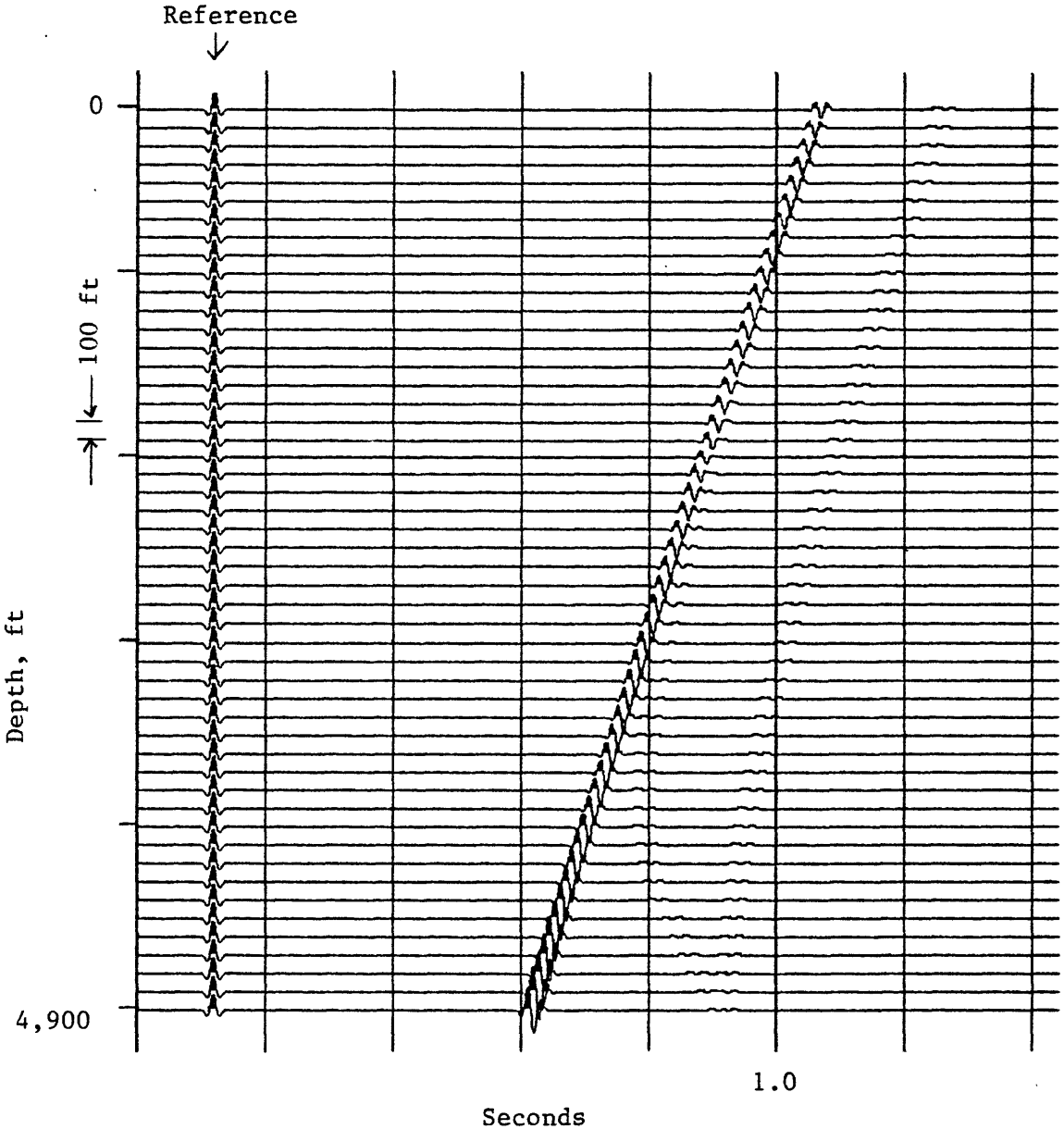

Figure 10b.--Same as figure 10a. Thickness = 50 ft.

amplitude is greater than the reference amplitude due to the constructive interference when the geophone is close to the body, and the amplitude decreases slowly with increasing well-phone distance from the body. When the bed thickness is 100 ft, shown in figure 10c, the interference effect due to bed thickness is reduced, and the seismic response from the top and the bottom of the body is now separated.

The amplitude variation of the diffraction response from a rectangular-type body is very complicated. Extensive model studies indicate that the following factors are all contributing to the amplitude variation on the VSP models.

1. The dimension and orientation of the body,
2. the depth and thickness of the body, and
3. the source and detector location and input frequency content.

Mapping of the edge of the rectangular body using the VSP method is complicated mainly due to the large variation of the edge amplitude. Generally, the edge amplitude appears to vary from 1/2 to 1/8 amplitude of the infinitely extended body when the width of the body is greater than the one wavelength of the input wavelet.

It is impractical to document all the edge amplitude variations with respect to the model parameters and field configurations, so an approximate approach to determine the edge amplitude for a simple model parameter is appropriate.

The approximate edge amplitude for a rectangular-type body with $X_o = Y_o = 0$ and $\emptyset = 0^o$ may be derived by substituting the diffraction response by a simple spike.

When $W < Z_d$, then the following approximate relation is adequate in analyzing the edge amplitude.

$$\tilde{W}^2 = \left(\frac{\sqrt{\tilde{Z}_d^2 + \tilde{X}_i^2}\sqrt{\tilde{Z}_s^2 + (\tilde{X}_s - \tilde{X}_i)^2}}{\sqrt{\tilde{Z}_d^2 + \tilde{X}_i^2}\sqrt{\tilde{Z}_s^2 + (\tilde{X}_s - \tilde{X}_i)^2}}\right) 8f\Delta T \qquad (10)$$

where the variable with a tilde is the quantity normalized by the input source wavelength.

Equation (10) shows the implicit relation of the edge amplitude with respect to the model dimension and VSP shooting geometry.

Figure 11 shows the relation of the model parameters to the edge amplitude with $\tilde{Z}_s = 20$, $\tilde{X}_e = 4$.

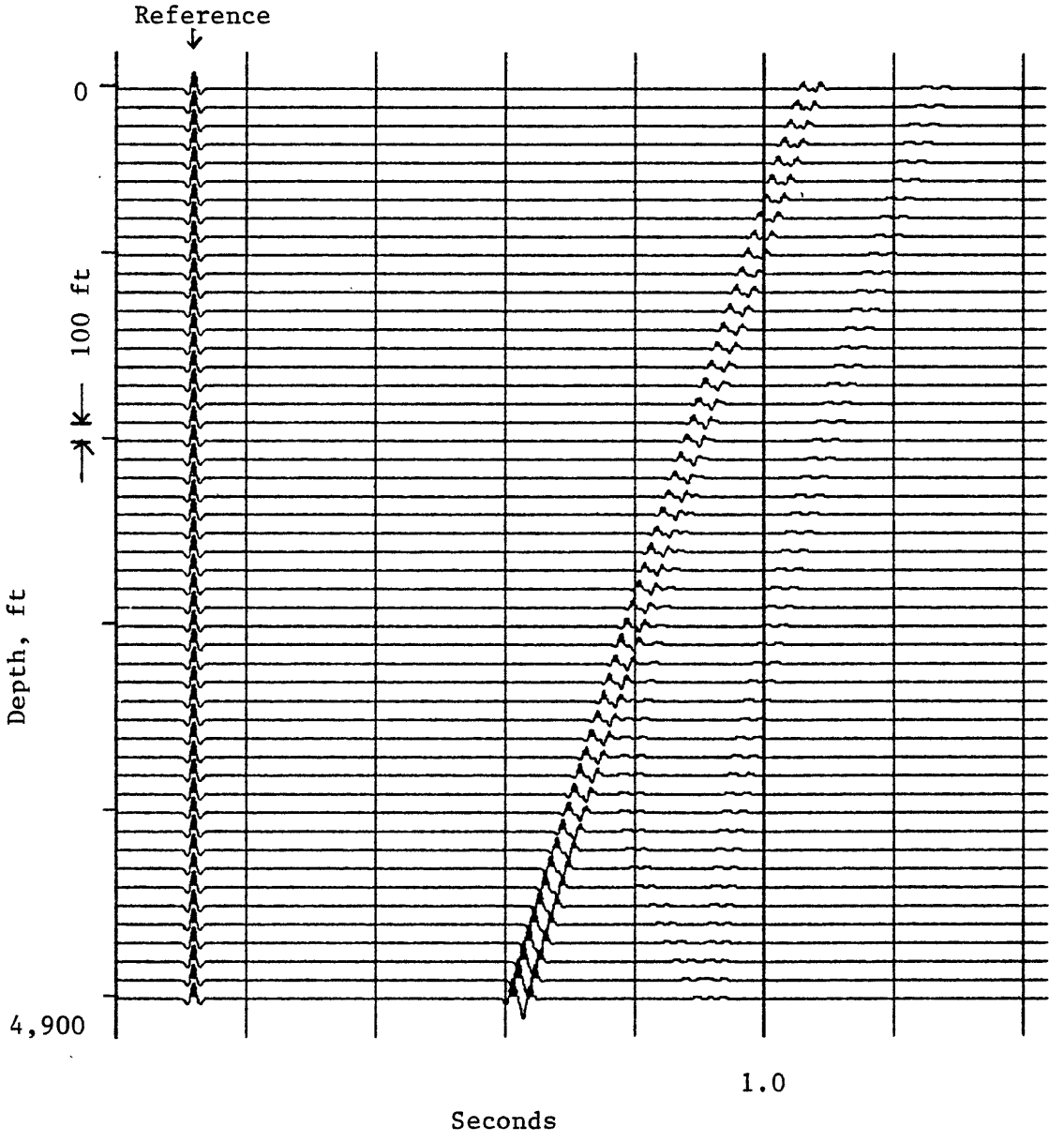

Figure 10c.--Same as figure 10a. Thickness = 100 ft.

For example, let

$W = 400$ ft

$L = 2{,}000$ ft

$H_r = Z_s = 5{,}000$ ft

$X_o = Y_o = 0$

$\emptyset = 0^o$

$V = 10{,}000$ ft/sec

$f = 40$ Hz.

Then,

$\lambda = 250$ ft

$\tilde{W} = 1.6$

$\tilde{X}_e = 4.0$

$\tilde{Z}_s = 20.$

From Figure 11, it can be seen that the edge amplitude will be between 1/4 and 1/8 of the amplitude of the infinitely extended body when $\tilde{Z}_d$ is less than 15, or equivalently the source offset is greater than about 2,500 ft. This kind of analysis could be useful in designing field configurations.

Figure 12 shows the actual plot of the peak amplitude ratio from the VSP models with respect to the detector location for three different widths of a rectangular body. The amplitude ratio in figure 12 is the ratio of the amplitude response from the rectangular-type body to the infinitely extended body and the model parameters are shown in figure 12. When W = 350, the edge amplitude is about 1/8 and when W = 500, the edge amplitude is about 1/4. These edge amplitudes correspond rather well to the approximate solution shown in figure 11. Also in figure 12, the range $X_e \pm \lambda$ is shown, and if Z_e is chosen in this depth range using VSP data to map the edge of the rectangular body, the possible error will be in the order of one wavelength of the source wavelet. This is an important observation in delineating lenticular-type sand bodies using the amplitude criteria. This figure shows that if the width of a lenticular-type sand body is in the order of two source wavelengths, the error in delineating the edge of the body using 1/4 amplitude criteria will be in the order of one source wavelength.

$\tilde{Z}_s = 20$

$\tilde{X}_e = 4.0$ (edge)

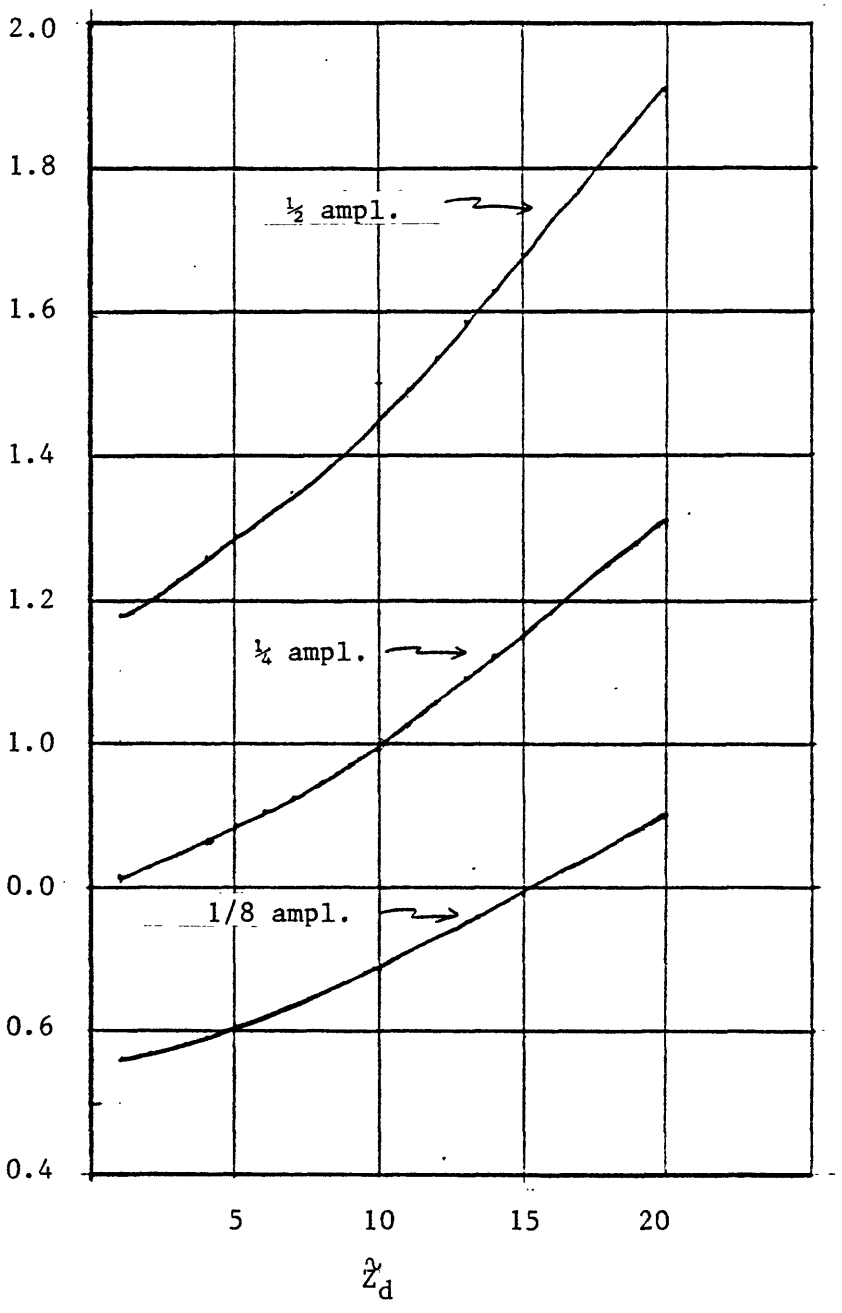

Figure 11.--Approximate edge amplitude relation among the geophone location, size of the rectangular body and the source locations in the dimensionless parameters. Model parameters are: L = 8.0 ($\tilde{X}_e = 4.0$), $X_o = Y_o = 0$, $\emptyset = 0^o$, and $\tilde{Z}_s = 20$.

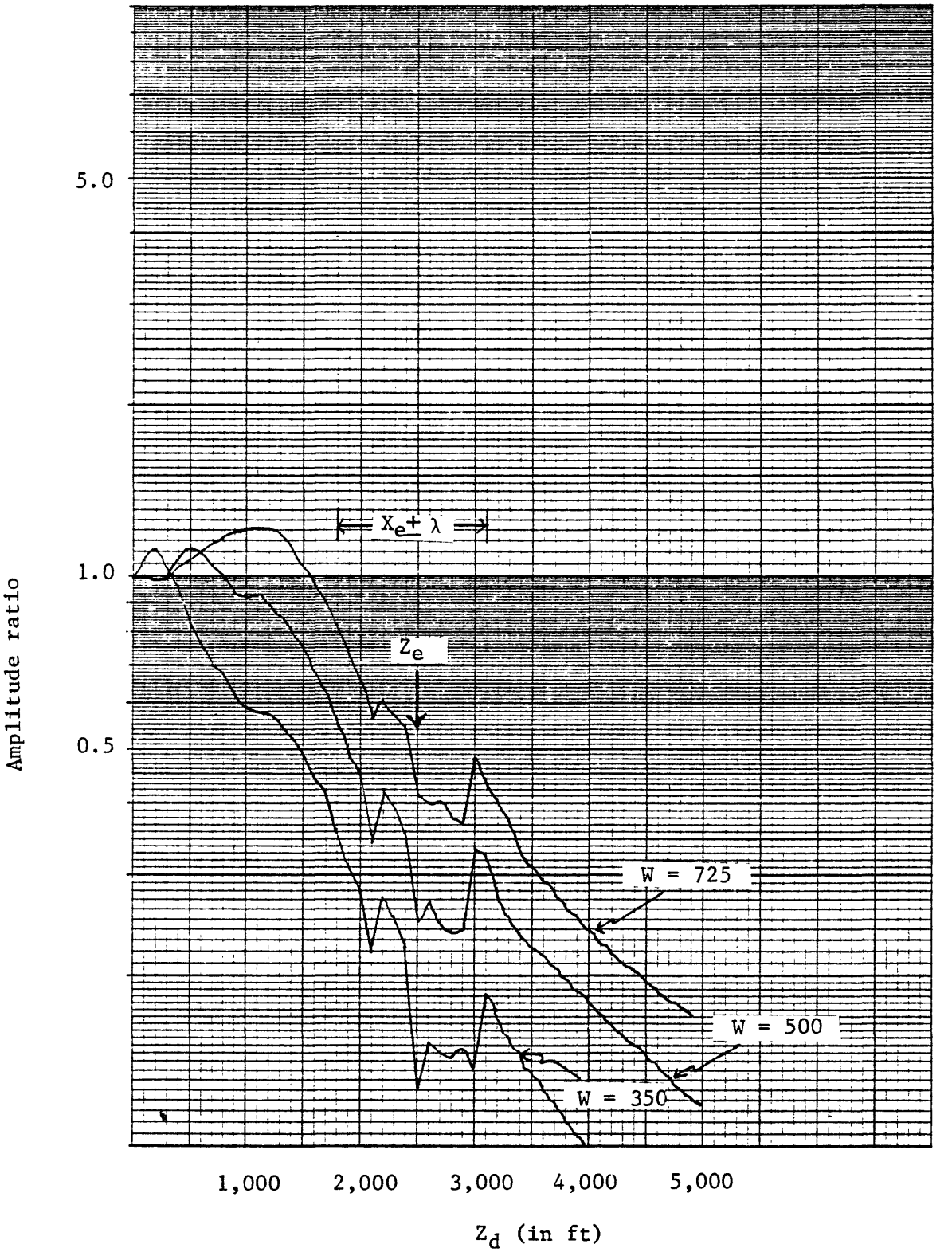

Figure 12.--Amplitude variation with respect to the width of the rectangular body. Model parameters are: L = 2,000 ft, Z_s = 5,000 ft, $X_o = Y_o = 0$, $\emptyset = 0^o$, X_s = 3,000 ft, and 40 Hz Ricker wavelet.

SEISMIC RESPONSE OF THE SELECTED SAND BODY AT MWX WELL SITE

The lenticular-type sand bodies at the MWX well site near Rifle, Colorado, are distributed in the depth range of 4,000-7,800 ft. Due to the differences in acoustic impedance, thickness, and vertical distribution of sand bodies in this area, a series of one-dimensional and three-dimensional modelings were performed in order to investigate the seismic characters of typical sand bodies.

One-dimensional seismic modeling will show the seismic characters, such as amplitude and waveform, based on the acoustic-impedance contrast and layering under the assumption that the sand bodies are extended over a large area compared to the wavelength considered.

On the other hand, three-dimensional VSP modeling will demonstrate the effect of the edges of the sand body with respect to the shooting geometry. If the result of one-dimensional modeling looks pessimistic, the chances of detecting and delineating the lenticular sand bodies using the VSP method are remote.

In making 3-dimensional models, the depths of the typical sand bodies were chosen arbitrarily. However, the acoustic parameters, such as velocity, density, and the layer thickness, are very representative for the lenticular sand bodies at the MWX well site. All of these parameters are derived from well logs, core analysis, and VSP data.

Throughout the VSP models of this section, it is assumed that the borehole penetrates the center of a rectangular body and the source is located in the direction of the axis of the rectangular body.

Three zones of interest--coastal, paludal, and coal--are studied in detail.

Coastal Zone

The depth of the coastal zone is from 6,000-6,500 ft at the MWX well site. Figure 13 shows the one-dimensional modeling result using 40 Hz Ricker wavelet. Acoustic parameters and reflection coefficients at the top and bottom of the sand body are also shown in this figure. There is not much of an interference pattern using 40 Hz Ricker wavelet because of the sand body thickness of 125 ft.

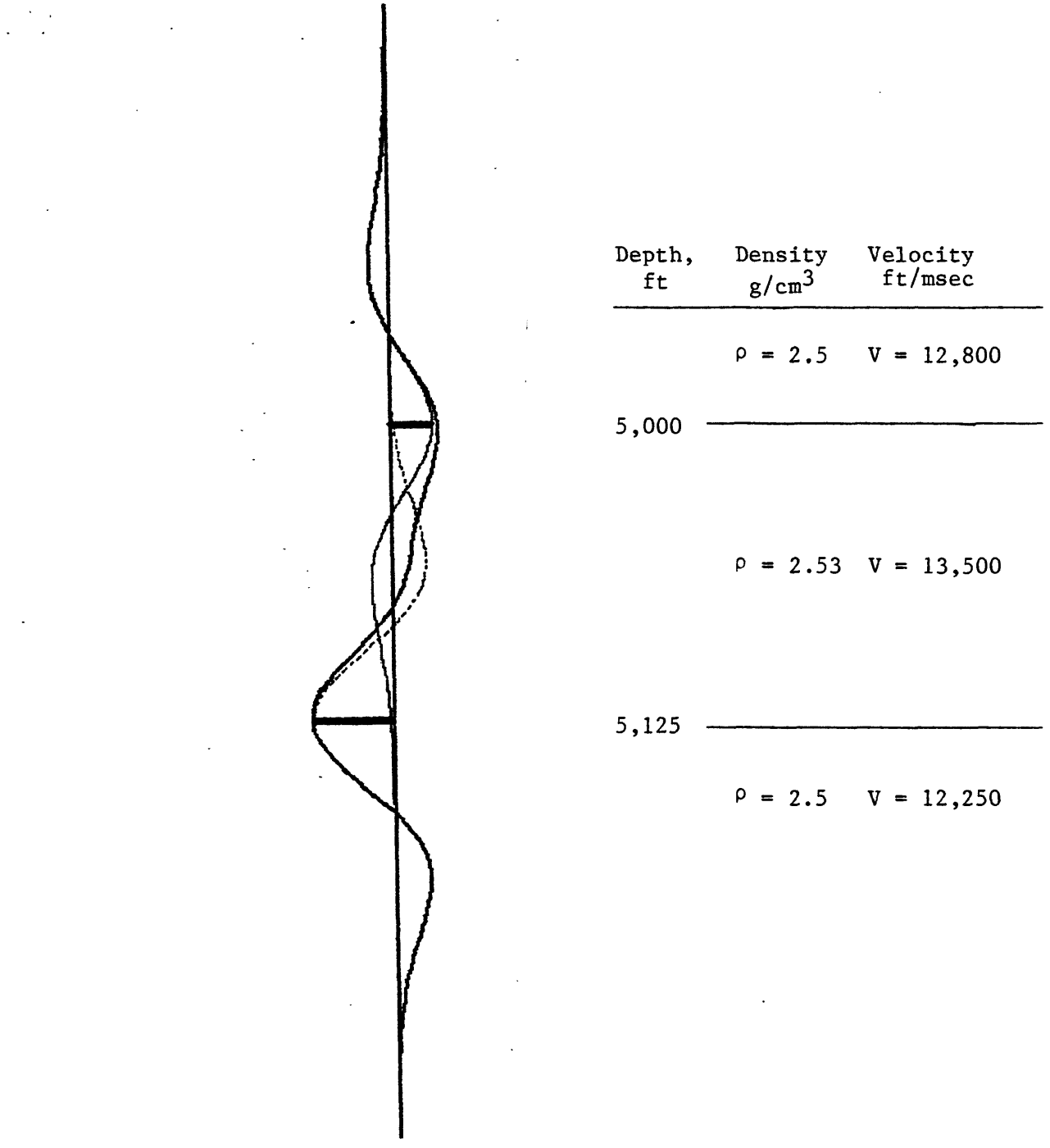

Figure 13.--One-dimensional seismic response for the coastal model. Each spike is convolved with 40 Hz Ricker wavelet which appears as lightweight solid or dashed line. The composite waveform appears as a heavy solid line.

Figure 14 shows the 3-dimensional VSP modeling with W = 400 ft, L = 4,000 ft, Z_s = 5,000 ft, and X_s = 2,000 ft along the axis of the body. The source waveform was 40 Hz Ricker wavelet. In this model, all the reflection points are located inside the body meaning that there is no ray path going through the edge of the body. The seismic signal at a depth of 4,750 ft, which is 250 ft above the body, is very similar to the one-dimensional model. The reference amplitude shown in figure 14 is the 40 Hz Ricker wavelet convolved with a reflection coefficient of 0.049, which is the reflection coefficient at the bottom of the sand body.

Figure 15 shows another VSP model result. The model parameters generating figure 15 are identical to those of figure 14 except that the source is located 4,500 ft away from the borehole. The low-frequence appearance of the seismic response in figure 15, compared with figure 14, is possibly due to the complex interference from the edges of the sand body. The edge amplitude, the amplitude at Z_e, is about 1/8 of the amplitude at 4,750 ft. The depth region shown as $X_e \pm \lambda$ in figure 15 is the depth range which will provide the edge of the lenticular sand body within one wavelength of the input source wavelet. For example, if an interpretation was made under the assumption that the edge amplitude appeared at the depth of about 1,750 ft, the interpreted edge of the body is about 1,750 ft which is one source wavelength less than the actual edge. The mapping of 1/8 amplitude location on the VSP section corresponds to detection of the reflection amplitude in the order of 0.006.

This order of amplitude detection could be possible for a very high signal-to-noise ratio VSP section. However, in the actual case, the probability of delineating the edge of the body could be at most fair considering the random and coherent noises introduced from the data acquisition and processing.

Paludal Zone

Two types of sand bodies were considered in the paludal zone, which is between 6,500-7,500 ft in depth.

Paludal model #1.--One-dimensional modeling of the paludal model #1 with 30 ft of bed thickness is shown in figure 16. Because the reflection coefficient at the bottom of the sand body is negligible compared with the top reflection coefficient, there is not much interference pattern due to layer thickness.

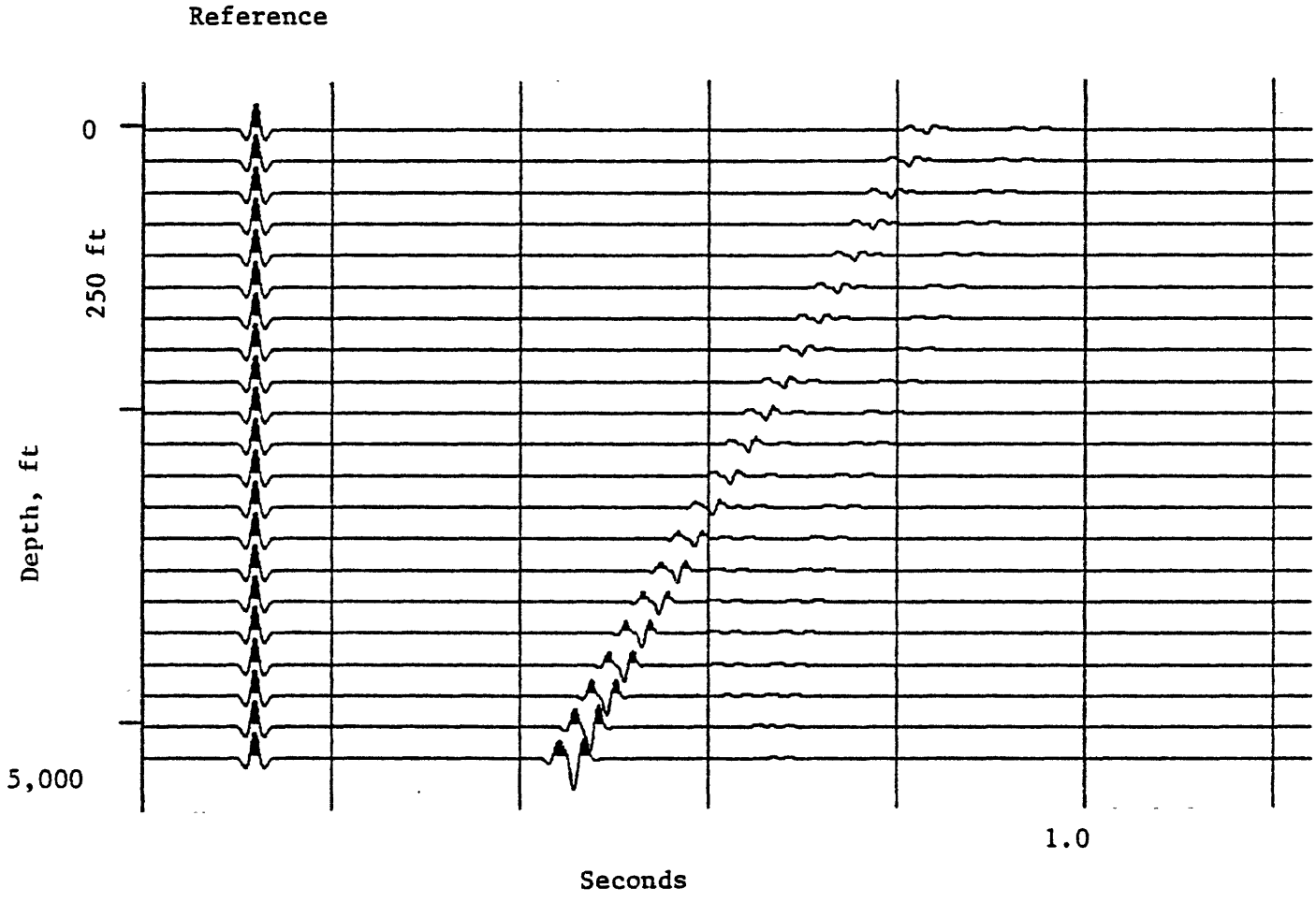

Figure 14.--Three-dimensional VSP response for the coastal model. Model parameters are: L = 4,000 ft, W = 400 ft, $X_o = Y_o = 0$, $\emptyset = 0^o$, Z_s = 5,000 ft, X_s = 2,000 ft, and 40 Hz Ricker wavelet.

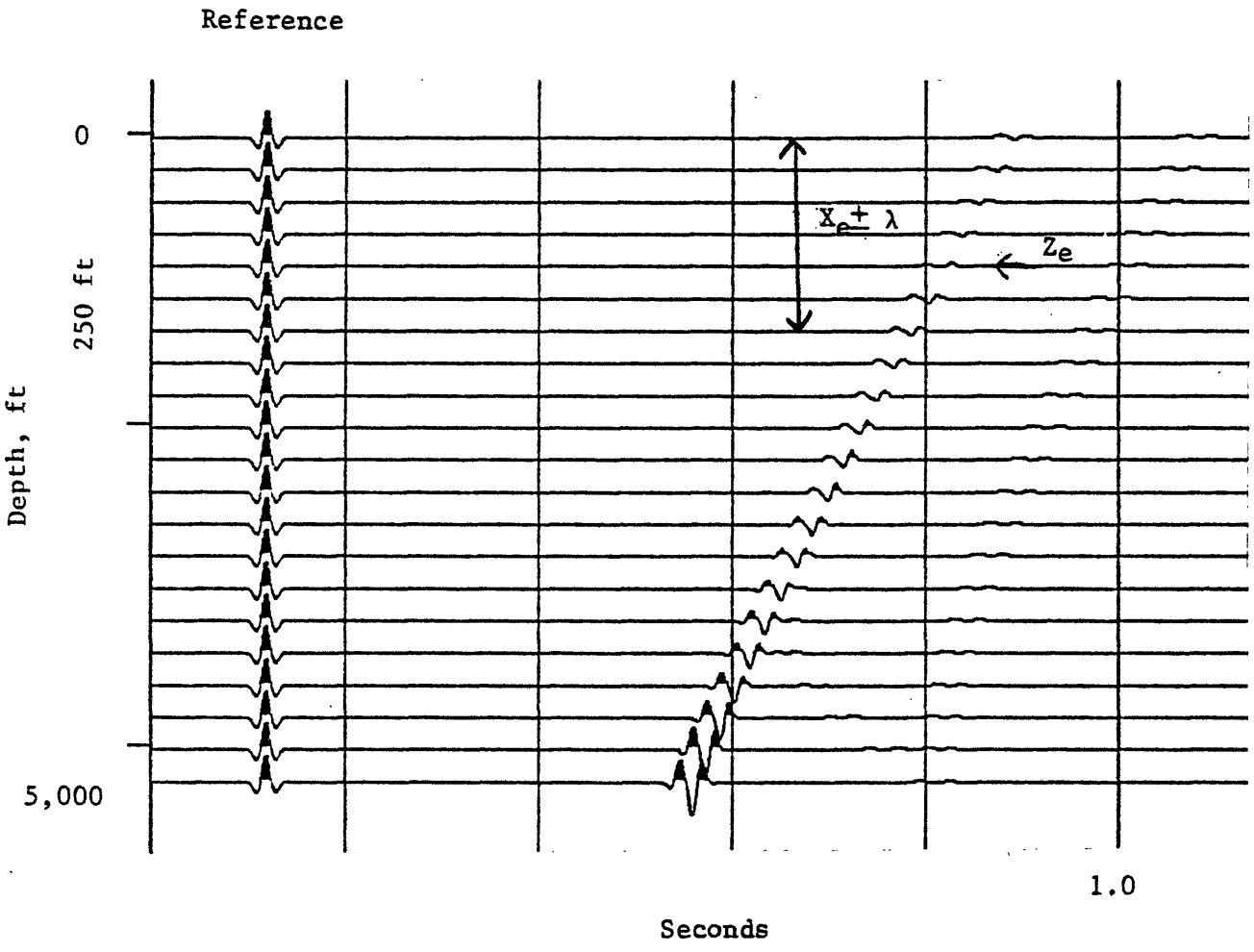

Figure 15.--Three-dimensional VSP response for the coastal model. Model parameters are: L = 4,000 ft, W = 400 ft, $X_o = Y_o = 0$, $\emptyset = 0^o$, Z_s = 5,000 ft, X_s = 4,500 ft, and 40 Hz Ricker wavelet.

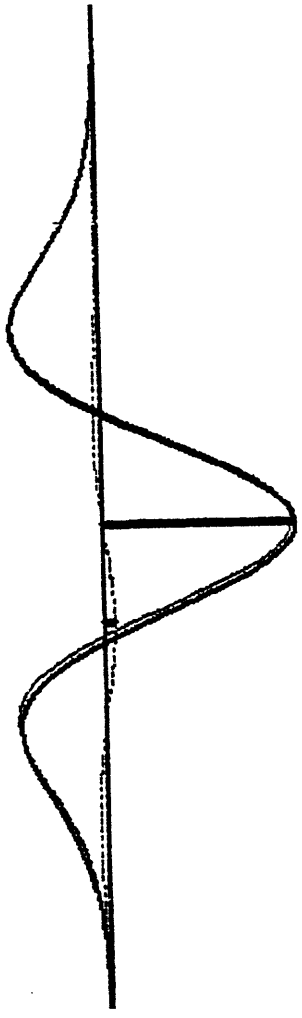

Depth, ft	Density g/cm^3	Velocity ft/msec
	ρ = 2.47	V = 10,000
5,000		
	ρ = 2.5	V = 12,000
5,030		
	ρ = 2.62	V = 11,600

Figure 16.--One-dimensional seismic response for the paludal model #1. Each spike is convolved with 40 Hz Ricker wavelet which appears as lightweight solid or dashed line. The composite waveform appears as a heavy solid line.

Three-dimensional VSP modeling with W = 300 ft, L = 1,500 ft, and X_s = 2,000 ft is shown in figure 17. The bed thickness in figure 17 is 30 ft. The waveform at the depth of 4,750 ft is different from that of the one-dimensional result. This difference in the waveform is due to the effect of interference from the edge of the body. Figure 18 shows VSP modeling with a bed thickness of 100 ft. As mentioned in the one-dimensional modeling, there are not many differences in the seismic response resulting from bed thickness.

The appearance of the edge amplitude is similar to the coastal model. However, since the reference amplitude of the paludal model #1 is about two times bigger than the coastal model, the probability of delineating the sand body in the paludal could be better than in the sand body in the coastal zone.

Paludal model #2.--The paludal model #2 consists of two sand bodies with varying inner-zone thickness. One-dimensional seismic modeling with the inner-zone thickness of 40 ft is shown in figure 19. Due to the constructive interference between the bottom reflection of the top sand body and the top reflection of the bottom sand body, the total seismic amplitude is bigger than the individual response.

The dimensions of the sand body in paludal model #2 are W = 400 ft and L = 4,000 ft. Figure 20 shows the VSP modeling with X_s = 2,000 ft, the top sand body depth of 5,000 ft, and the inner-zone thickness of 40 ft. The result of VSP modeling with the top sand body depth of 6,800 ft is shown in figure 21. The seismic responses in both figures are very similar. The seismic character a few hundred feet above the sand body is very similar to that of the one-dimensional response.

The VSP model results of locating the source at 4,500 ft from the well are shown in figures 22 and 23. Based on the amplitude characteristics near the edge of the model, the probability of delineating the sand bodies of the paludal model #2 is good.

One-dimensional modeling with the inner-zone thickness of 140 ft is shown in figure 24. Due to the large thickness of the inner zone compared with the source wavelength, the effect of constructive interference shown in figure 19 is negligible.

Figure 25 shows the one-dimensional model with a 240 ft inner-zone thickness. The seismic response from the top sand body is entirely separated from the response of the bottom sand body.

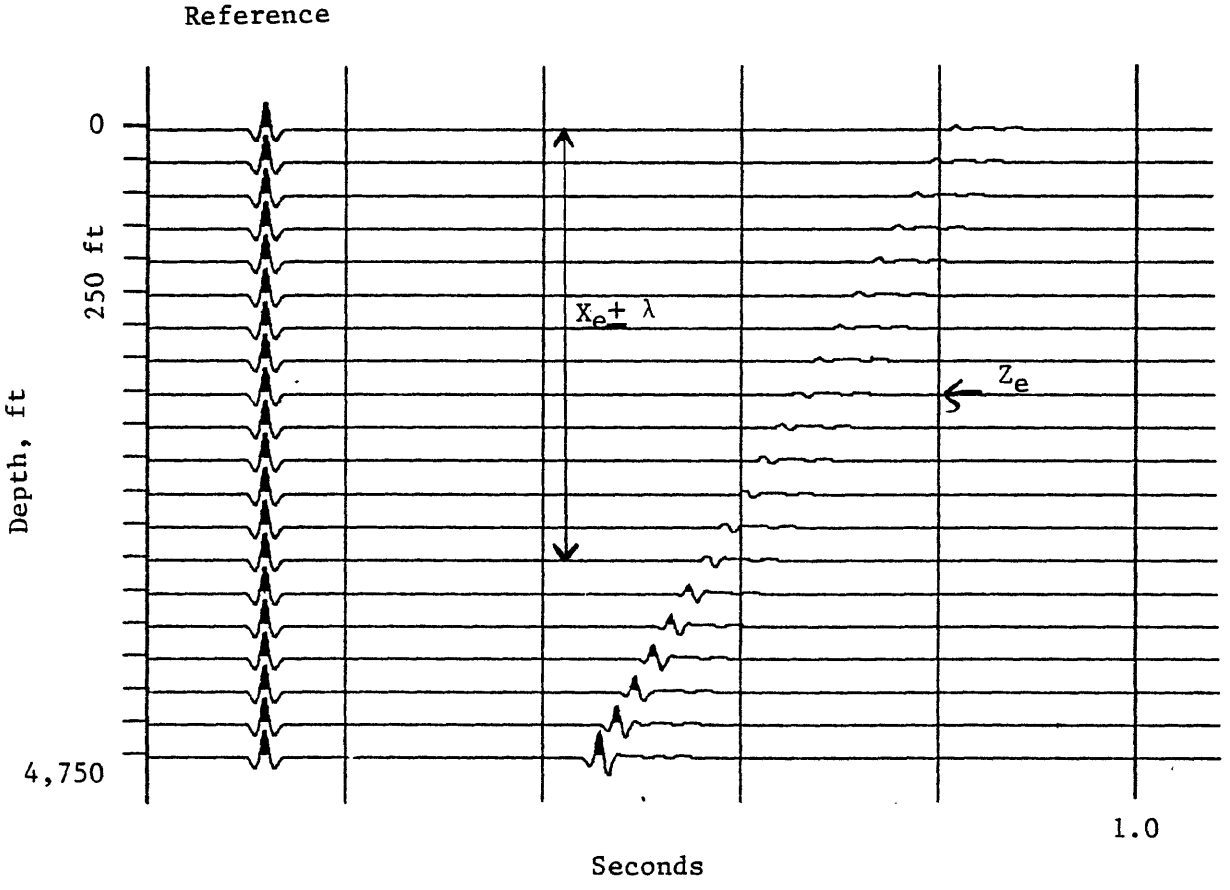

Figure 17.--Three-dimensional VSP response for the paludal model #1. Model parameters are: L = 1,500 ft, W = 300 ft, $X_o = Y_o = 0$, $\emptyset = 0^o$, Z_s = 5,000 ft, X_s = 2,000 ft, bed thickness of 30 ft, and 40 Hz Ricker wavelet.

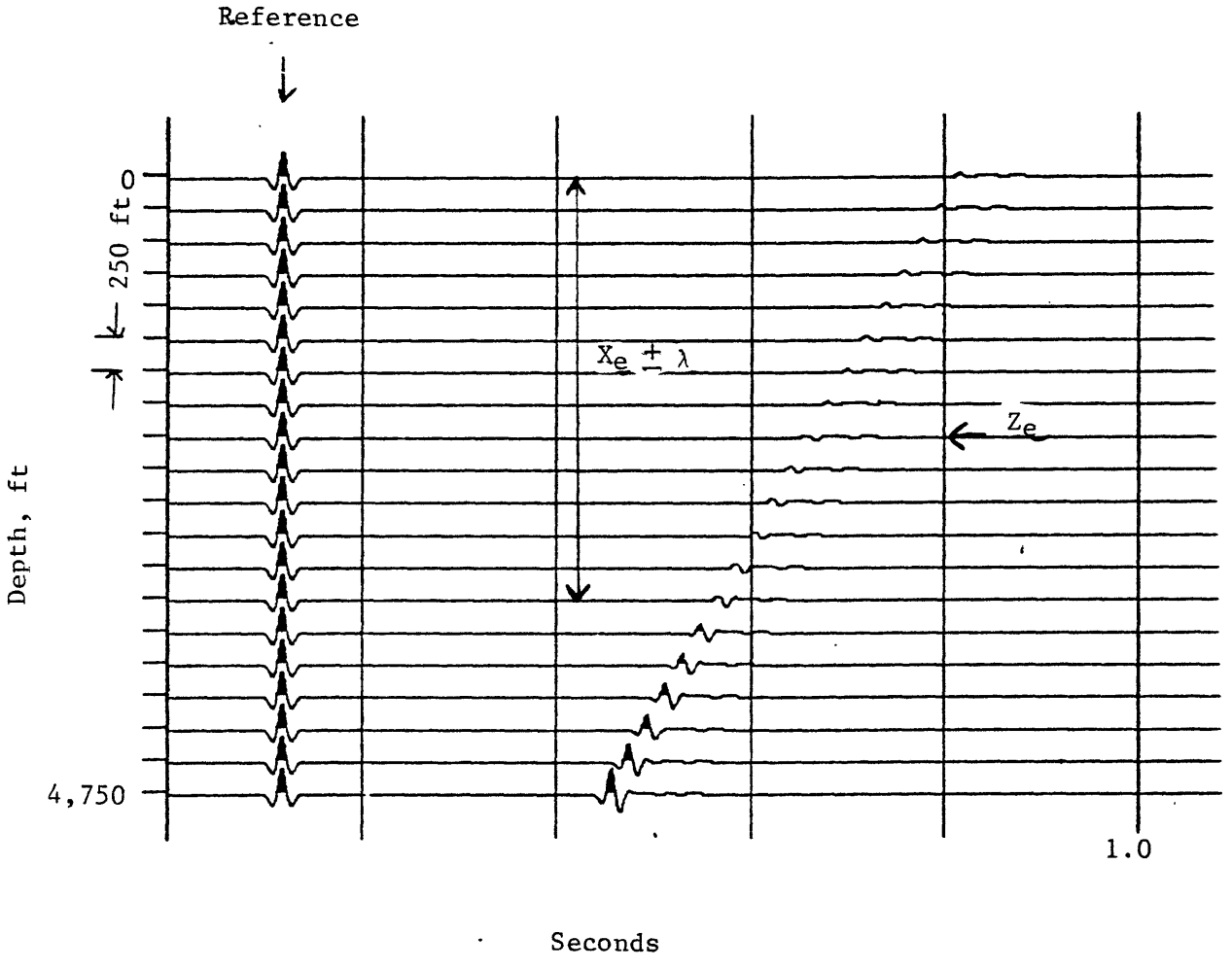

Figure 18.--Three-dimensional VSP response for the paludal model #1. Model parameters are: L = 1,500 ft, W = 300 ft, $X_o = Y_o = 0$, $\emptyset = 0^o$, Z_s = 5,000 ft, X_s = 2,000 ft, bed thickness of 100 ft, and 40 Hz Ricker wavelet.

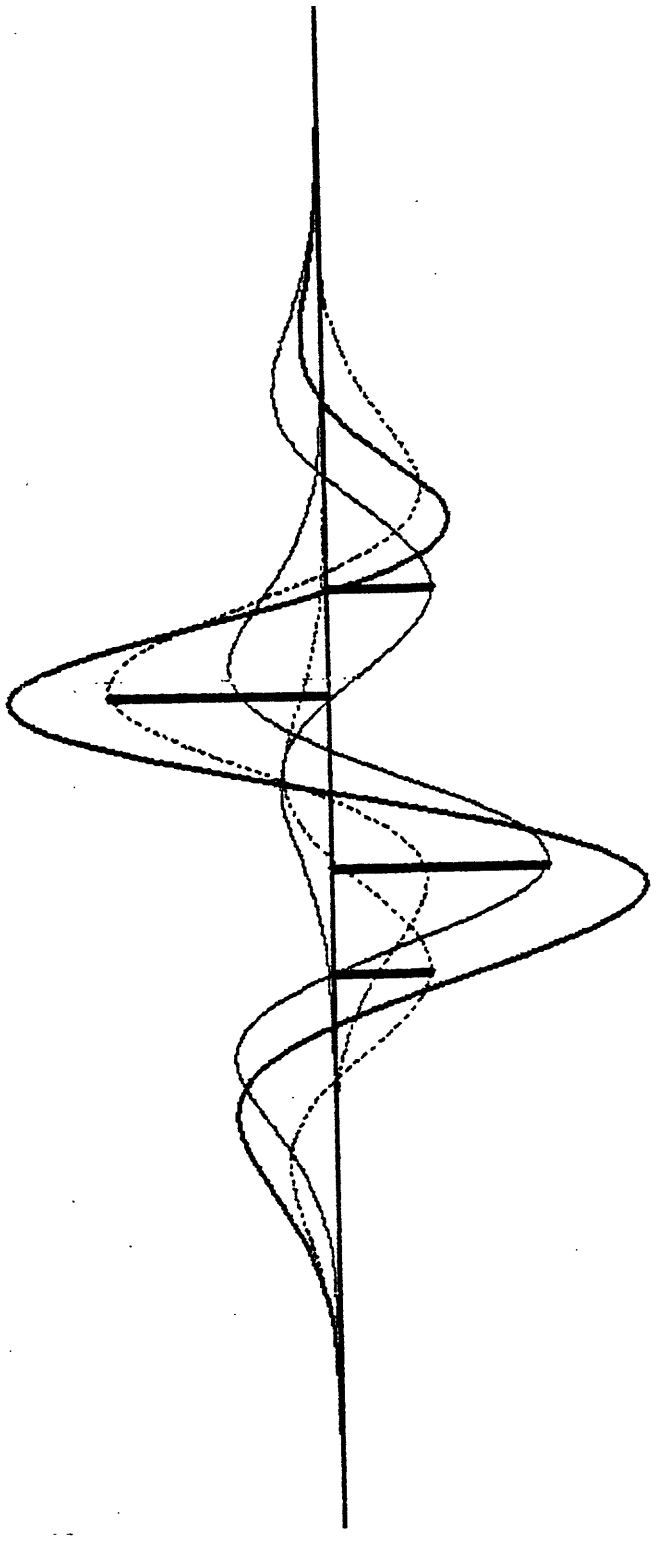

Depth, ft	Density g/cm^3	Velocity ft/msec
	ρ = 2.47	V = 10,000
5,000		
	ρ = 2.5	V = 11,000
5,030		
	ρ = 2.45	V = 9,000
5,070		
	ρ = 2.5	V = 11,000
5,100		
	ρ = 2.62	V = 11,600

Figure 19.--One-dimensional seismic response for the paludal model #2 with inner zone thickness of 40 ft. Each spike is convolved with 40 Hz Ricker wavelet which appears as lightweight solid or dashed line. The composite waveform appears as a heavy solid line.

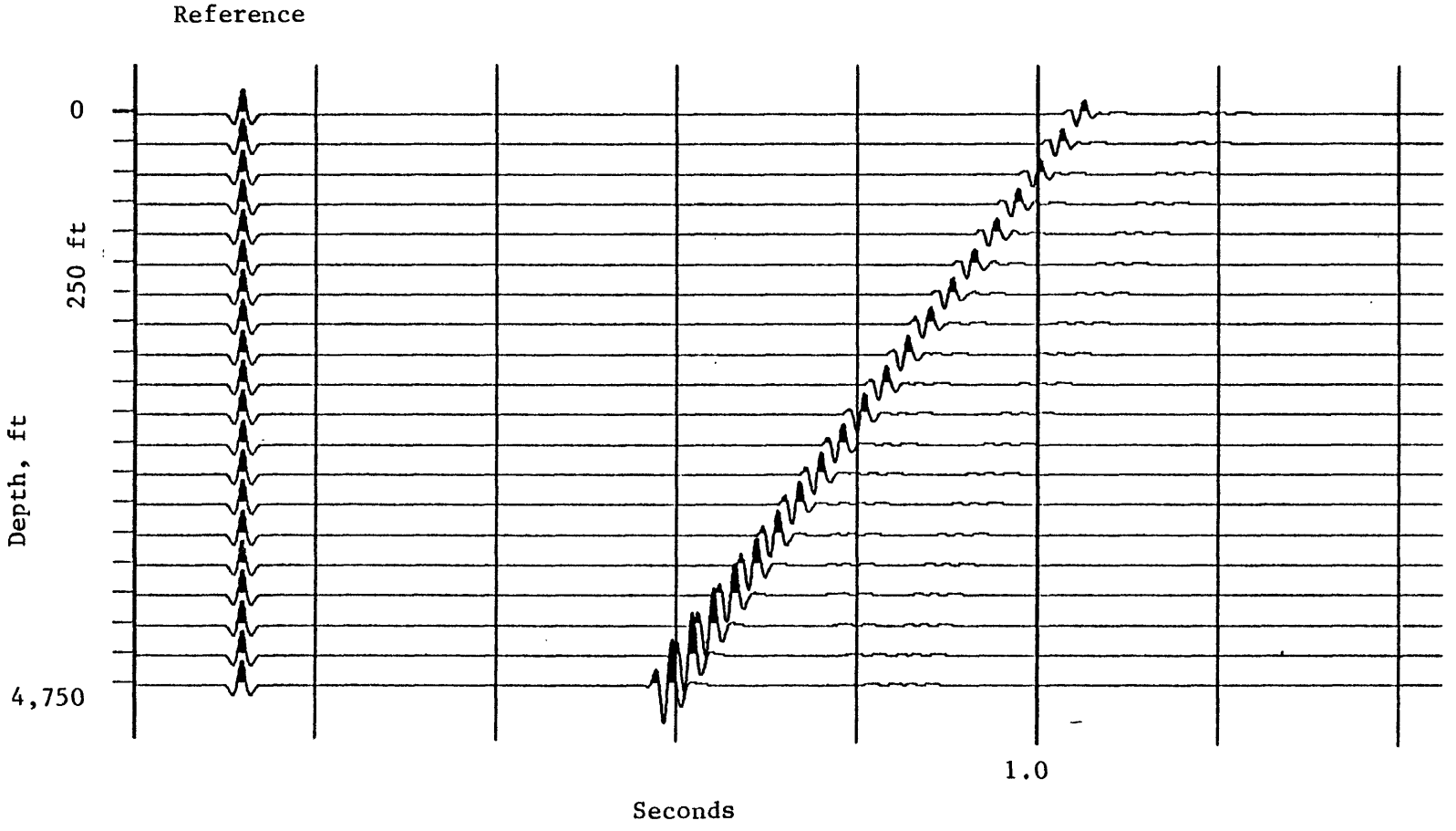

Figure 20.--Three-dimensional VSP response for the paludal model #2 with inner zone thickness of 40 ft. Model parameters are: L = 4,000 ft, W = 400 ft, $X_o = Y_o = 0$, $\emptyset = 0^o$, Z_s = 5,000 ft, X_s = 2,000 ft, and 40 Hz Ricker wavelet.

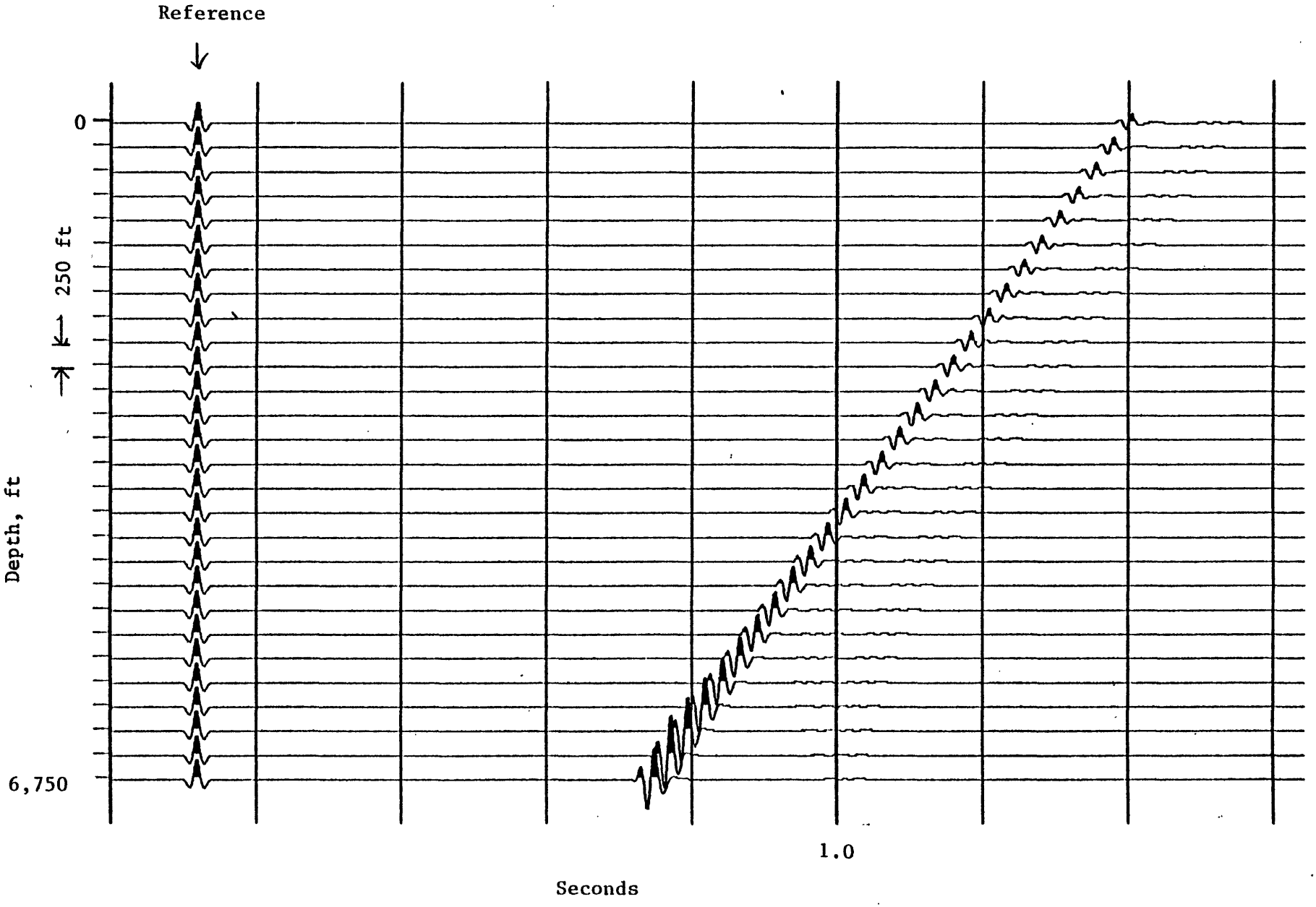

Figure 21.--Three-dimensional VSP response for the paludal model #2 with inner zone thickness of 40 ft. Model parameters are: L = 4,000 ft, W = 400 ft, $X_o = Y_o = 0$, $\emptyset = 0^o$, Z_s = 6,800 ft, X_s = 2,000 ft, and 40 Hz Ricker wavelet.

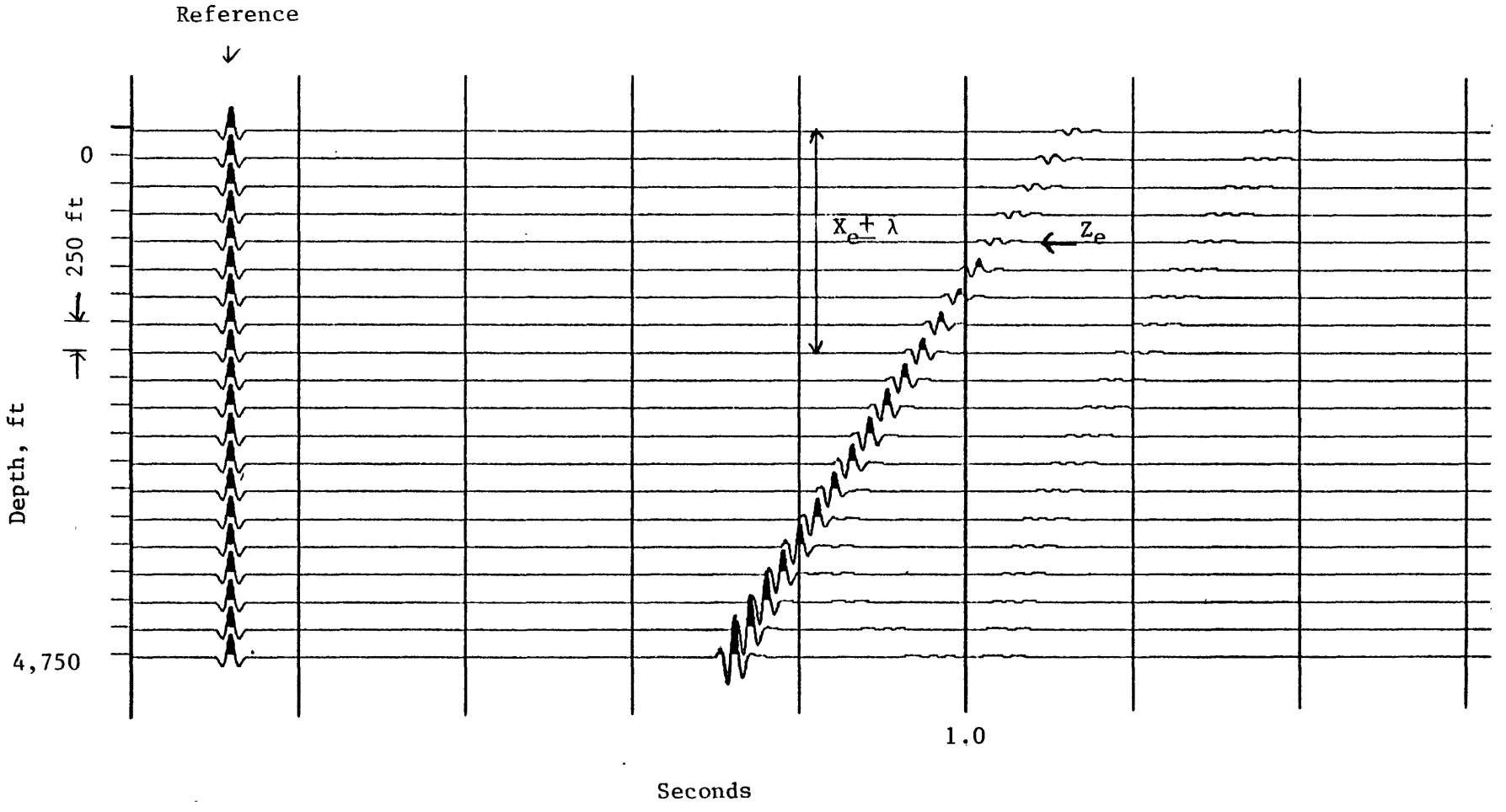

Figure 22.--Three-dimensional VSP response for the paludal model #2 with inner zone thickness of 440 ft. Model parameters are: L = 4,000 ft, W = 400 ft, $X_o = Y_o = 0$, $\emptyset = 0^o$, Z_s = 5,000 ft, X_s = 4,500 ft, and 40 Hz Ricker wavelet.

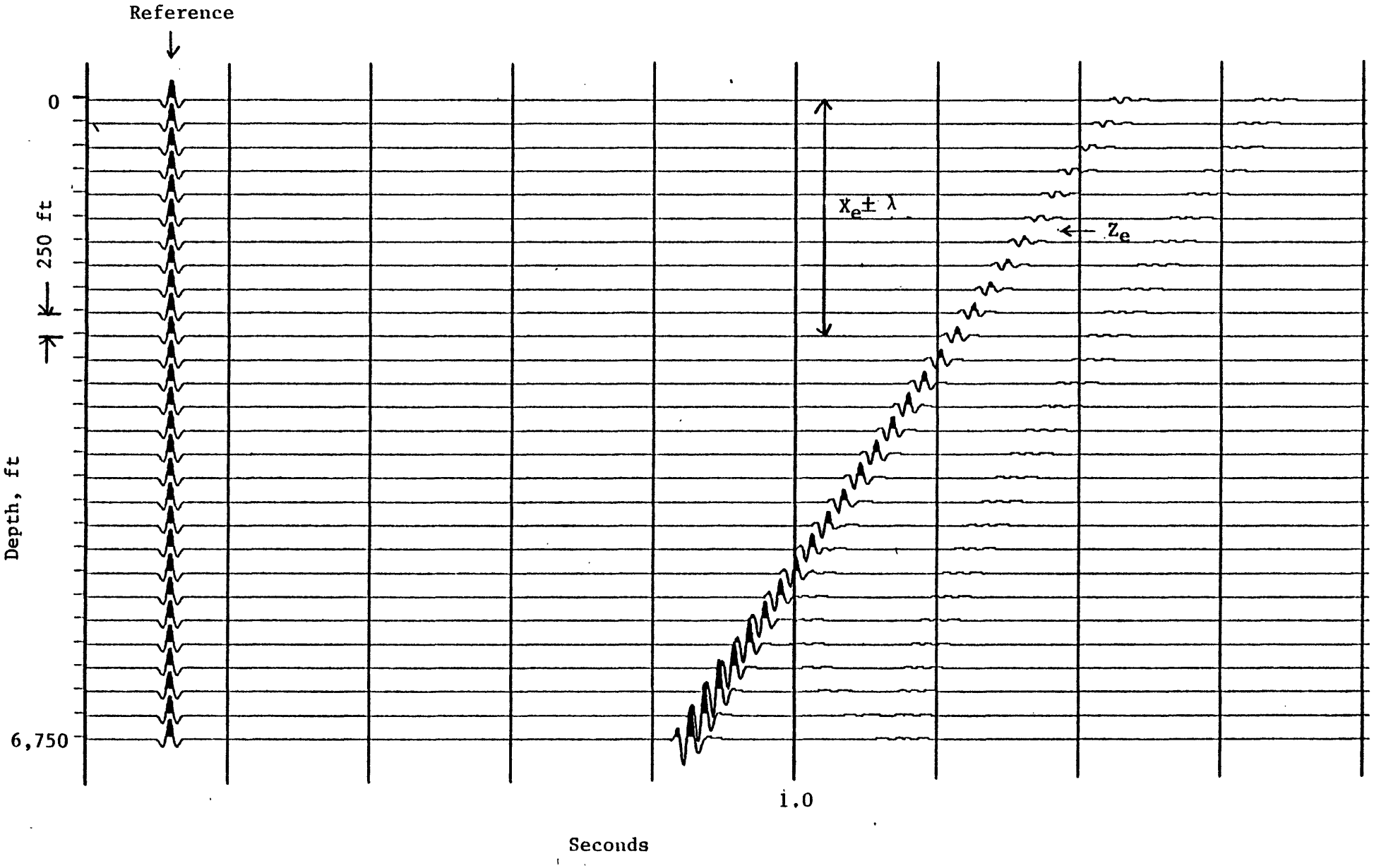

Figure 23.--Three-dimensional VSP response for the paludal model #2 with inner zone thickness of 40 ft. Model parameters are: L = 4,000 ft, W = 400 ft, $X_o = Y_o = 0$, $\emptyset = 0^o$, Z_s = 6,800 ft, X_s = 4,500 ft, and 40 Hz Ricker wavelet.

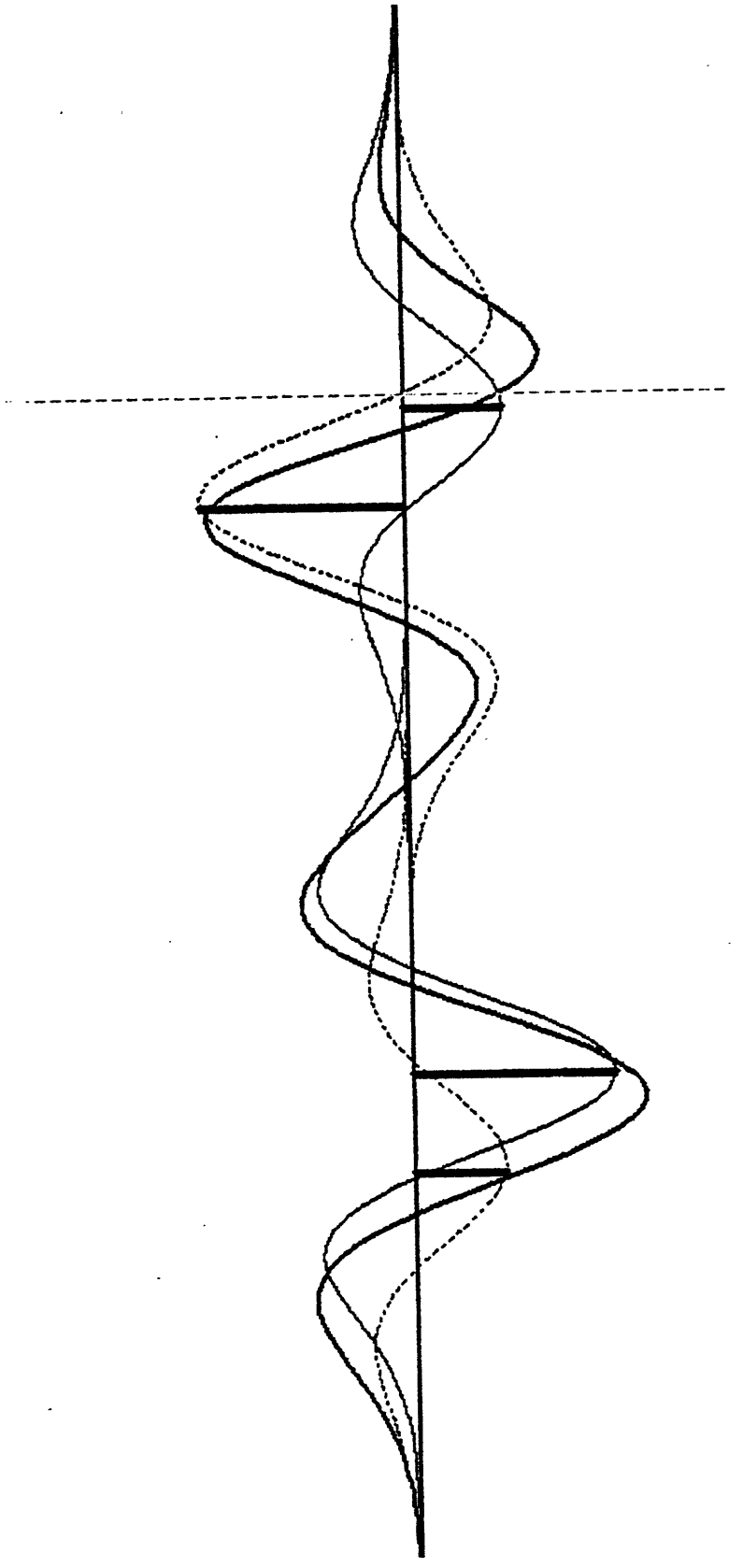

Depth, ft	Density g/cm^3	Velocity ft/msec
	ρ = 2.47	V = 10,000
5,000		
	ρ = 2.5	V = 11,000
5,030		
	ρ = 2.45	V = 9,000
5,170		
	ρ = 2.5	V = 11,000
5,200		
	ρ = 2.62	V = 11,600

Figure 24.--One-dimensional seismic response for the paludal model #2 with inner zone thickness of 140 ft. Each spike is convolved with 40 Hz Ricker wavelet which appears as lightweight solid or dashed line. The composite waveform appears as a heavy solid line.

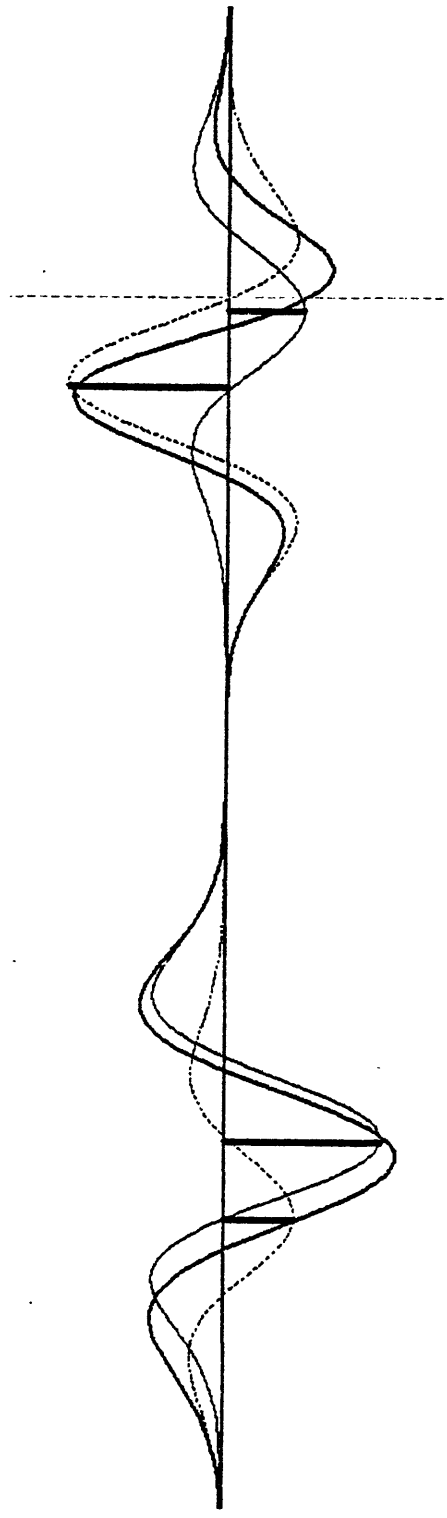

Depth, ft	Density g/cm^3	Velocity ft/msec
	ρ = 2.47	V = 10,000
5,000		
	ρ = 2.5	V = 11,000
5,030		
	ρ = 2.45	V = 9,000
5,270		
	ρ = 2.5	V = 11,000
5,300		
	ρ = 2.62	V = 11,600

Figure 25.--One-dimensional seismic response for the paludal model #2 with inner zone thickness of 240 ft. Each spike is convolved with 40 Hz Ricker wavelet which appears as lightweight solid or dashed line. The composite waveform appears as a heavy solid line.

Figure 26 shows the VSP response with X_s = 4,500 ft and the top sand body depth of 5,000 ft. The response with the top sand body depth of 6,800 ft is shown in figure 27.

In both cases, the chances of delineating two separate sand bodies are good.

Coal Zone

Figure 28 shows one-dimensional modeling of the coal zone. Figure 28a shows the response with 25 Hz Ricker wavelet. Due to the severe destructive interference of the individual coal bed, the amplitude of the total response is small. Seismic response using 40 Hz Ricker wavelet is shown in figure 28b. The overall seismic response is very similar to that of figure 28a, except that the apparent frequency content is high and the peak amplitude increases by a factor of 3. Figure 28c shows the one-dimensional model with 80 Hz Ricker wavelet. The seismic response of the upper coal beds are separated from that of the lower coal beds.

Figure 29 shows three-dimensional VSP modeling with W = 400 ft, L = 4,000 ft, X_s = 4,500 ft, and the depth of the top coal bed of 6,764 ft. The edge amplitude, amplitude at Z_e, is about 1/3 of the reference amplitude. If the exploration objective is mapping the coal bed and each coal bed is distributed uniformly in a lateral direction, the probability of delineating coal beds may be high. However, delineating sand bodies inside the coal zone appears to be impossible due to a severe interference phenomena of the coal bed on the seismic response.

In summary, based on the one- and three-dimensional seismic responses of the lenticular-type sand bodies present in the MWX well site, the sand bodies in the paludal zone have the highest potential to be detected and delineated seismically.

PROCESSING TECHNIQUE IN DELINEATING SAND BODIES

One of the problems in delineating the lateral extent of a lenticular-type sand body comes from the complicated interference phenomena owing to the diffracted events from the edges of the body. In the surface seismic profiling method, these diffracted events collapse at the apex of the diffraction curve when the data are properly migrated. Thus, the migration process increases the spatial resolution and, consequently, it is

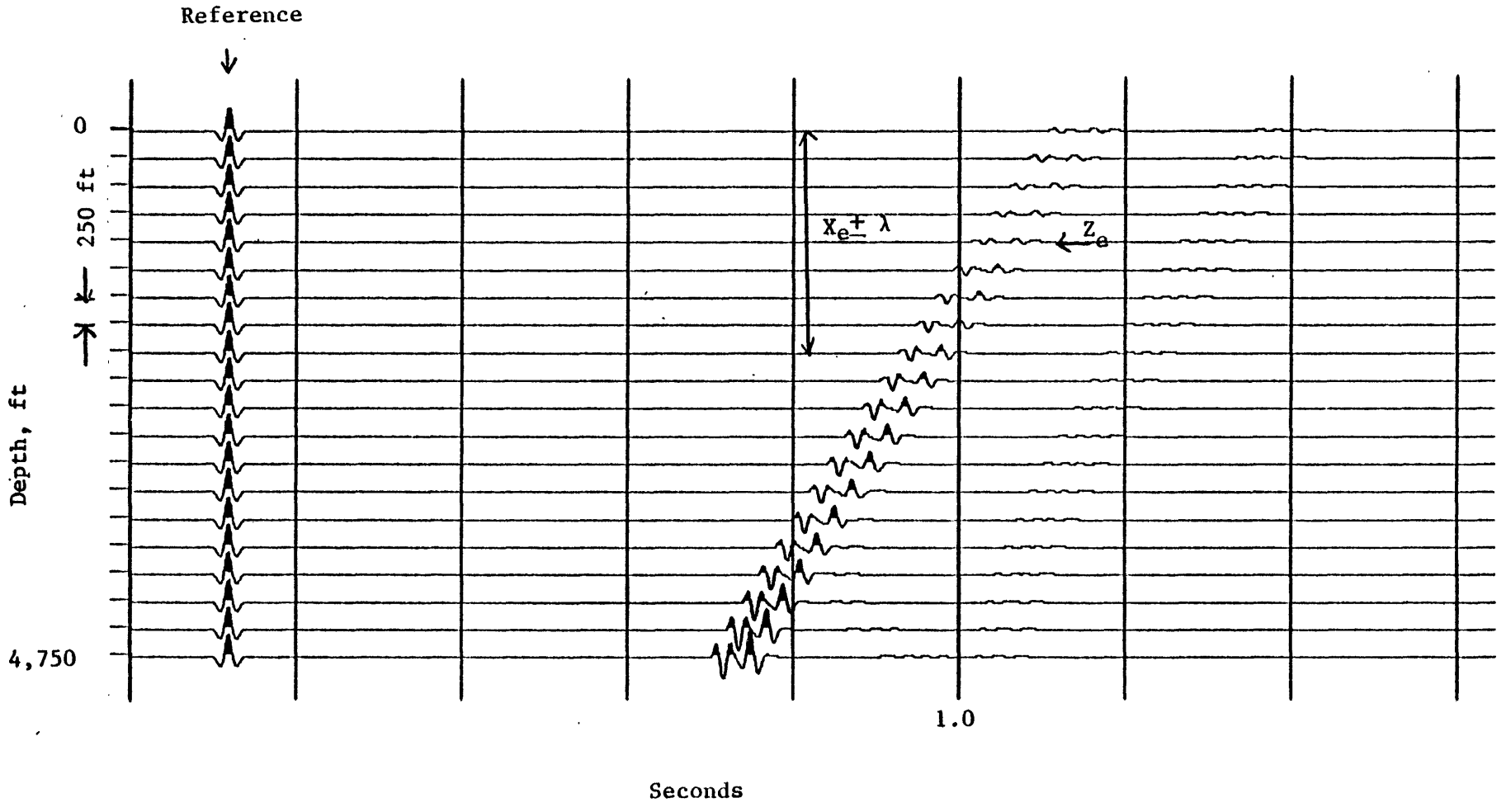

Figure 26.--Three-dimensional VSP response for the paludal model #2 with inner zone thickness of 240 ft. Model parameters are: L = 4,500 ft, W = 400 ft, $X_o = Y_o = 0$, $\emptyset = 0^o$, Z_s = 5,000 ft, X_s = 4,500 ft, and 40 Hz Ricker wavelet.

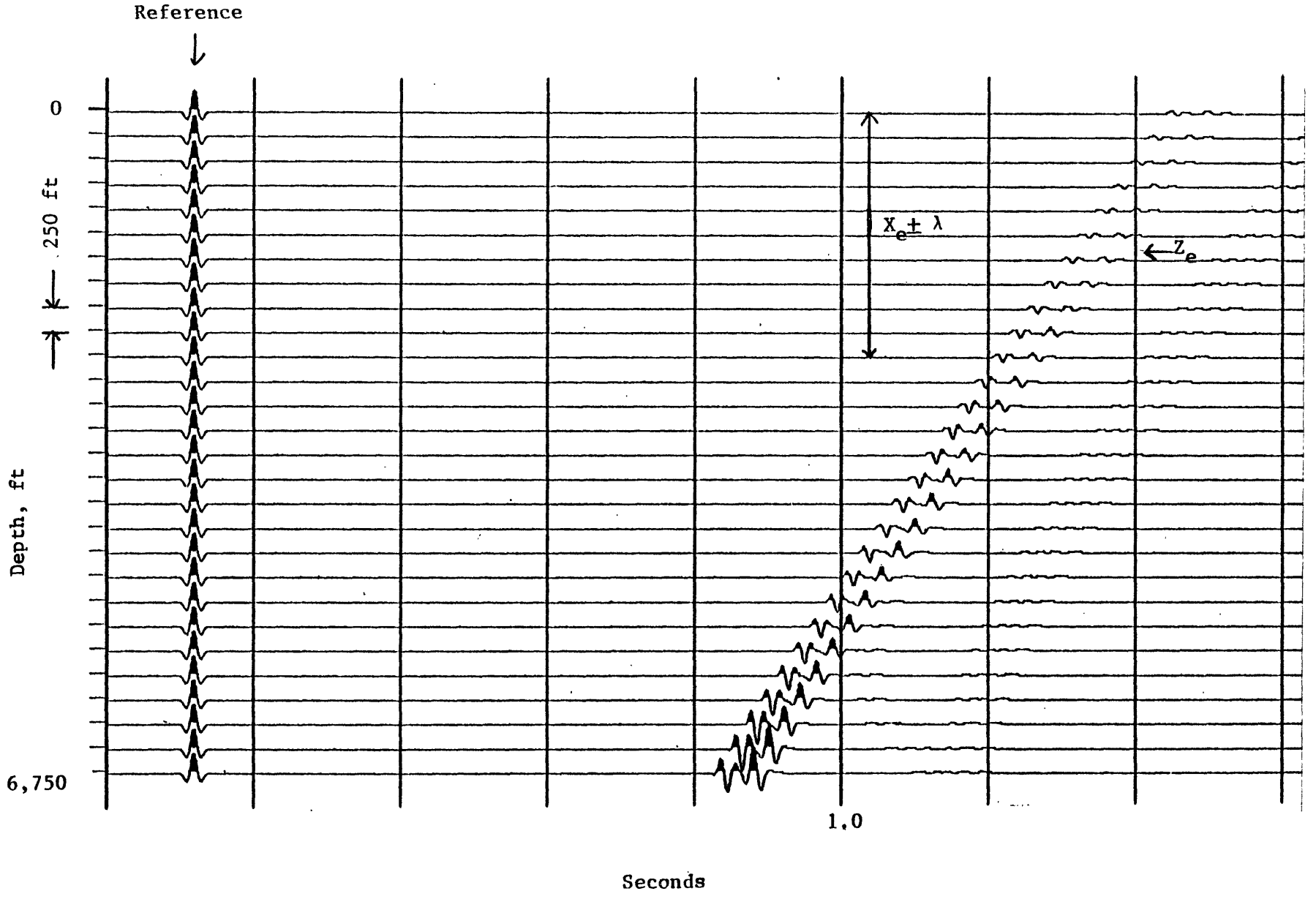

Figure 27.--Three-dimensional VSP response for the paludal model #2 with the inner zone thickness of 240 ft. Model parameters are: L = 4,000 ft, W = 400 ft, $X_o = Y_o = 0$, $\emptyset = 0^o$, Z_s = 6,800 ft, X_s = 4,500 ft, and 40 Hz Ricker wavelet.

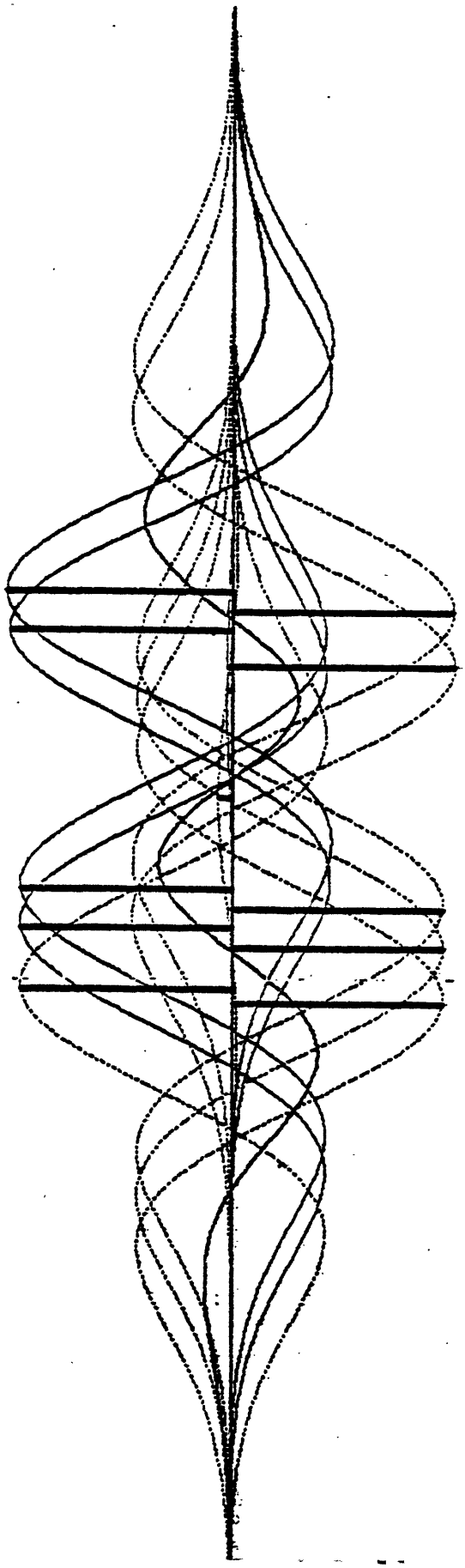

Depth, feet	Density g/cm^3	Velocity ft/msec
	ρ = 2.5	V = 12,250
6,764		
	ρ = 1.3	V = 7,200
6,770		
	ρ = 2.5	V = 12,000
6,780		
	ρ = 1.3	V = 7,200
6,790		
	ρ = 2.8	V = 10,800
6,800		
	ρ = 2.55	V = 11,600
6,850		
	ρ = 2.53	V = 11,000
6,890		
	ρ = 1.3	V = 7,200
6,896		
	ρ = 2.43	V = 11,000
6,904		
	ρ = 1.3	V = 7,200
6,910		
	ρ = 2.53	V = 11,000
6,928		
	ρ = 1.3	V = 7,200
6,932		
	ρ = 2.53	V = 11.000

Figure 28a.--One-dimensional seismic modeling for the coal beds in the paludal zone at MWX 2 well. Model parameters are shown in the figure. Using 25 Hz Ricker wavelet.

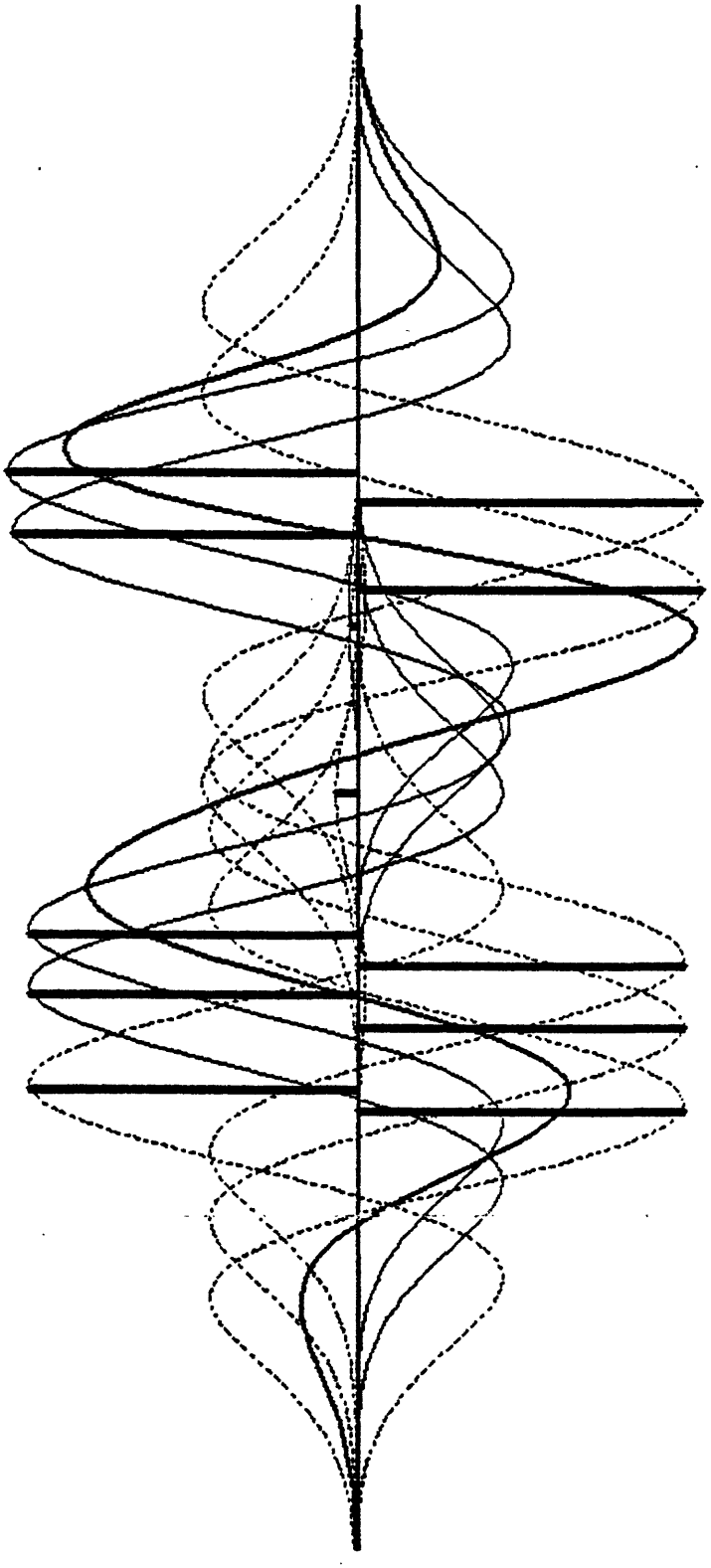

Depth, ft	Density g/cm^3	Velocity ft/msec
	ρ = 2.5	V = 12,250
6,764	ρ = 1.3	V = 7,200
6,770	ρ = 2.5	V = 12,000
6,780	ρ = 1.3	V = 7,200
6,790	ρ = 2.8	V = 10,800
6,800	ρ = 2.55	V = 11,600
6,850	ρ = 2.53	V = 11,000
6,890	ρ = 1.3	V = 7,200
6,896	ρ = 2.53	V = 11,000
6,904	ρ = 1.3	V = 7,200
6,910	ρ = 2.53	V = 11,000
6,928	ρ = 1.3	V = 7,200
6,932	ρ = 2.53	V = 11,000

Figure 28b.--Same as figure 28a. Using 40 Hz Ricker wavelet.

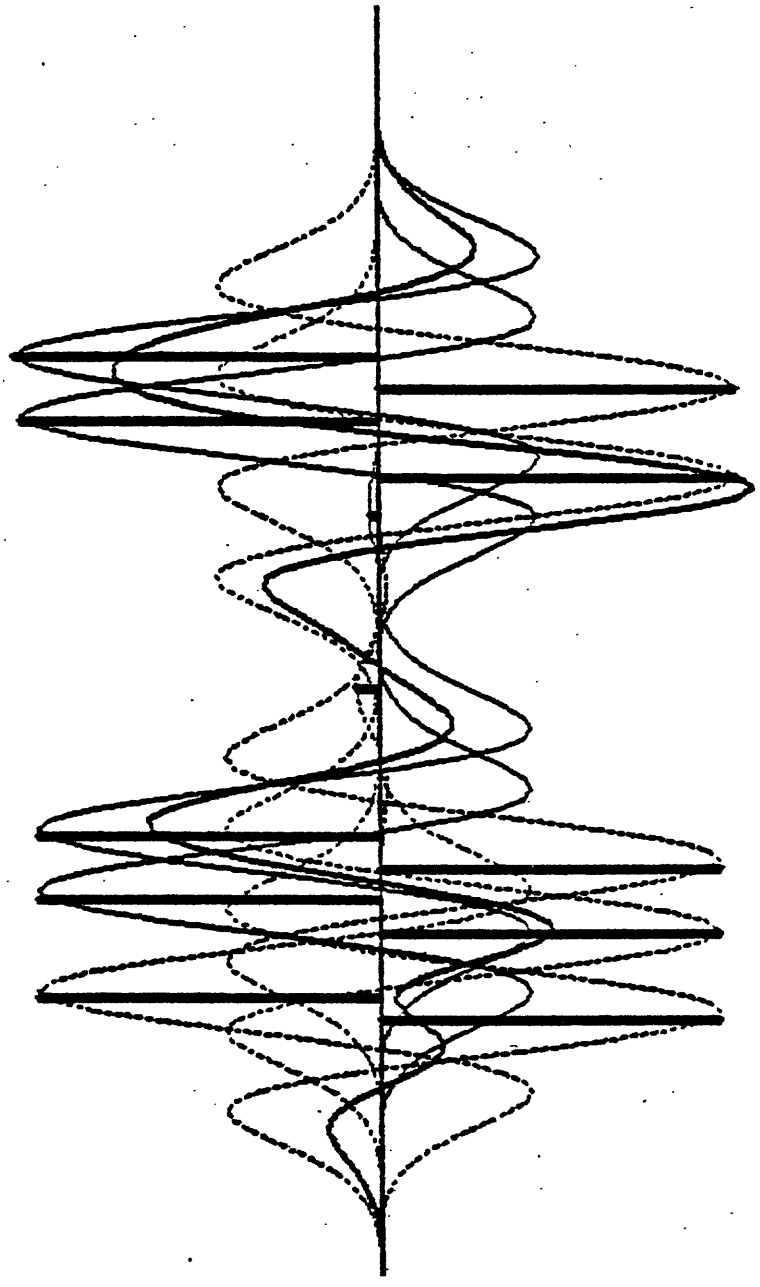

Depth, feet	Density g/cm^3	Velocity ft/msec
	ρ = 2.5	V = 12,250
6,764		
6,760	ρ = 1.3	V = 7,200
6,780	ρ = 2.5	V = 12,000
	ρ = 1.3	V = 7,200
6,790	ρ = 2.8	V = 10,800
	ρ = 2.55	V = 11,600
6,850		
	ρ = 2.53	V = 11,000
6,890		
6,896	ρ = 1.3	V = 7,200
6,904	ρ = 2.53	V = 11,000
6,910	ρ = 1.3	V = 7,200
6,928	ρ = 2.53	V = 11,000
6,932	ρ = 1.3	V = 7,200
	ρ = 2.53	V = 11,000

Figure 28c.-- Same as figure 28a. Using 80 Hz Ricker wavelet.

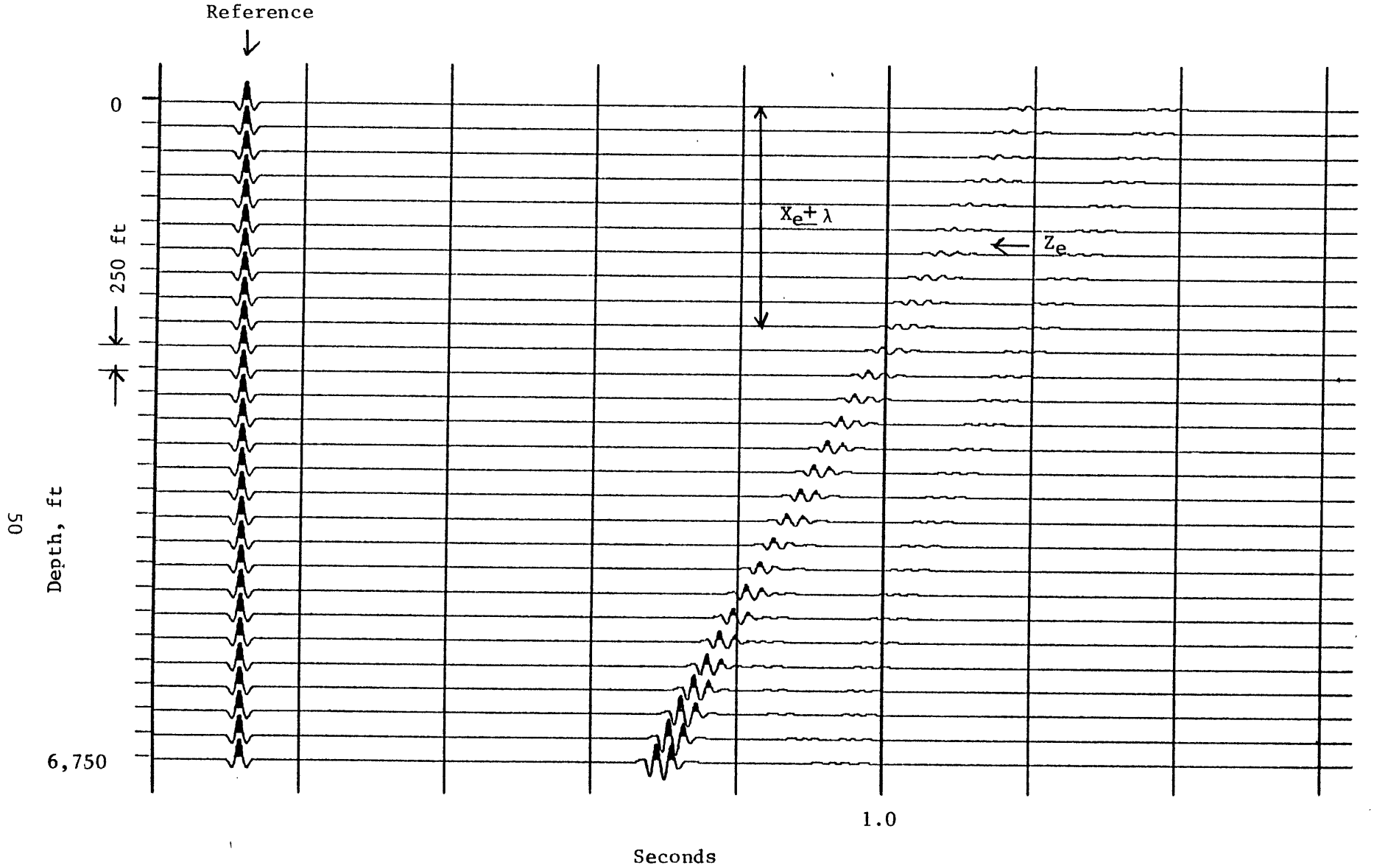

Figure 29.--Three-dimensional VSP response for the coal model. Model parameters are: L = 4,000 ft, $X_o = Y_o = 0$, $\emptyset = 0^o$, Z_s = 6,764 ft, X_s = 4,500 ft, and 40 Hz Ricker wavelet.

possible to delineate the spatial distribution of a lenticular-type sand body. On the other hand, there are no available migration techniques directly applicable to the conventional VSP data, which is defined as VSP data acquired at many depth levels in the borehole from a single surface source.

Previous model studies indicate that the spatial extent of a lenticular-type sand body in the VSP configuration manifests itself as an amplitude variation with respect to the downhole geophone location. This amplitude variation, recorded on the borehole axis, can be translated into an equivalent amplitude variation along the reflecting body by stacking the VSP data laterally away from the borehole. These laterally stacked VSP data are very similar to the stacked surface seismic profile data around the borehole. By measuring the amplitude variation along the horizontal direction away from the borehole, the spatial extent of a lenticular sand body could be determined. The same information can be extracted directly from the VSP section. However, by laterally stacking VSP data, interpretation capability of delineating the edges of a body will be enhanced. Also, laterally stacked VSP data could be migrated in order to increase the spatial resolution in certain cases.

The migration process utilizes the downward continuation of wavefields observed at the surface. If geophones or sources or both can be located very close to the target body, such as a lenticular sand body, the observed seismic section looks similar to the migrated surface data. Therefore, downward continuation of the receiver gather, or equivalently, source gather could have some potential in delineating the lenticular-type sand bodies.

In this section, laterally stacking VSP data and downward continuation of source gather or receiver gather will be discussed.

VSP Lateral Stacking

The observed reflected events on the far-offset VSP section come from the different subsurface locations. Figure 30 shows a schematic raypath diagram for a two-layered media for a far-offset VSP configuration. The reflected event observed at well-phone location Z_1 comes from the reflector H, and lateral position X_1 along the reflector; the reflected event observed at well-phone location Z_2 comes from the same reflector but the lateral position along the reflector is X_2. The procedure of VSP lateral stacking is to sum the reflected events whose lateral location from the borehole axis

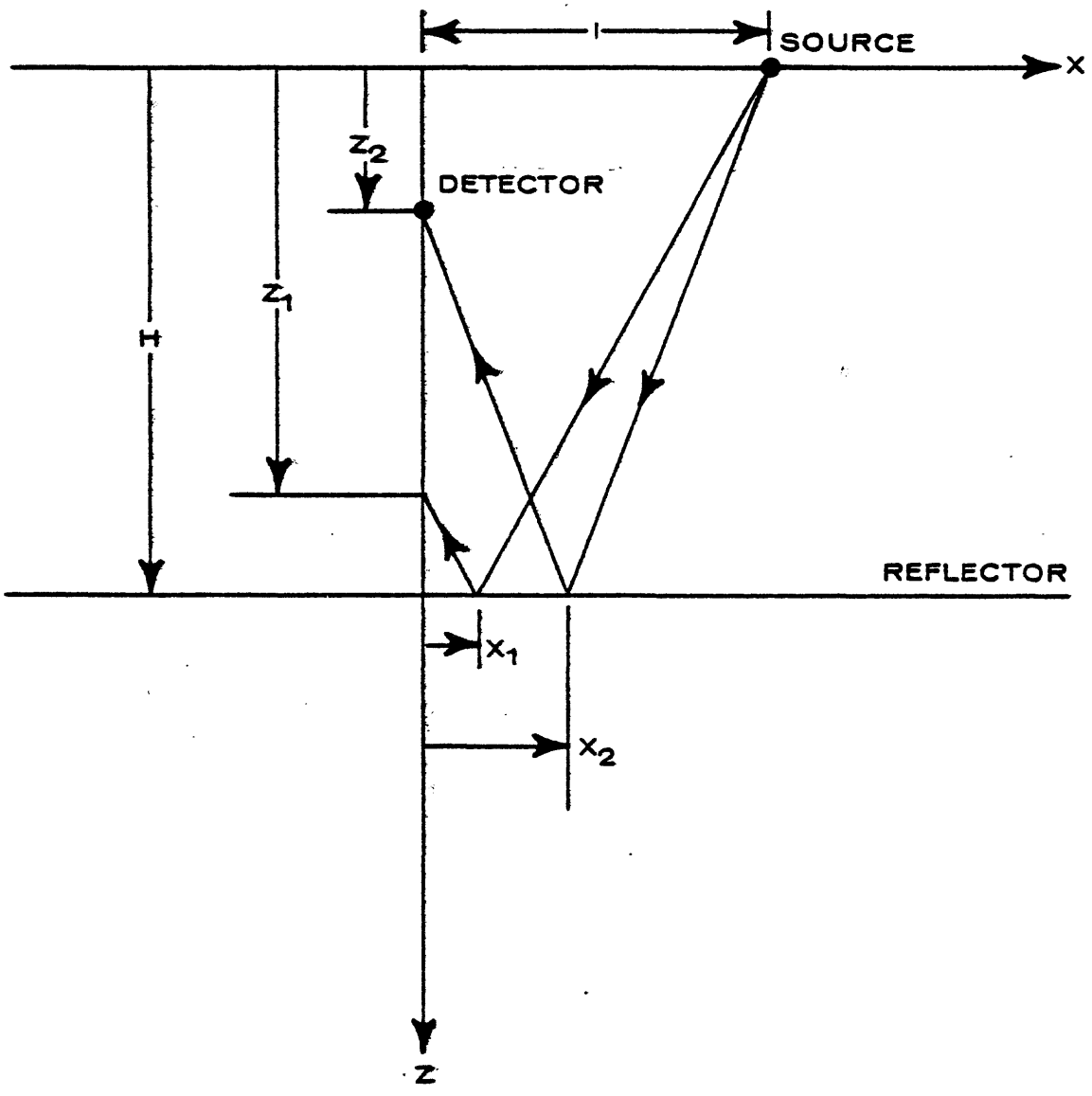

Figure 30.--Schematic ray path diagram for the lateral stacking of VSP data.

is constant and is very similar to conventional common-depth-point stacking for surface profiles. For a horizontally layered media, the maximum lateral distance away from the borehole that can be investigated from the VSP data is one-half the source offset distance.

The relation between reflector depth H, well-phone location Z, and the lateral reflection point along a reflector X_i, can be written for a homogeneous medium as:

$$Z = \frac{(\ell - 2X_i)H}{\ell - X_i} \triangleq r_i H$$

where

$$0 \leq X_i \leq \frac{\ell}{2}$$

Because common lateral reflection point X_i is a function of H and Z for a given source offset, the lateral stacking of VSP data is time and space variant.

Let $T_R(Z, X_i, H_k)$ be the reflection arrival time from the reflector depth H_k and lateral location X_i observed at geophone depth Z. Then we can write $T_R(Z, X_i, H_k)$ as

$$T_R(Z,X_i,H_k) = \frac{\sqrt{\ell^2 + (2H_k - Z)^2}}{V_{NMO}} \tag{11}$$

with V_{NMO} defined as shot-offset correction velocity (Lee, 1983).

If a source-offset correction is applied for the reflected event, Equation (11) can be written, using straight raypath assumption, as

$$T_R^o(Z,X_i,H_k) = \frac{2H_k - Z}{V_{NMO}} \tag{12}$$

$$= \frac{2Z}{v(Z/r_k)r_k} - T_D^o(Z)$$

where $T_D^o(Z)$ is the shot-offset corrected direct arrival time at geophone location Z, T_R^o is the shot-offset corrected reflection arrival time, and $\bar{v}$ is the average velocity.

Equation (12) will provide depth vs. arrival time for a given X_i. For example, when $X_i = 0$, then

$$T_R^o(Z, o, H_k) = T_D^o(Z).$$

This means that the reflected event along the first arrival time comes from the lateral location $X_i = 0$, for all the reflectors, which is intuitively correct.

Let $L^k(t)$ be the laterally stacked data in which the lateral reflection points fall within X_{k-1} and X_k. Then the VSP data can be laterally stacked by the following steps.

1) Apply source offset correction to the reflected events.

2) Let $X_k = k\Delta X$, where $\Delta X = \ell/2N$, N is the total number of laterally stacked data, and k = 1, 2---N.

3) Compute arrival time T_i^k by

$$T_i^k = \frac{2Z_i}{\bar{v}(Z_i/r_k)r_k} - T_D^o(Z_i)$$

for k = 1, 2---N

i = 1, 2---M

where Z_i is the detector location and M is the total number of depth levels.

4) Sort the VSP section whose lateral reflection points fall with X_{k-1} and X_k. Let $S_i^k(t)$ be the sorted VSP data. Then

$$S_i^k(t) = S_i(t)W_i^k(t),$$

where $W_i^k(t) = U(t - T_i^{k-1}) = U(t - T_i^k)$, $S_i(t)$ is the upgoing wave at i-th location, and U(t) is unit step function.

5) Stack CRP (common reflection point) by

$$L^k(t) = \sum_i S_i^k(t - \tau_i)F_k(t)$$

where τ_i is the static time shift to vertically align the reflected event and $F_k(t)$ is a gain function which will compensate the effect of the number of traces within the CRP gather.

Figure 31 shows the concept of VSP lateral stacking pictorially without source-offset correction. The line X_i's in this figure represent the time-space pair corresponding to Equation (12). For example, X_{i+1} curve maps the reflected events that come from the lateral location X_{i+1} away from the borehole in the direction of a source on the VSP section. If the cross-hatched portion in figure 31 is stacked, the result is equivalent to the stacking of reflected events whose lateral position away from the borehole fall within X_i and X_{i+1}.

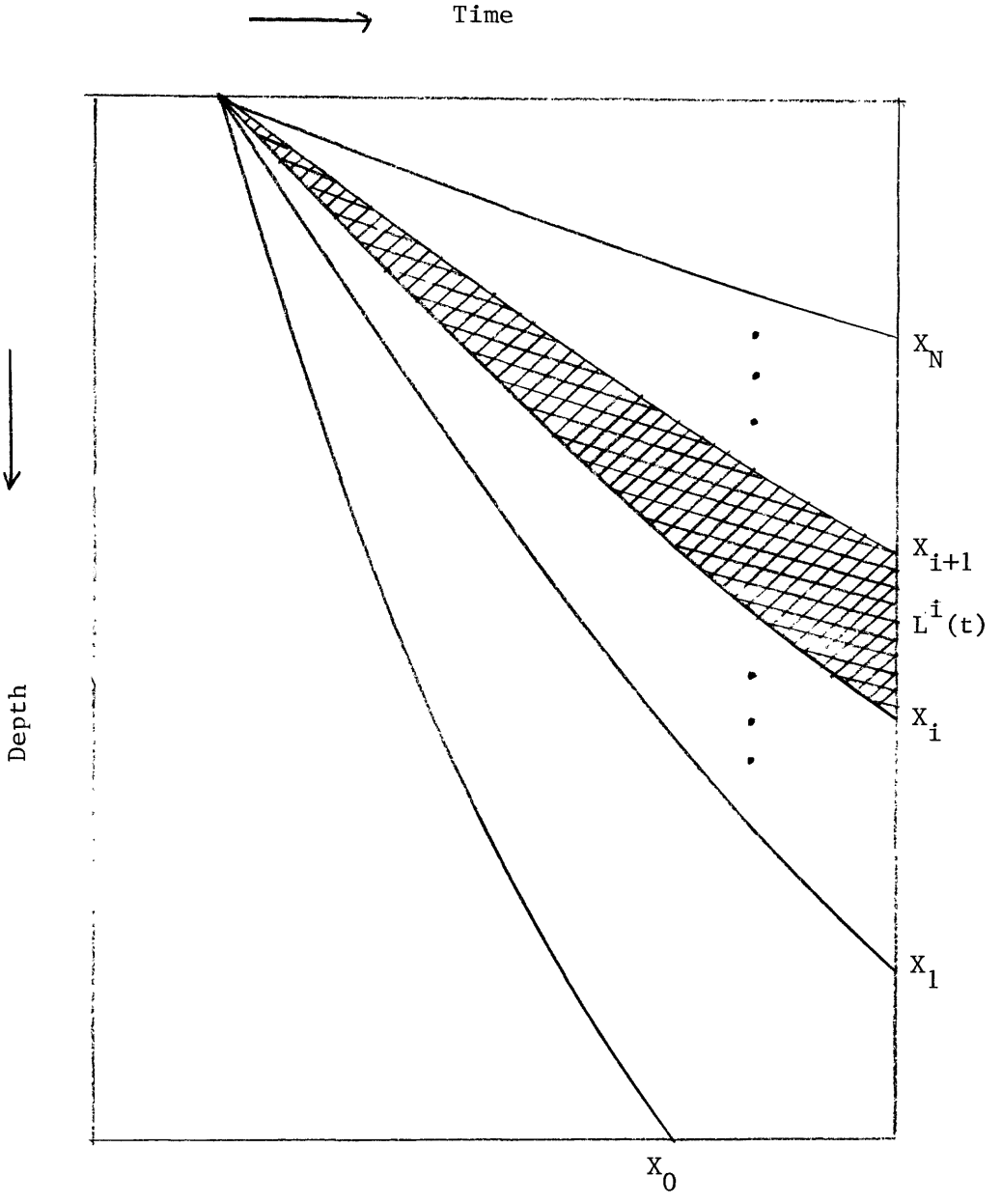

Figure 31.--Pictorial presentation of the VSP lateral stacking without source-offset correction.

Figure 32 shows an example of VSP lateral stacking applied to the real VSP data, acquired at the MWX 2 well site with source offset of 1,900 ft. The top portion of the figure is the laterally stacked VSP data with a trace interval of 25 ft, and the bottom part represents the cumulative summed (Lee, 1983) VSP data with a trace interval of 25 ft. Combining laterally and cumulatively stacked VSP data, it could be possible to interpret the spatial extents of the sand bodies and their depth distribution.

Downward Continuation

Downward continuation is a well known seismic processing technique (Claerbout, 1976; Berkhout, 1980). In this study, downward continuation is performed in the frequency-wavenumber domain assuming constant velocity.

The two-dimensional downward continuation operator in the frequency-wavenumber domain can be written as:

$$F_{d_2}(k_x, \omega) = F_{d_1}(k_x, \omega) e^{-i(\omega^2/v^2 - k_x^2)^{1/2}(d_2 - d_1)}$$

with $\frac{\omega}{v} > k_x$

where ω : angular frequency,

k_x : angular wavenumber, and

$F_{d_i}(k_x, \omega)$: two-dimensional Fourier-transformed wave field at depth d_i.

Figure 33 shows the common receiver gather from a lenticular-type sand body with 40 Hz Ricker wavelet. The model parameters are:

W = 400 ft

L = 2,000 ft

X_o = 500 ft

Y_o = 100 ft

Ø = 0.0

Z_s = 5,000 ft

V = 10,000 ft/sec.

The receiver is located on the surface and the source locations are from -3,000 ft to 3,000 ft with 100 ft intervals.

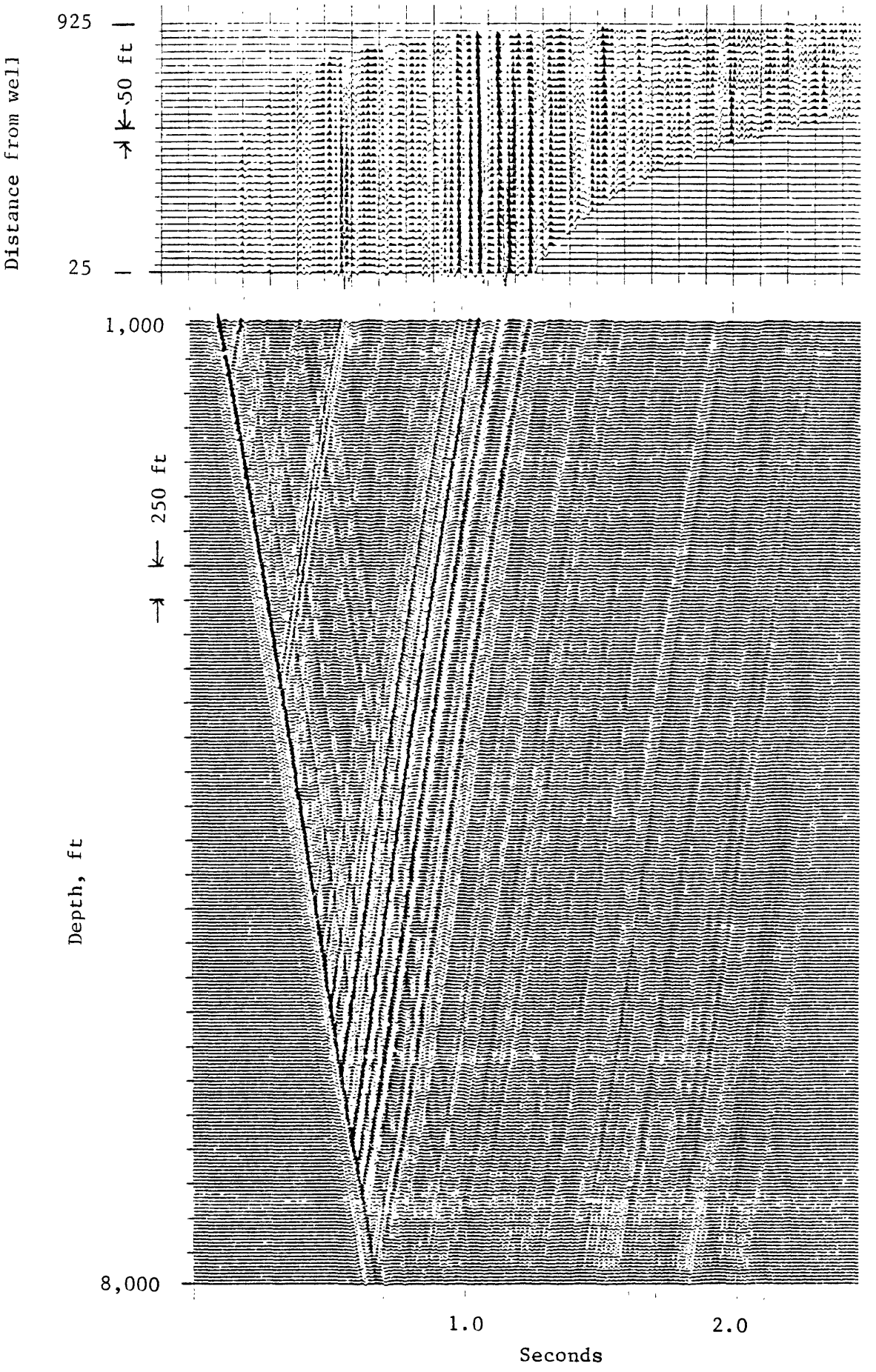

Figure 32.--An example of VSP cummulative and lateral stacking for the for-offset VSP data at MWX 2 well. Bottom: cummulative stacking; top: lateral stacking.

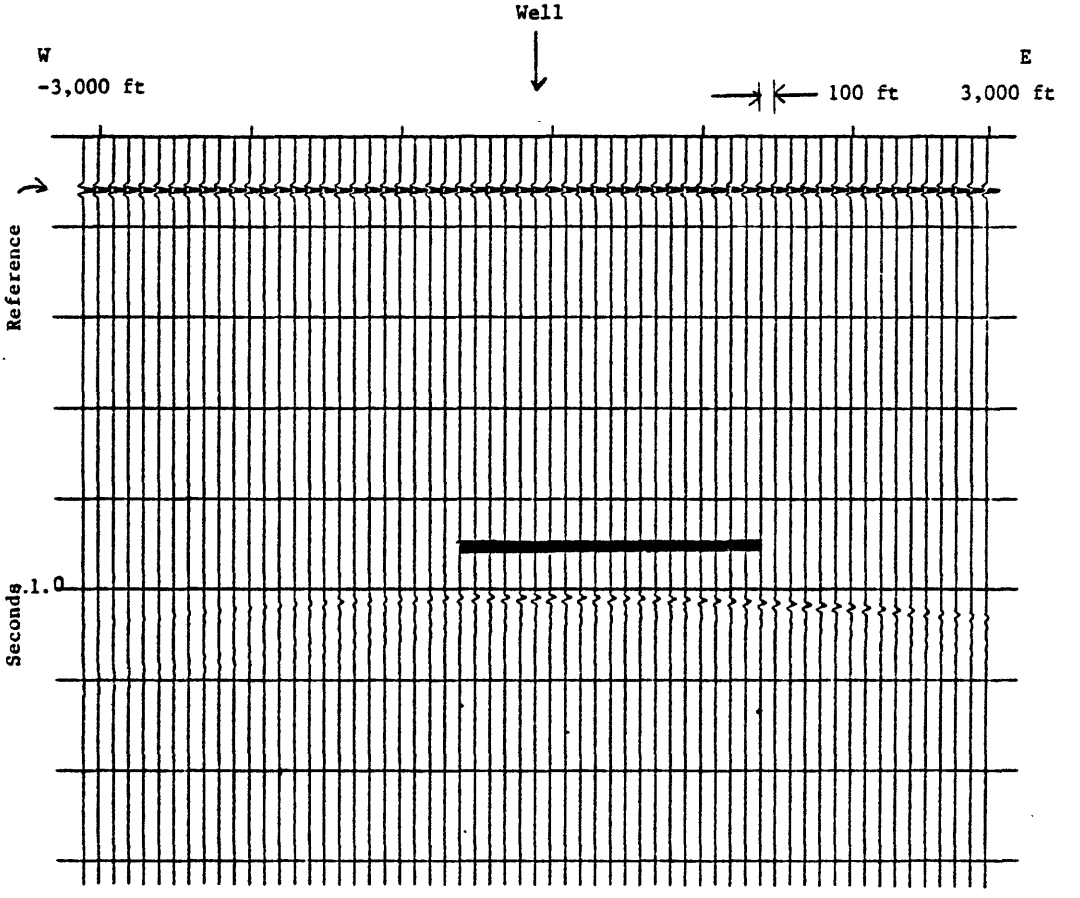

Figure 33.--Common receiver gather for the rectangular body. Model parameters are: L = 2,000 ft, W = 400 ft, X_o = 500 ft, Y_o = 150 ft, $\emptyset = 0^o$, V = 10,000 ft/sec, Z_s = 5,000 ft, X_s = -3,000 ft to 3,000 ft with 100 ft interval, and 40 Hz Ricker wavelet. Horizontal bar indicates the lateral extent of the body.

The spatial extent of the sand body in the direction of the source is represented with a horizontal bar. Because the sources and receiver are located far away from the small target, it is extremely difficult to delineate the spatial extent of the body.

The result of the downward-continued wave field is shown in figure 34. Now the edges of the lenticular sand bodies are clearly resolved in this figure.

Figure 35 shows the hypothetical results when the sources are buried at a depth of 4,900 ft, which is 100 ft above the target. Except for the high amplitude and diffraction tails, the results are very similar to the downward-continued wave field shown in figure 34.

Figure 36 shows another example of common receiver gather with 40 Hz Ricker wavelet. The model parameters are:

$W = 400$ ft

$L = 2{,}000$ ft

$X_o = 0.0$

$Y_o = 0.0$

$\emptyset = 0.0$

$Z_s = 5{,}000$ ft

$V = 10{,}000$ ft/sec.

In this case, the source line is perpendicular to the axis of the body. The downward-continued receiver gather is shown in figure 37. Both illustrations clearly indicate the advantage of downward continuation of the wave field in delineating the lenticular-type sand bodies. Some of the problems and limitations associated with this technique will be addressed in a later chapter.

FEASABILITY STUDY OF DELINEATING LENTICULAR SAND BODY

The main purpose of this study is to determine whether a lenticular-type sand body can be delineated by the VSP method. Previous model studies indicate that there is some probability of detecting and delineating lenticular sands, particularly in the paludal zone using the VSP method. However, the actual VSP data are not as simple as shown in the previous model studies. In actual VSP data, there are seismic responses from many sand bodies and many layers, interferences between strong downgoing waves and weak upgoing reflected events, and other effects excluded from the previous model studies. So extensive computer processing is required to detect and delineate sand bodies using actual VSP data.

The previous section indicates that a lateral stacking of VSP data could be used in order to delineate the spatial distribution of lenticular-type sand bodies. In order for this processing technique to be effective, multichannel velocity filtering to separate the upgoing waves from the downgoing waves and the dynamic time correction procedure to compensate for the source offset distance should be applied to the actual VSP data.

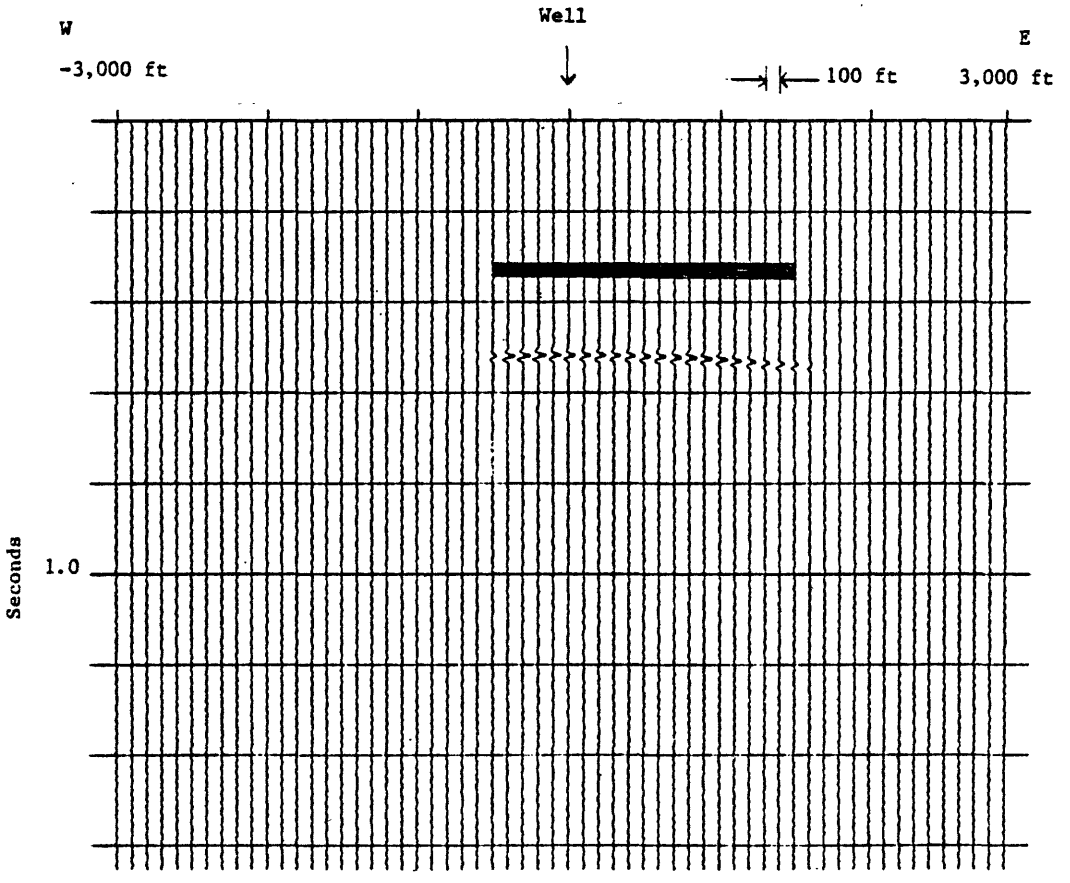

Figure 34.-- Downward continued wavefield of the data shown in figure 33.

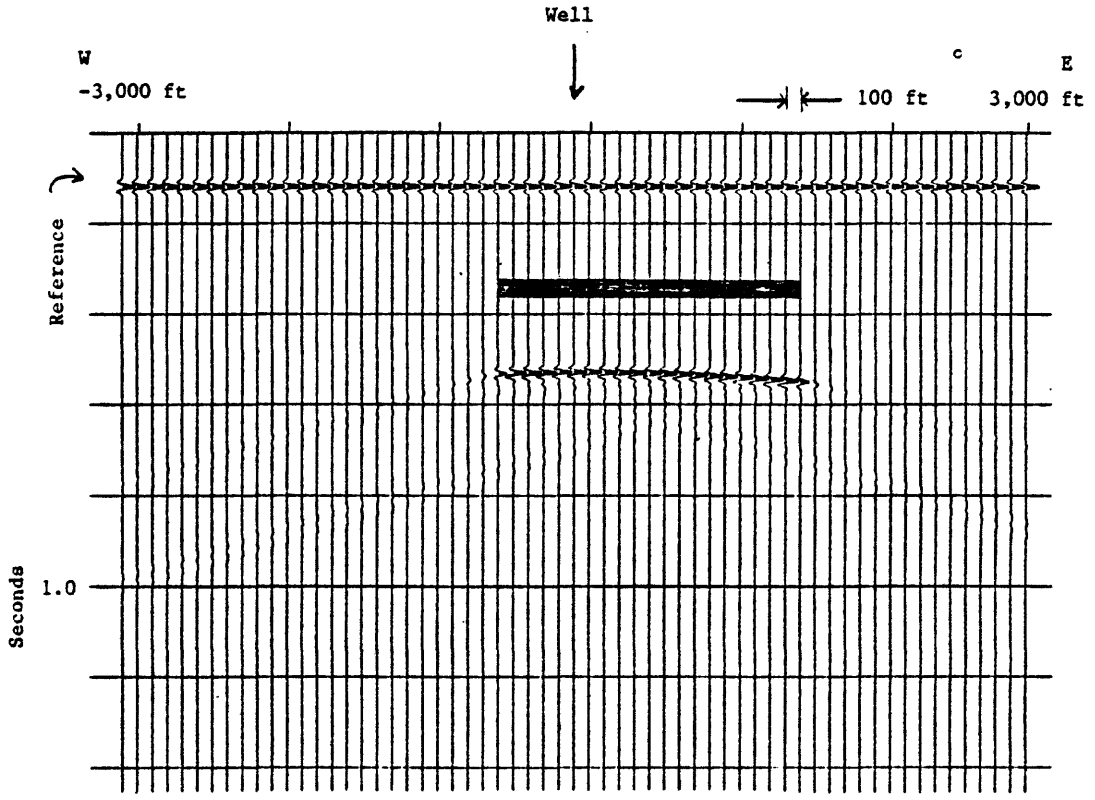

Figure 35.--Hypothetical common receiver gather for the buried source. Model parameters are identical to those of figure 33 except that the sources are located 100 ft above the rectangular body. Horizontal bar indicates the lateral extent of the body.

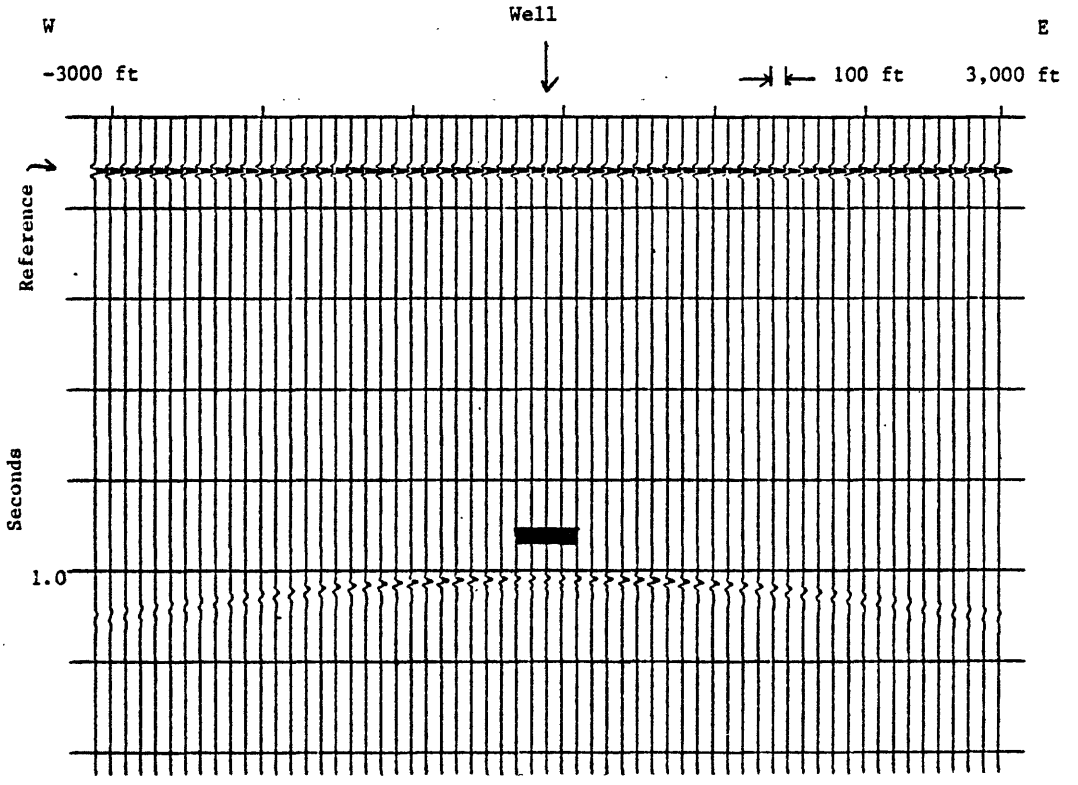

Figure 36.--Common receiver gather for the rectangular body. Model parameters are: L = 2,000 ft, W = 400 ft, $X_o = Y_o = 0$, $\emptyset = 0^o$, $Z_s = Z_d$ = 5,000 ft, and 40 Hz Ricker wavelet. The sources are located from -3,000 ft to 3,000 ft with 100 ft interval perpendicular to the axis of the body. Horizontal bar indicates the lateral extent of the body.

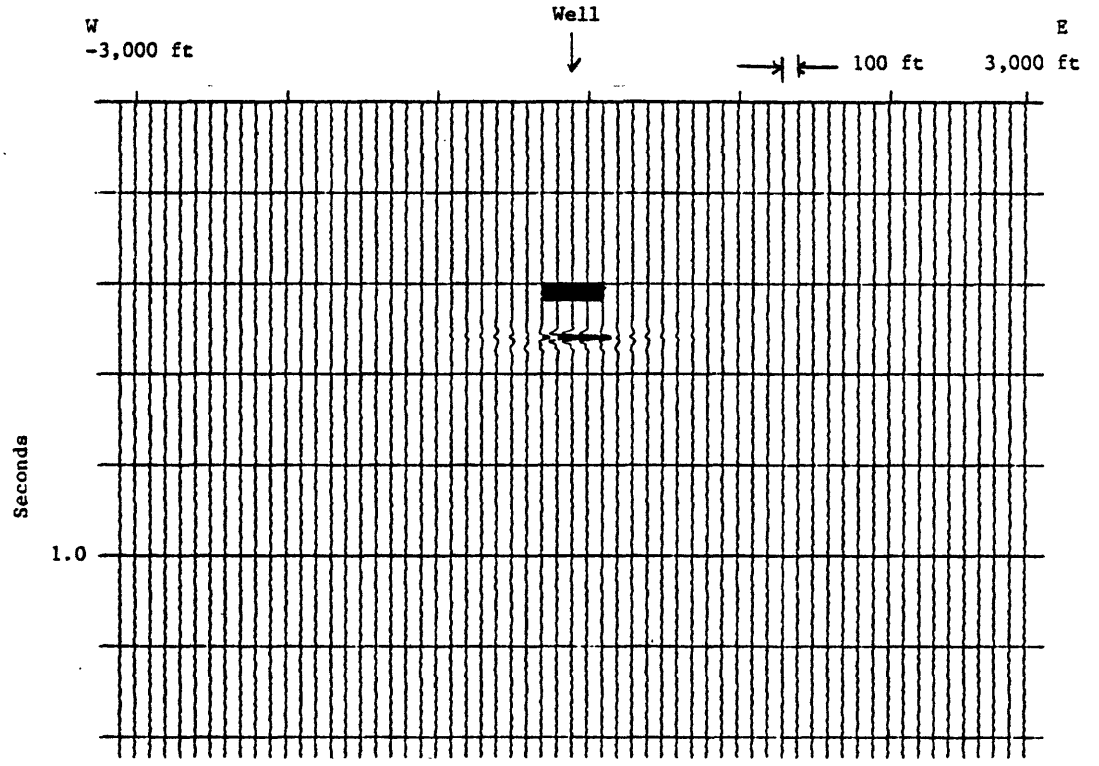

Figure 37.--Downward continued wavefield of the data shown in figure 36. Horizontal bar indicates the lateral extent of the body.

To analyze the effect of the main processing steps (multichannel filtering, dynamic time correction, and VSP lateral stacking) on mapping the lateral extent of the sand body, the model parameters shown in figure 38 were used.

The velocity of the model is constant with 10,000 ft/sec. Four infinitely extended layers and three lenticular sand bodies (A, B, and C) are included in the model. In the left column of figure 38, the depths of the reflecting bodies and reflection coefficients at the interface are shown. The reflection coefficient of sand body A is similar to that of the coastal model and the reflection coefficients of sand bodies B and C are similar to that of the paludal model. The bottom two layers are simulated as a coal bed with a reflection coefficient of 0.53.

The axis of the lenticular sand bodies is in an E-W direction, and sand body A is symmetrically located at the borehole; the center of sand body B is 750 ft shifted to the west; and the center of sand body C is shifted 750 ft to the east. A depth increment of 25 ft from 6,200 ft to 1,000 ft and 40 Hz Ricker wavelet was used to generate the VSP models. Figure 39a shows the zero-offset VSP modeling. Constant-amplitude upgoing events (moveout to the right) are responses from the infinite extended layer, and variable amplitude events are the seismic responses from the finitely extended sand bodies.

The amplitudes of the downgoing waves shown in this section are reduced by a factor of 5 in order to see the weak upgoing waves in the same plot.

Figure 39b shows the zero-offset VSP modeling under the assumption that the areal extent of the sand bodies are infinite. Comparing figure 39a with figure 39b, the effect of small lenticular-type bodies on the VSP section can be clearly observed.

Zero-offset VSP data will provide accurate depth locations of a reflecting horizon of either an infinitely extended or a finitely extended body by applying the cumulative summation technique of VSP processing. Zero-offset VSP data also will provide some information about the size of the body, actually the width of the lenticular-type sand body, analyzing the amplitude variation with respect to the downhole geophone location.

Figure 40 shows VSP modeling when the source offset is 3,000 ft in the east direction. The responses of sand body A are very similar to those from the zero-offset data. However, the seismic responses of the sand body B are quite different from those of the zero-offset data. The amplitude responses of sand body B above 5,000 ft are almost negligible.

Figure 41 shows the VSP model when the source offset is 3,000 ft in the west direction. Now the amplitude responses of sand body C are neglible when the detector is above 5,000 ft.

The differences in the amplitude responses with respect to the source locations will provide information about the edges of the sand bodies.

To apply the lateral stacking procedure effectively to the data shown in figures 40 and 41, multichannel velocity filtering and dynamic time correction should be applied. Figure 42 shows the VSP data shown in figure 40 after velocity filtering, dynamic time correction, and remergence of downgoing and upgoing waves. Arrival times of the seismic events shown in figure 42 accurately match with the zero-offset VSP data shown in figure 38a, but the amplitude variations due to the source offset distance are preserved. Processing noise due to the edge effect of multichannel velocity filtering is clearly shown in the upper part of figure 42.

Using dynamic time-corrected upgoing waves, the lateral stacking procedure is applied to the data shown in figures 40 and 41. The result of lateral stacking is shown in figure 43. The maximum investigation distance

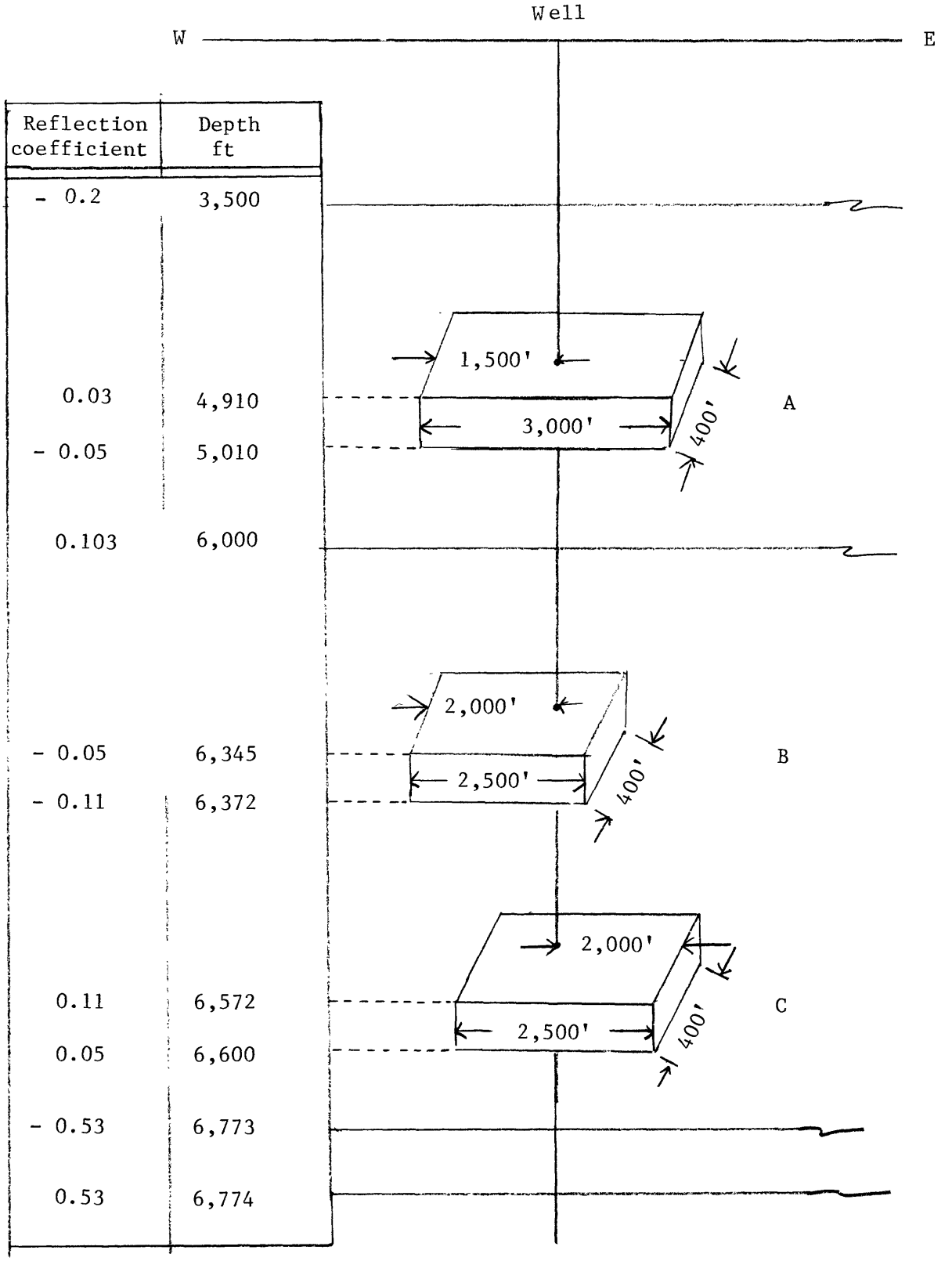

Figure 38.--Model parameters for the composite lenticular-type sand bodies.

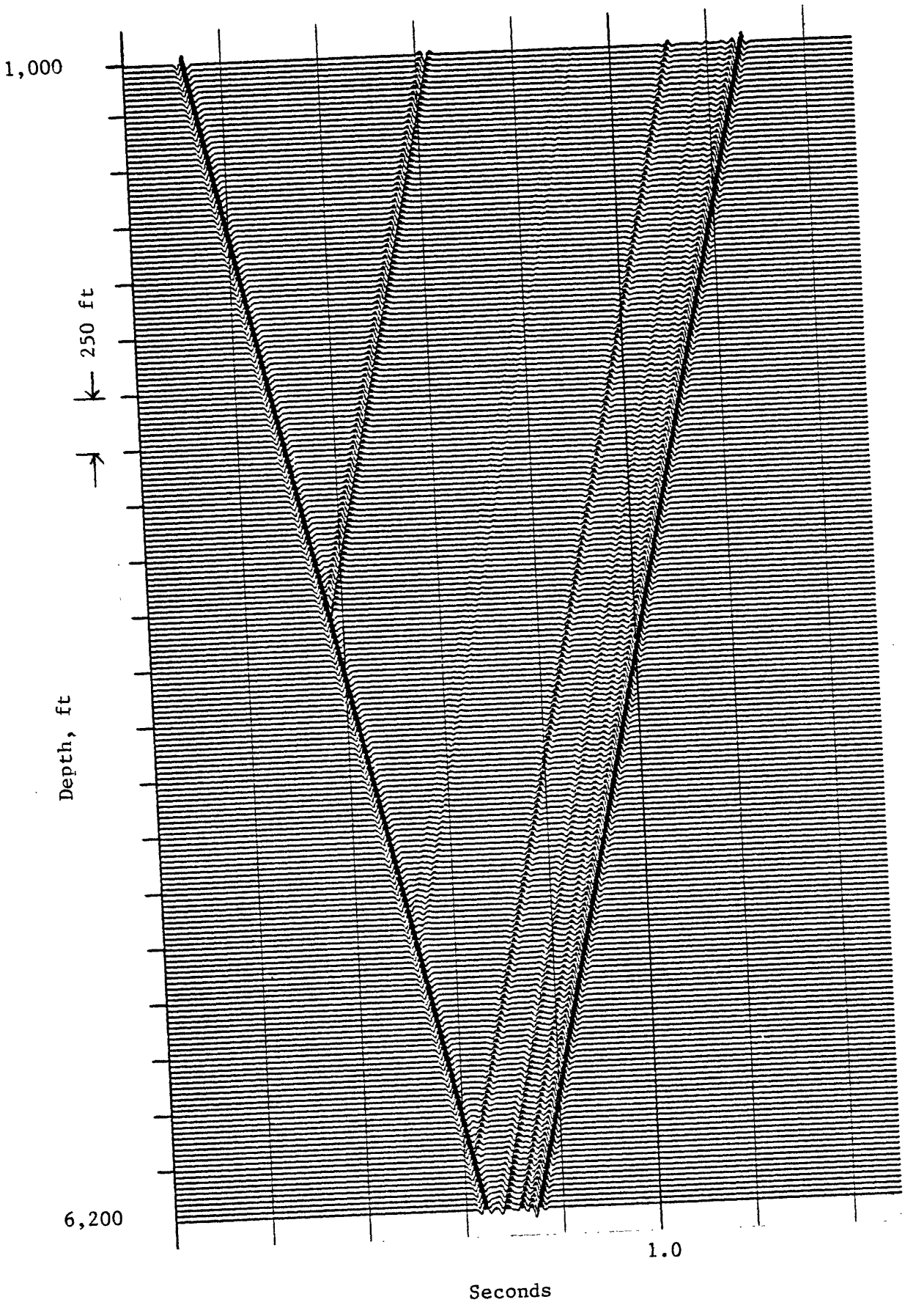

Figure 39a.--Three-dimensional VSP response for the model shown in figure 38. The source offset is zero and 40 Hz Ricker wavelet was used.

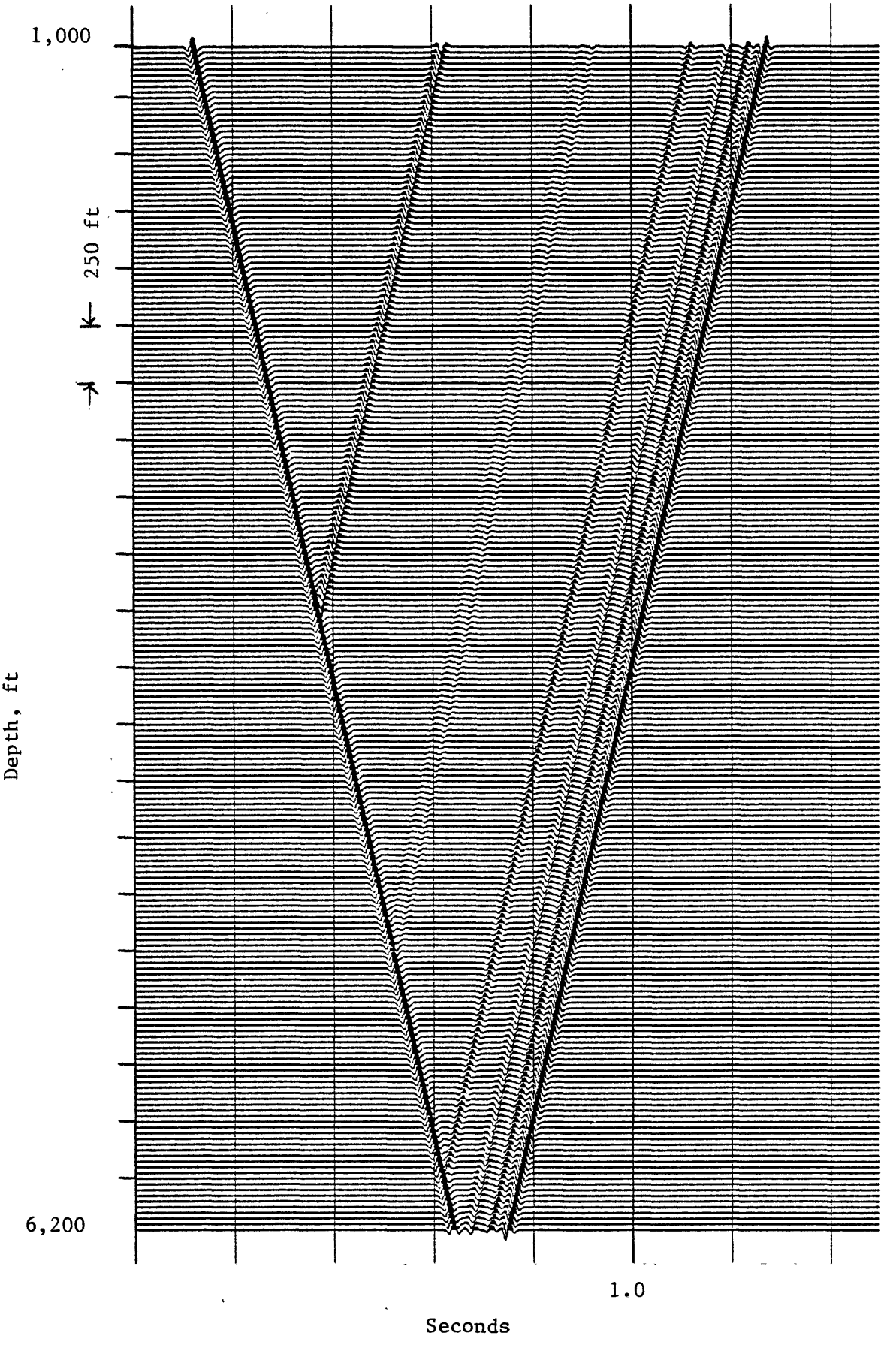

Figure 39b.--Same as figure 39a, with the assumption that the sand bodies are extended infinitely. The source offset is zero and 40 Hz Ricker wavelet was used.

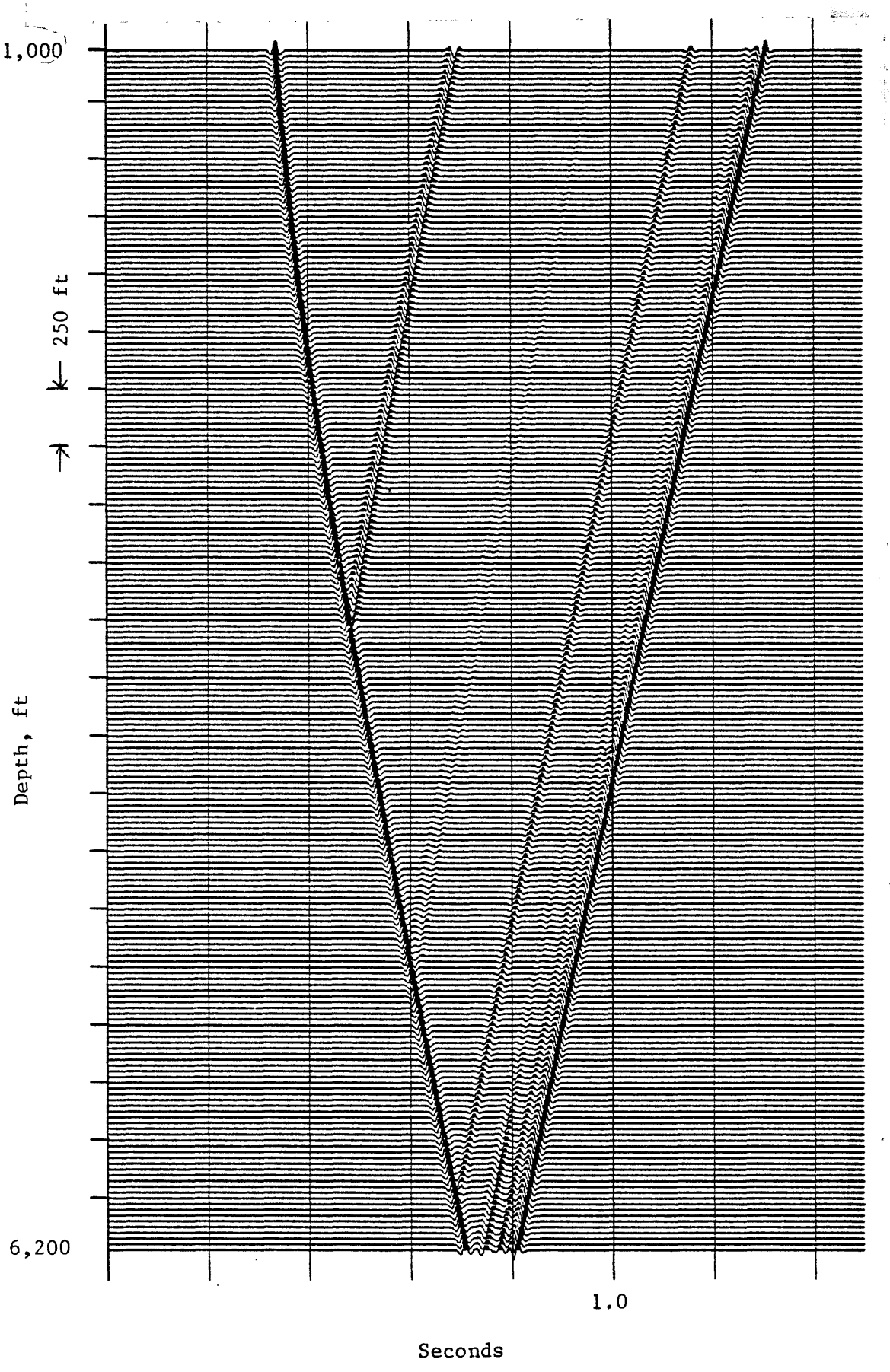

Figure 40.--Three-dimensional VSP response for the model shown in figure 38. The source is located 3,000 ft away from the well to the east.

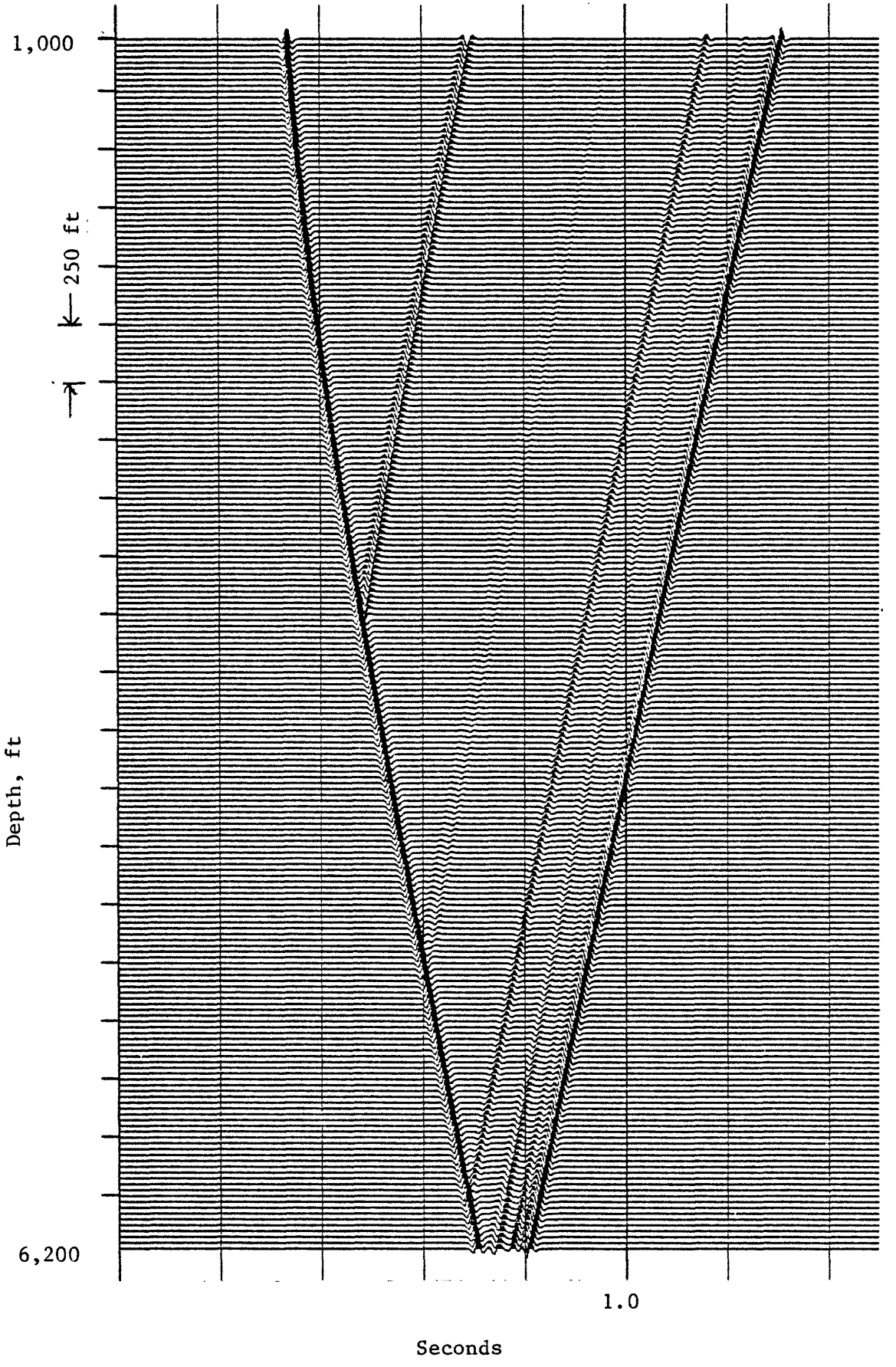

Figure 41.--Three-dimensional VSP response for the model shown in figure 38. The source is located 3,000 ft away from the well to the west.

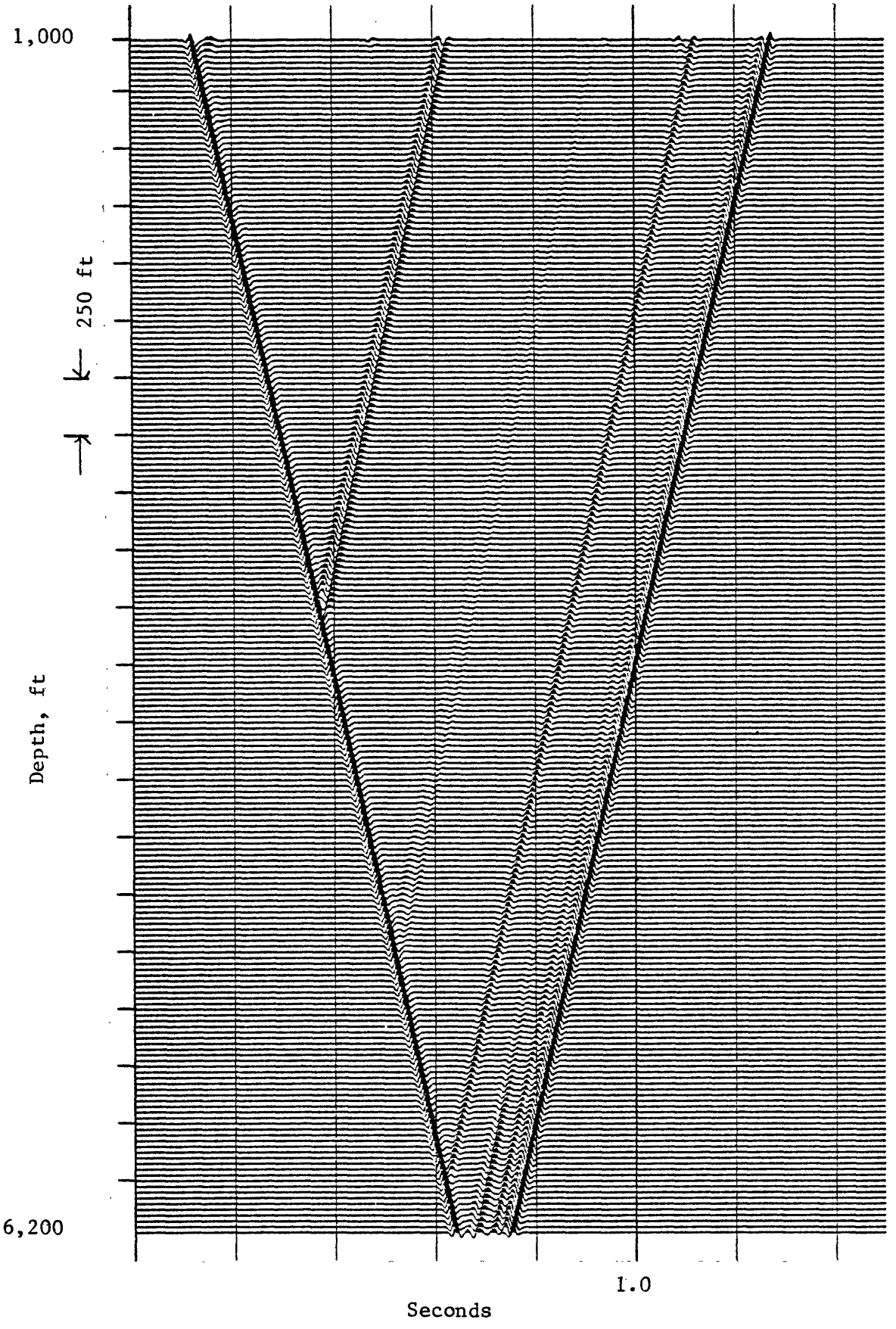

Figure 42.--The velocity-filtered, source-offset corrected and remerged upgoing and downgoing waves from the data shown in figure 40.

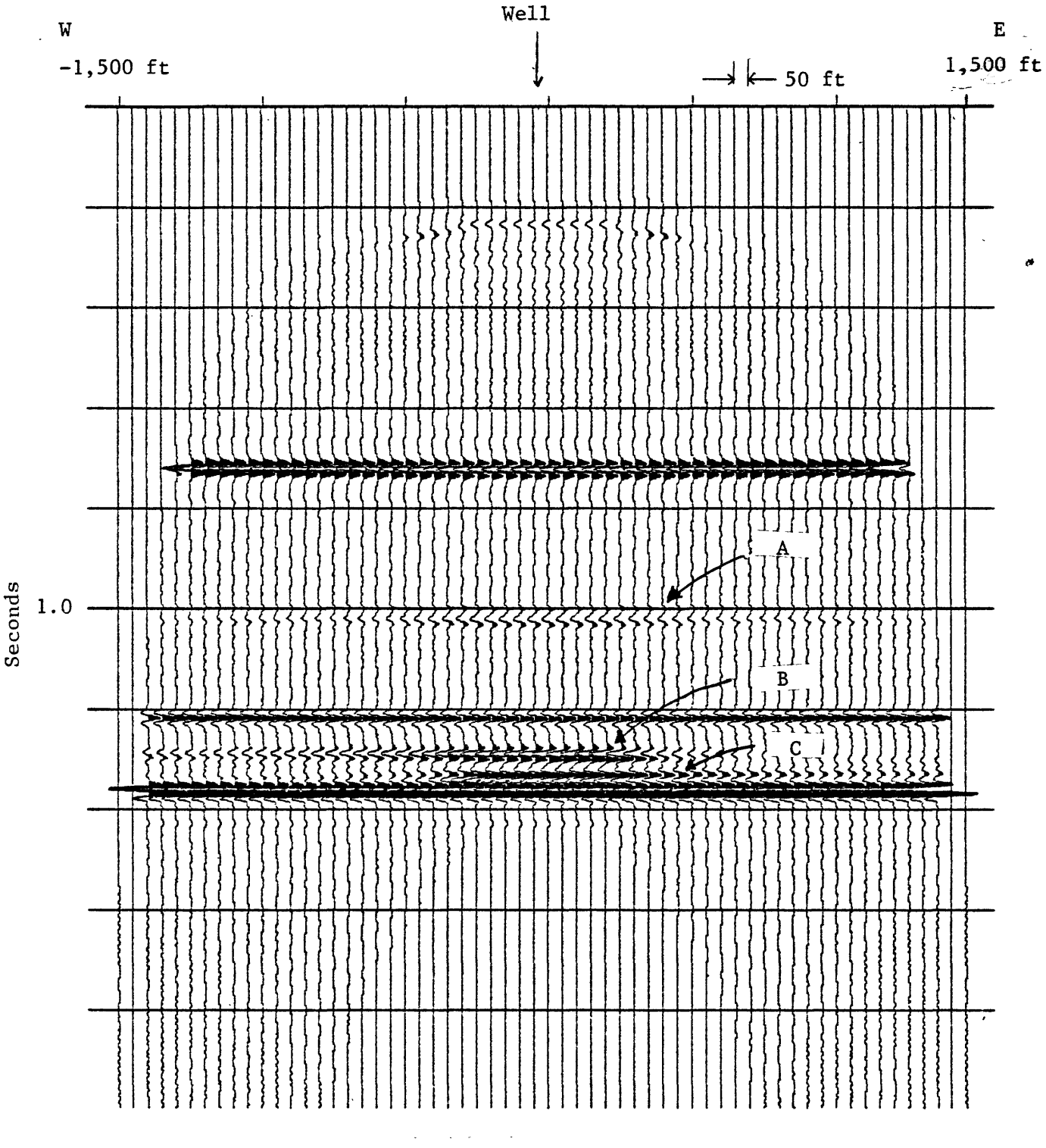

Figure 43.--Laterally stacked VSP data showing the lateral extent of the sand bodies.

away from the borehole by VSP lateral stacking for the horizontally layered media is one-half the source offset distance. Therefore, the west edge of sand body B and the east edge of sand body C cannot be interpreted from figure 43. Notice the amplitude variations of the sand bodies with respect to the lateral location away from the borehole. The edges of sand body A are difficult to determine due to the processing noise. However, it would be possible to say that sand body A is at least 2,000 ft long. If the 1/4 amplitude criteria are used in determining the east edge of sand body B and the west edge of sand body C, the laterally stacked VSP data shown in figure 43 is very reasonable in the error range of one source wavelength.

In order to compare the laterally stacked VSP data with conventional surface seismic data, three-dimensional, normal-incident diffraction modeling was performed on the model shown in figure 37. The normal-incidence seismic model of the E-W line from -4,000 to 4,000 ft is shown in figure 44. The trace interval in figure 44 is 100 ft, and 40 Hz Ricker wavelet was used. To see the edges of the sand bodies, a two-dimensional, finite-difference migration technique was applied to the data shown in figure 44. The migrated data, shown in figure 45, clearly show the lateral extents of the sand bodies. Comparing the result of the laterally stacked VSP data and the 2-D migrated surface data, the advantages and disadvantages of the VSP method are obvious.

As far as mapping sand bodies B and C is concerned, migrated surface data indicates the better definition of the spatial distribution of sand bodies, even if the overall amplitudes are less than those of the VSP data. However, mapping sand body A, using actual surface seismic data, would be difficult because of the low amplitude response. This example also shows the advantage of using the VSP method to detect small bodies around a borehole in the seismic frequency band.

As shown in the previous examples, when the source is located in the direction of the axis of the sand body, the results of the two-dimensionally migrated surface seismic data or laterally stacked VSP data could provide a reasonable estimate of the lateral extent of the body.

In order to see the effect of orientation of the sand body with respect to the source location on the seismic responses, a series of models was generated by rotating sand body C to the north.

Figure 46 shows the two-dimensional, migrated, normal-incident seismic section with a rotation angle of 45° for sand body C. The events above sand body C shown in figure 46 are identical to those shown in figure 45. Now sand body C looks like an anticlinal surface in the migrated section and the lateral extent of sand body C is about three times the true lateral extent. This indicates that general three-dimensional bodies cannot be mapped using two-dimensional analysis. This conclusion is also applicable to the VSP data.

Figure 47 shows the VSP model when the source offset is 3,000 ft to the west with a rotatation angle of 45° for sand body C, and figure 48 shows the VSP model when the source is 3,000 ft to the east. Notice that the response of sand body C in figure 47 is entirely missing, because none of the ray paths go through sand body C.

However, the amplitude responses of sand body C shown in figure 48 do not decay in an appreciable amount with respect to the well phone location except in the bottom part of the section. This indicates that the lateral extent of sand body C would be highly overestimated if lateral stacking of VSP data was attempted.

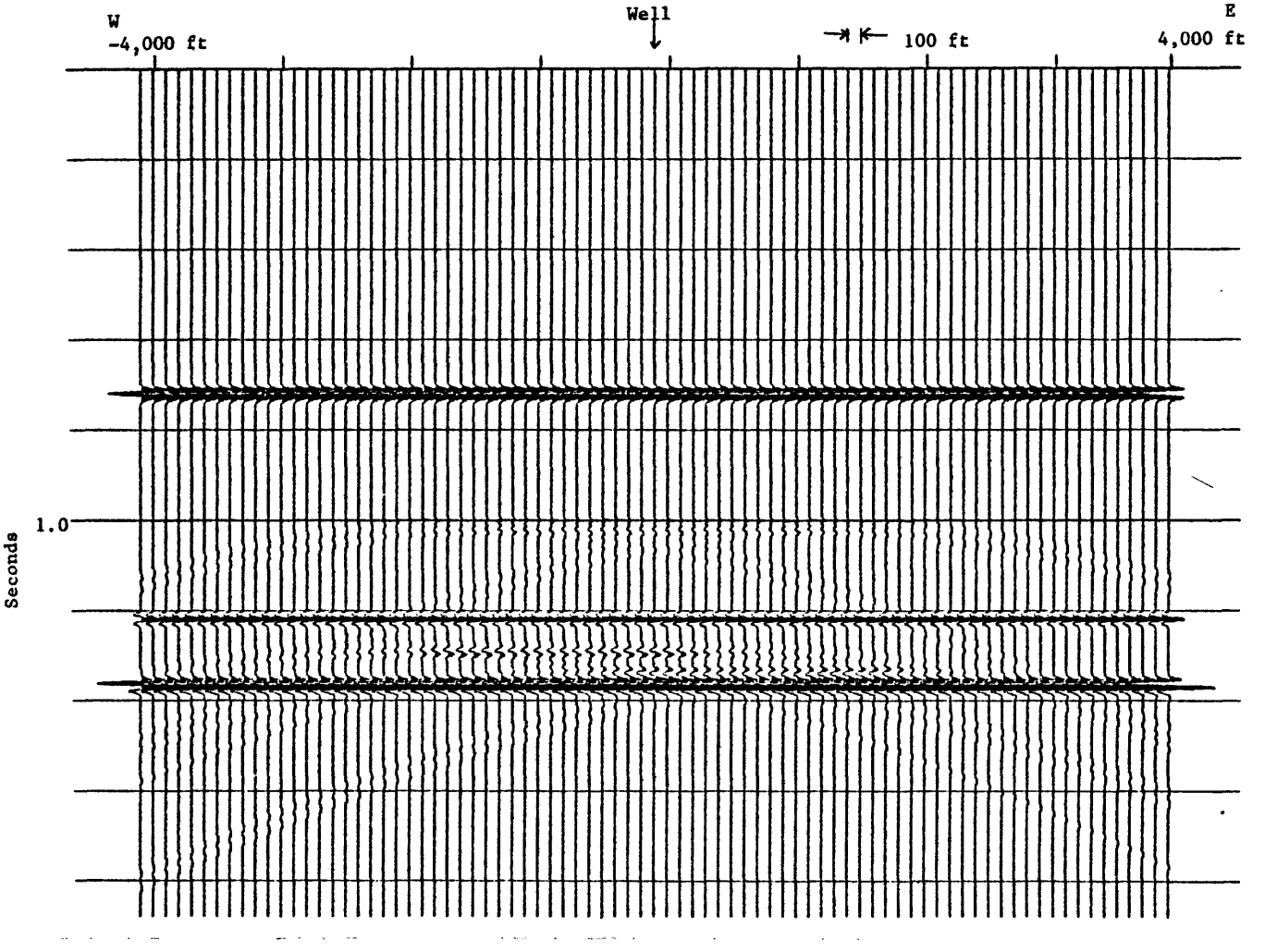

Figure 44.--Normal incident seismic response with 100 ft trace interval for the model parameters shown in figure 38.

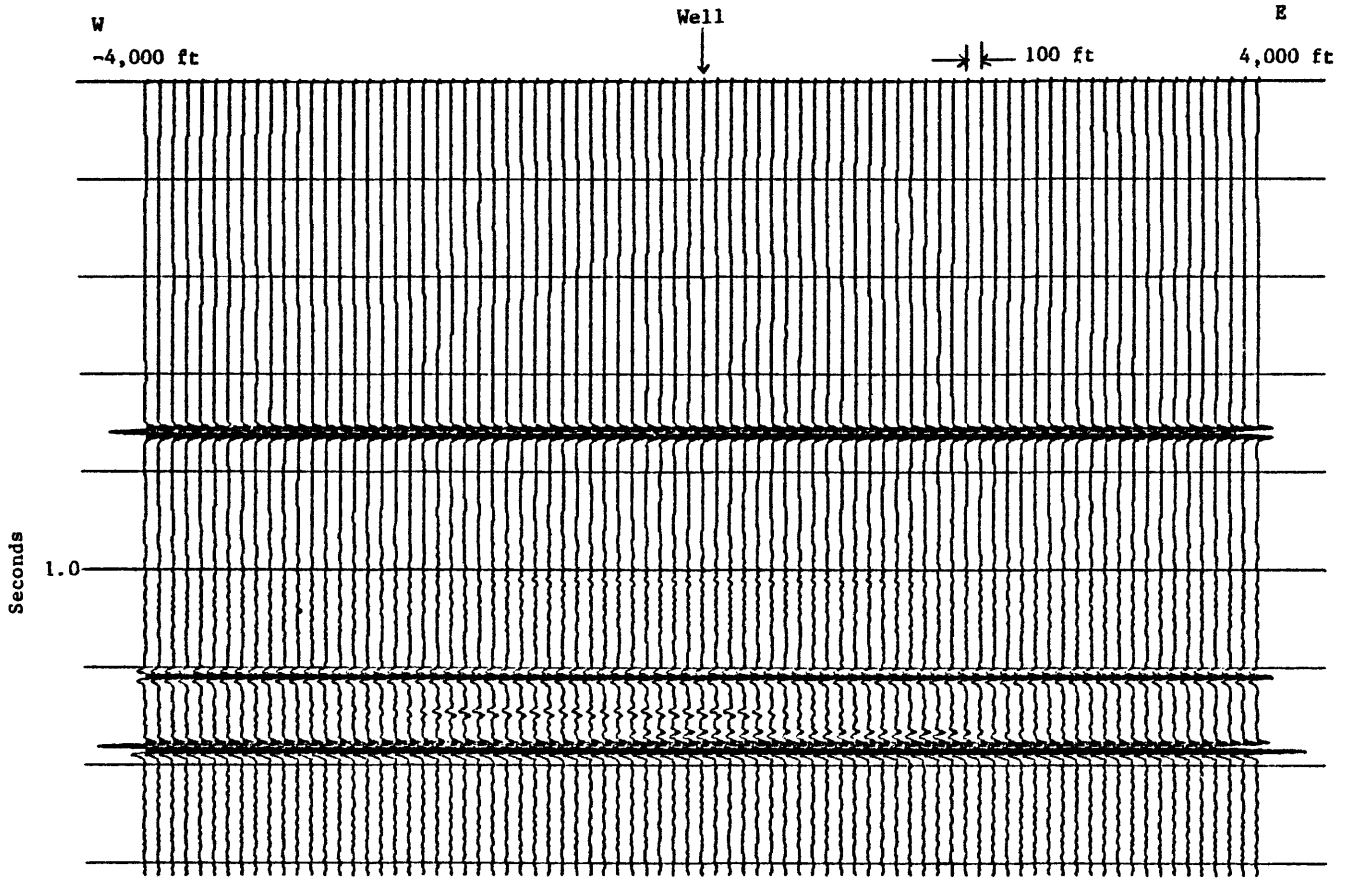

Figure 45.--Migrated section of figure 44.

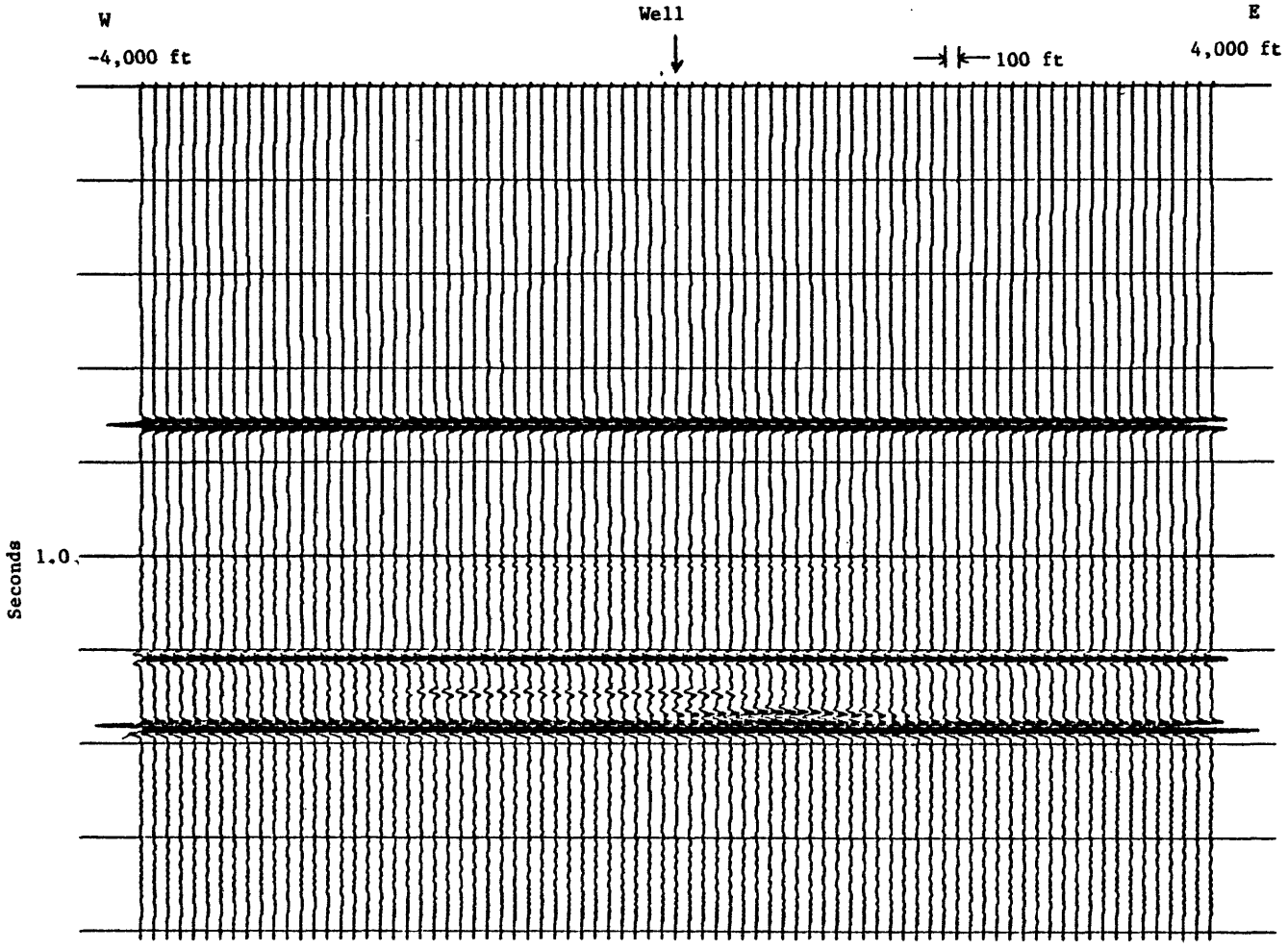

Figure 46.--Migrated section of the normal incident seismic response for the model shown in figure 38 with a rotation angle of 45° to the north for the sand body C.

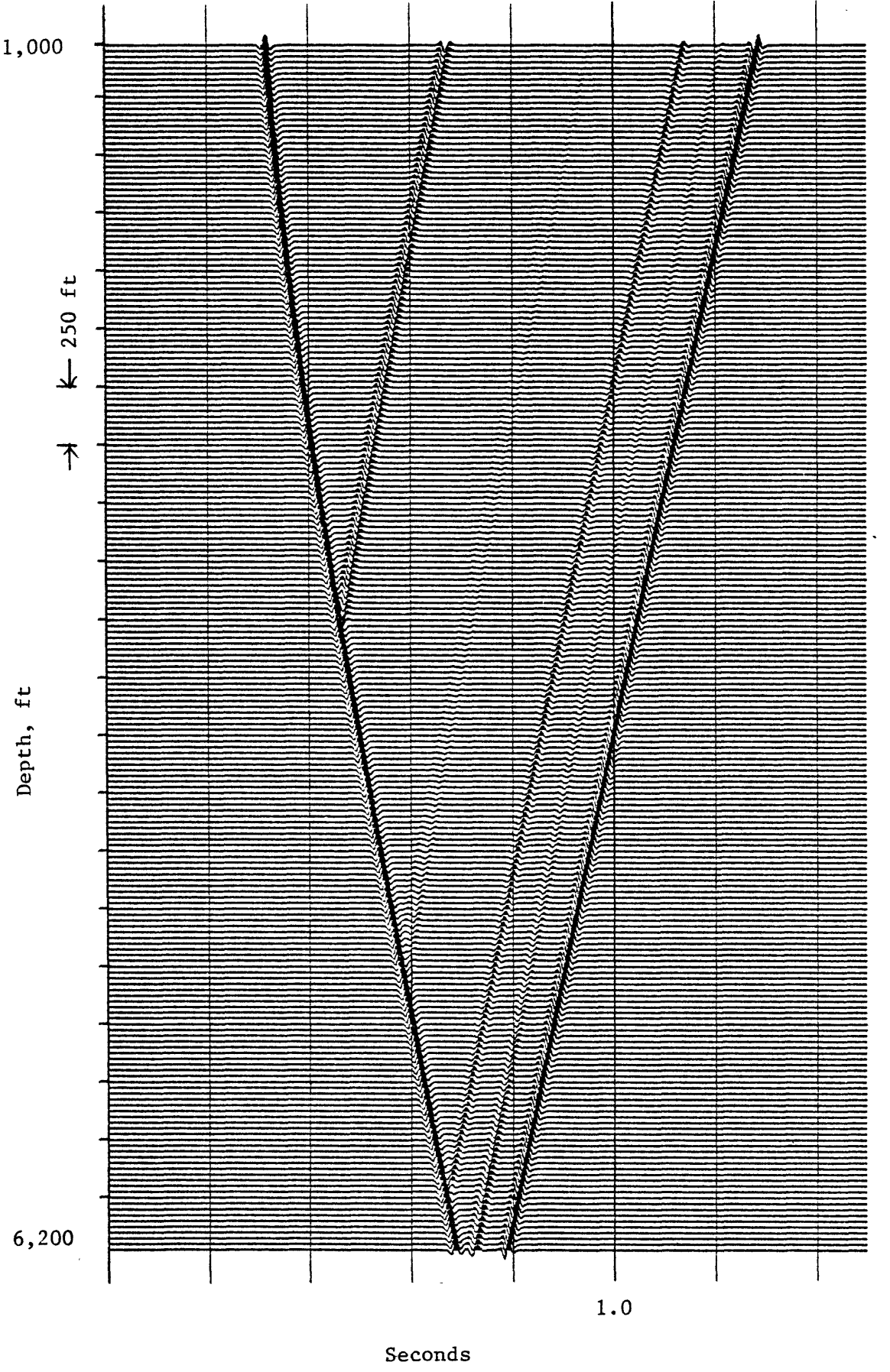

Figure 47.--Three-dimensional VSP response for the model shown in figure 38 with a rotation angle of 45° to the north for the sand body C. The source is located 3,000 ft away from the well to the west.

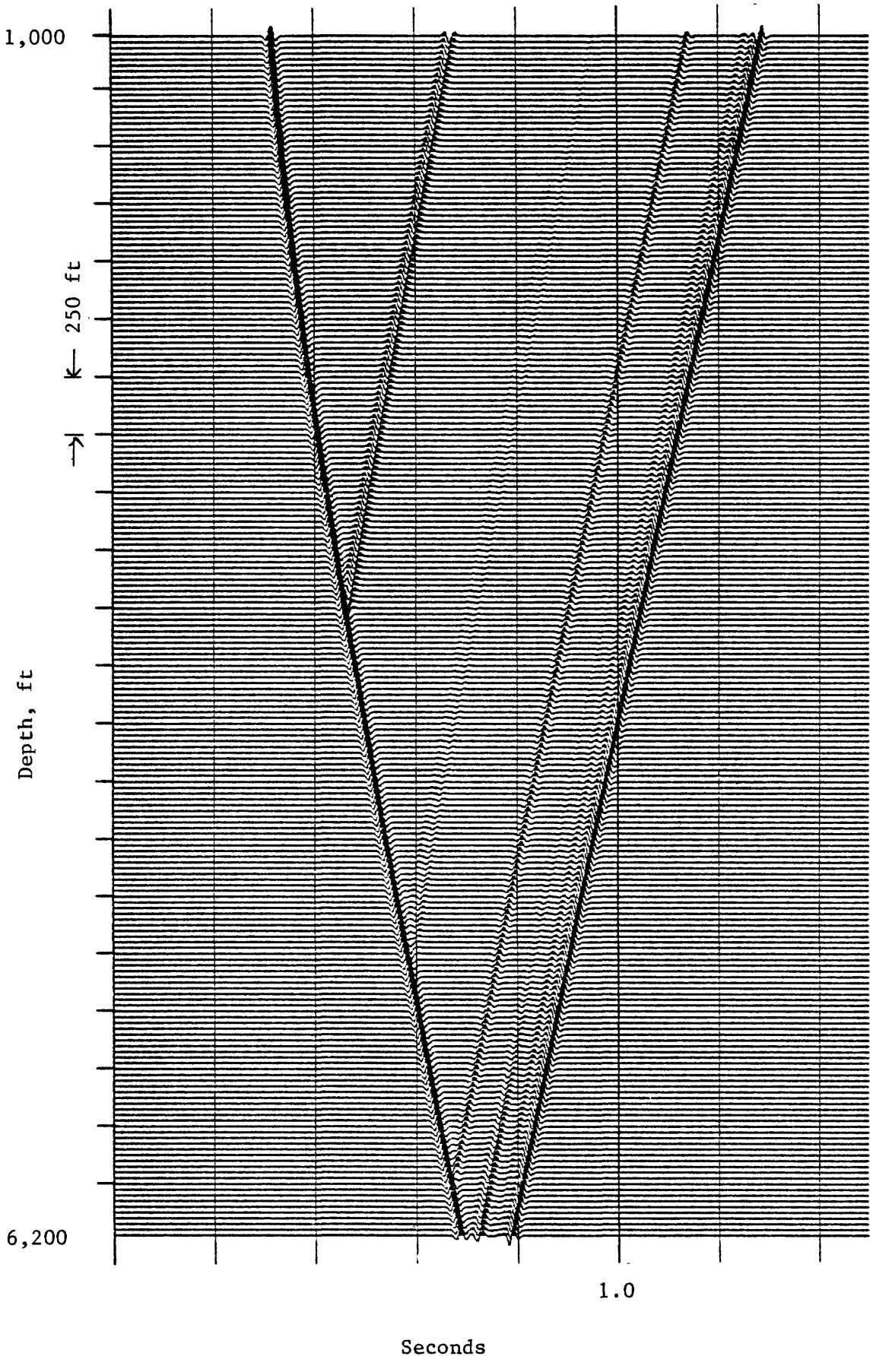

Figure 48.--Three-dimensional VSP response for the model shown in figure 38 with a rotation angle of 45° to the north for the sand body C. The source is located 3,000 ft away from the well to the east.

In summary, the application of conventional VSP methods to delineate the spatial extent of lenticular-type sand bodies is very limited. If the approximate orientation of a lenticular-type sand body is known, the VSP method seems to be feasible in mapping the edges of the body. When there is no knowledge of the orientation of the sand body and the borehole does not penetrate the sand body, application of conventional VSP techniques may not be a practical approach, since many source locations could be required in the azimuthal direction around the boreheole. Even if many problems exist, detailed three-dimensional surface seismic surveys and three-dimensional processing techniques could be the optimum approach in delineating lenticular-type sand bodies seismically.

SOME CONSIDERATIONS ON FIELD VSP EXPERIMENT AND PROCESSING

Based on the model studies, lenticular-type sand bodies at the MWX well site near Rifle, Colorado, particularly in the paludal zone, have a good chance of being detected and delineated seismically using the VSP method, when the approximate orientation of the sand body is known. This result suggests that the arbitrarily oriented sand bodies which intersect the borehole can be delineated seismically, if many sources are utilized in the azimuthal direction around the well.

If measurements are made along the borehole, such as in a conventional VSP method, the lateral stacking technique of VSP data could be an appropriate approach to investigate the lateral distribution of sand bodies. The downward continuation or migration technique could be applied if measurements are made in the horizontal direction, like source gathers or conventional surface profile data. In both cases, the amplitude responses from the edge of the body are the criteria for delineating the spatial location. Therefore, an accurate estimation of the amplitude of reflected events is important.

In the model study, the size and depth of the target body, the orientation of the body with respect to the source-receiver line, source offset, geophone location, and the frequency content of input-source wavelet cause the amplitude variation. But some other factors control the amplitude variation in the real data. The other factors to be considered in the processing and interpretation of VSP data, except for the well known geometrical spreading effect, are:

1. Source radiation pattern--In the model study, the source radiation pattern is assumed to be isotropic. But the actual seismic sources have a highly directional radiation pattern.
2. Attenuation--The earth materials are not perfectly elastic, thus there is some degree of high-frequency losses due to earth attenuation.
3. Reflection coefficient variation with respect to the angle of incidence--The angle of incidence highly depends on the source and receiver location relative to the target. There could be some additional variation of the reflection amplitude when the source-offset is excessively large.
4. Variable geophone and source coupling to the medium.
5. Mode conversion at the interface due to the non-normal incident ray path.

The above mentioned amplitude controlling factors should be considered in designing field VSP configuration in addition to considering the interferences between various waves registered in the actual VSP data. Factors 1 and 3 actually dictate the maximum source-offset to be allowed in the field configuration.

In the following, three possible VSP configurations are considered.

A. Conventional VSP configuration.--Figure 49 shows the conventional VSP configuration. In this configuration, only one downhole geophone can be utilized for each shot. To accomplish a complete azimuthal survey, for example 15^{o} azimuthal source interval with 25 ft depth sampling for a 8,000 ft deep well, the data acquisition time and cost will be tremendous. Therefore, this approach may not be practical in delineating arbitrarily oriented, lenticular-type sand bodies. However, this conventional VSP technique could be the most reliable method, simply because this configuration has been used for almost all VSP applications to earth investigations.

B. Downhole source and surface geophone.--This VSP configuration is shown in figure 50. This is very similar to the conventional VSP technique if the source and receiver are interchanged. By shooting a downhole source inside a borehole, as many surface locations as the upper limit of the recording instrument can be measured simultaneously. Arranging the surface geophones azimuthally around the borehole, a complete azimuthal survey would have been accomplished with a single trip of the downhole source along the borehole. Therefore, the data acquisition time and cost would be tremendously reduced in this VSP configuration. But there are some problems to this approach. The main problems are:

1. Limit of depth of a downhole source.--Currently, there is no reliable downhole source which can operate at great depth. The maximum depth of a downhole source used in VSP configuration was about 2,500 ft.

2. Complicated downhole source radiation pattern.--Downhole sources generate complicated body-wave radiation patterns in addition to tremendous tube waves (Lee and Balch, 1982). This complicated downhole-source radiation pattern will cause problems in analyzing the subtle amplitude variations from the lenticular-type sand bodies.

3. Coupling of tube waves into body waves.--There are large secondary body-wave radiations due to the tube-wave coupling into body waves (Balch and Lee, 1982). These strong secondary radiations could mask all the reflection events of interest.

This kind of VSP configuration has a great future potential in mapping subsurfaces, but it may not be feasible at the present time.

C. Single downhole geophone and multiple surface sources.--The most time-consuming part of the conventional VSP configuration is locating a downhole geophone at many depth levels along the borehole axis. To overcome this problem, a downhole geophone is positioned at a certain depth level and multiple sources are located on the surface. This VSP configuration is shown in figure 51. In this VSP configuration, the mapping of the lateral extent of the lenticular-type sand bodies could be achieved by a downward continuation of the common receiver gathers. Conceptually, the same result could be achieved using common surface source gathers. The main advantages of the common receiver gathers in the well, compared to the common receiver gathers on the surface, are that the complicated near-surface effect could be reduced by using a deep downhole geophone and the frequency content of the data could be increased due to less attenuation. Some problems associated with this approach include:

1. Calibration of the source wavelet.--Surface sources could be located at very inhomogeneous surface media, except in the marine case; thus the calibration of the source signature could be the main problem.

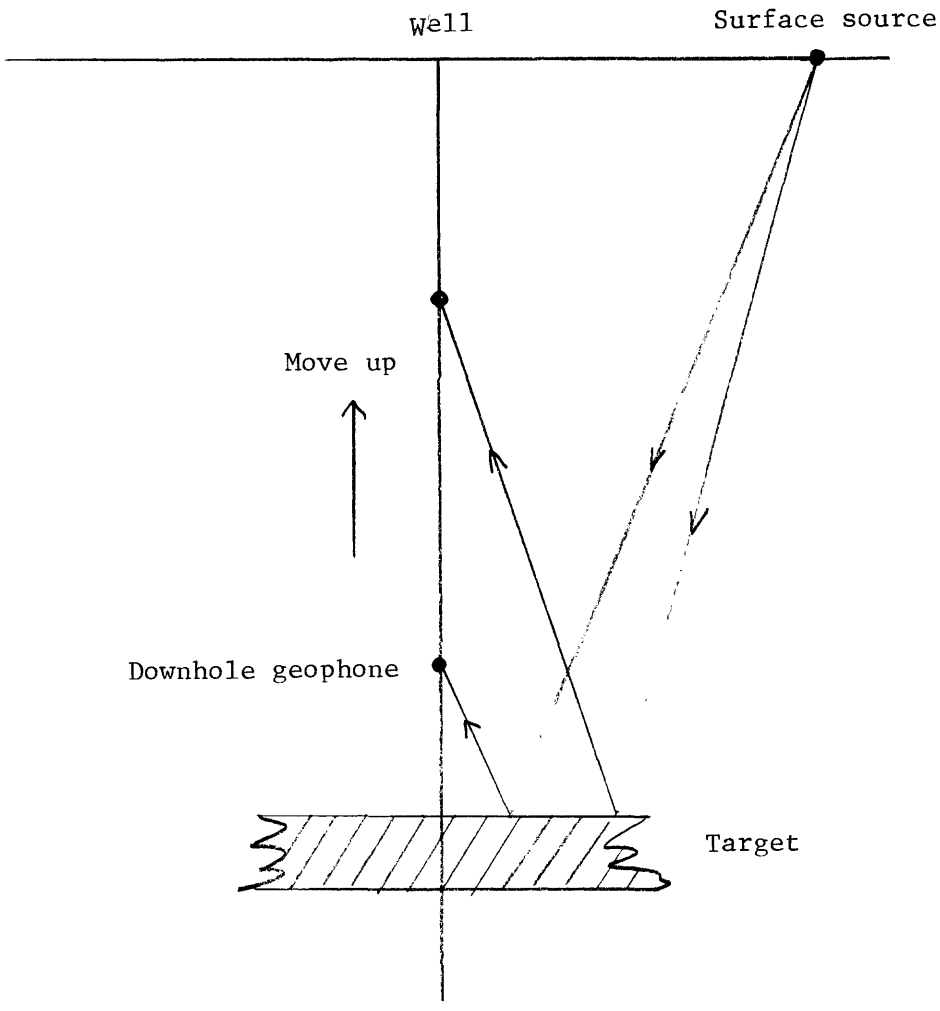

Figure 49.--Schematic diagram for the conventional VSP configuration.

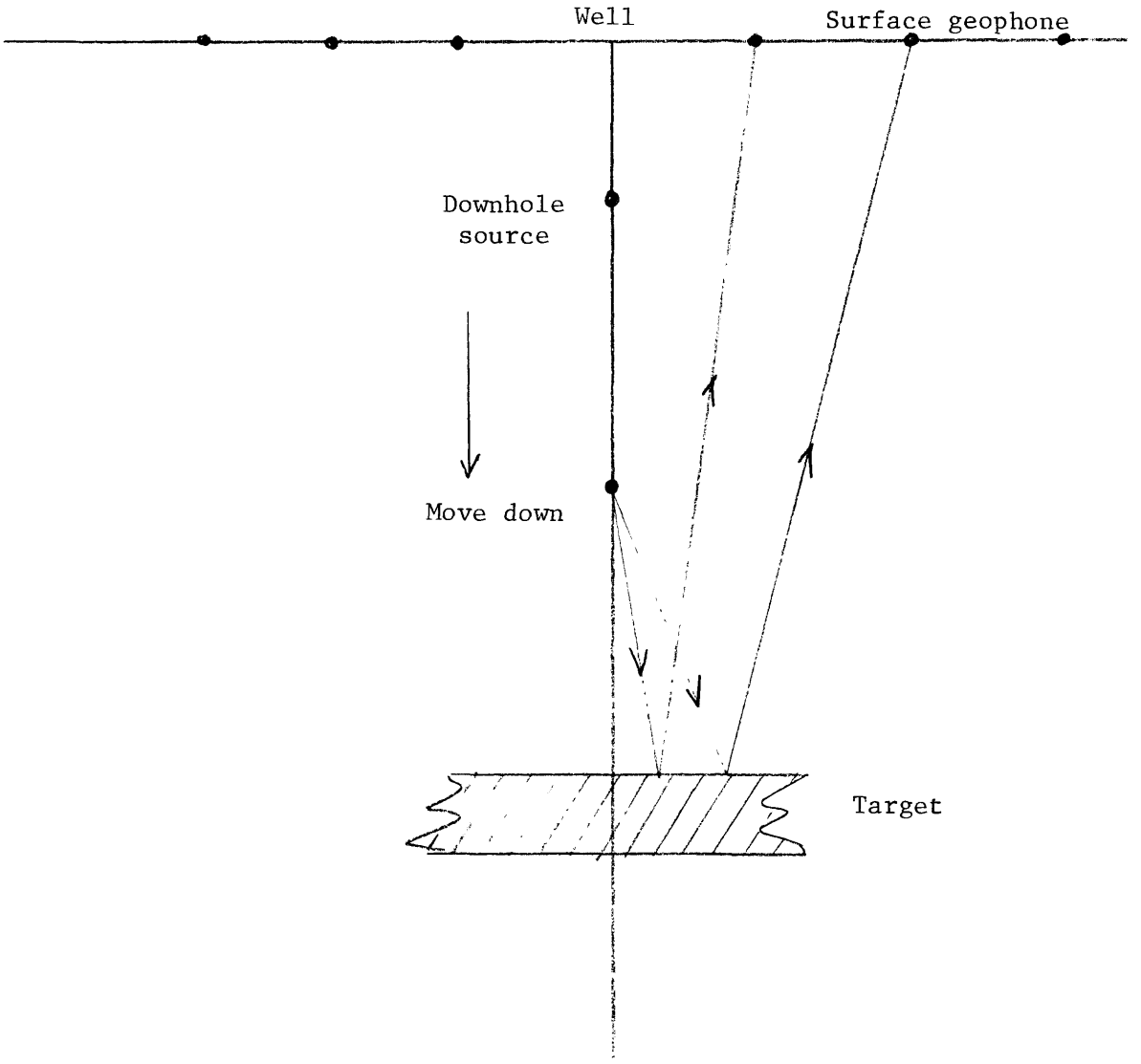

Figure 50.--Schematic diagram for the downhole source and surface geophones.

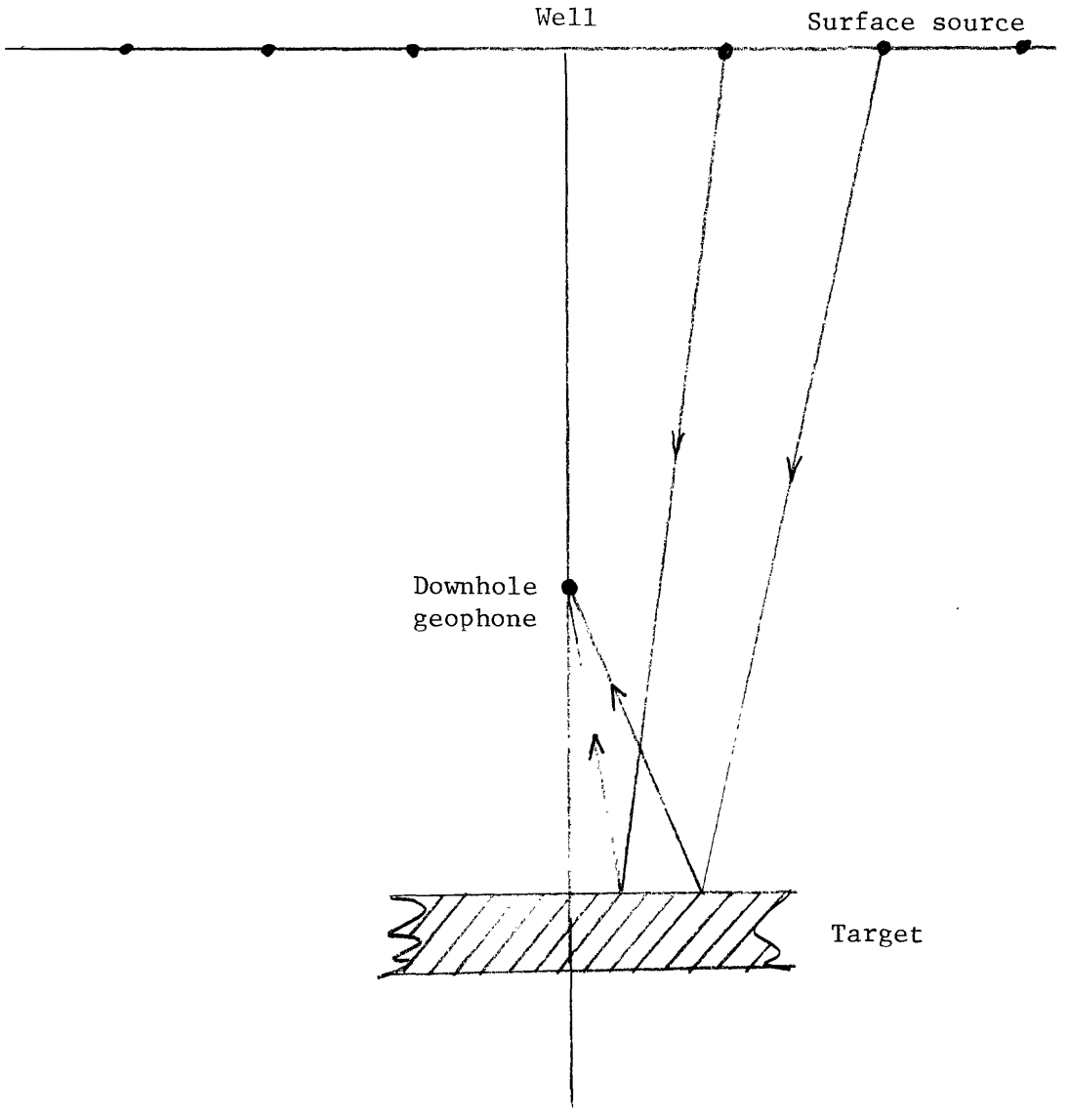

Figure 51.--Schematic diagram for the single downhole geophone and surface sources.

2. Limited region of investigation.--The optimum depth of a single downhole phone should be determined by the depth of the target, so the region of the investigation will be constrained by the location of the geophone.

3. Lack of data and experience.--There are no VSP data available to the public based on this configuration. Thus, there remains some degree of uncertainty in this approach.

Among the three possible VSP configurations, the conventional VSP technique (Method A), and the single downhole geophone with multiple surface source (Method C) seem to be most practical in the field operation. Based on these two VSP methods, some modified field configurations will be discussed. Before discussing field configuration, some of the advantages of VSP methods over surface seismic methods are appropriate.

The advantages of the conventional VSP method over surface seismic methods are:

1. Better estimate of input wavelet.--Using multichannel velocity filtering and monitor-phone, shaping-filter application, a reliable downgoing wave can be extracted at any depth location. In consequence, the vertical resolution of the small target bodies can be increased by downgoing-wave deconvolution.

2. Less attenuation.--In contrast to the surface seismogram, the input wavelet passes only once the highly attenuating surface medium. Therefore, the horizontal and vertical resolution improves.

3. Increased detectability.--By locating downhole geophones very close to the target, the detectability of small bodies increases.

4. Accurate interpretation of the lithological boundaries.

The processing advantage of each VSP method, in addition to the field operational constraints and limitations, should be considered in designing an optimum field procedure to detect and delineate lenticular-type sand bodies at the MWX well site. If the following assumptions about the sand bodies at the MWX well site are applicable, a conventional VSP method could be a practical approach in delineating sand bodies. The assumptions are:

1. Approximate orientation of the lenticular sand is known.

2. The maximum lateral extension of the sand body to be mapped is in the order of 1,500 ft, and the borehole penetrates the sand body.

3. The widths of the sand bodies of interest are in the order of, or greater than, 300 ft, and the target depth is around 6,500 ft.

Figure 52 shows the conventional VSP configuration with a series of surface spreads in an attempt to map the lateral extents of the sand bodies under the above assumptions.

In this configuration, three surface-source locations--one location with an offset distance in the order of 300 ft (near offset), and two locations with an offset distance in the order of 3,000 ft (far offset)--will be used in conjunction with surface geophones with a group interval of 100 ft. The near-offset VSP data were utilized in the estimation of an approximate width of a sand body and in the interpretation of the accurate lithological boundaries, and served as a reference data set in order to check the processed results of the far-offset VSP data.

To map the edges of the sand body, two far-offset VSP data sets are used. In addition to the VSP data, surface source gathers will be recorded at the same time of VSP recording. For example, line A will be recorded simultaneously with VSP data from the source location A. Additional cost and time in recording surface spread are negligible compared with those of

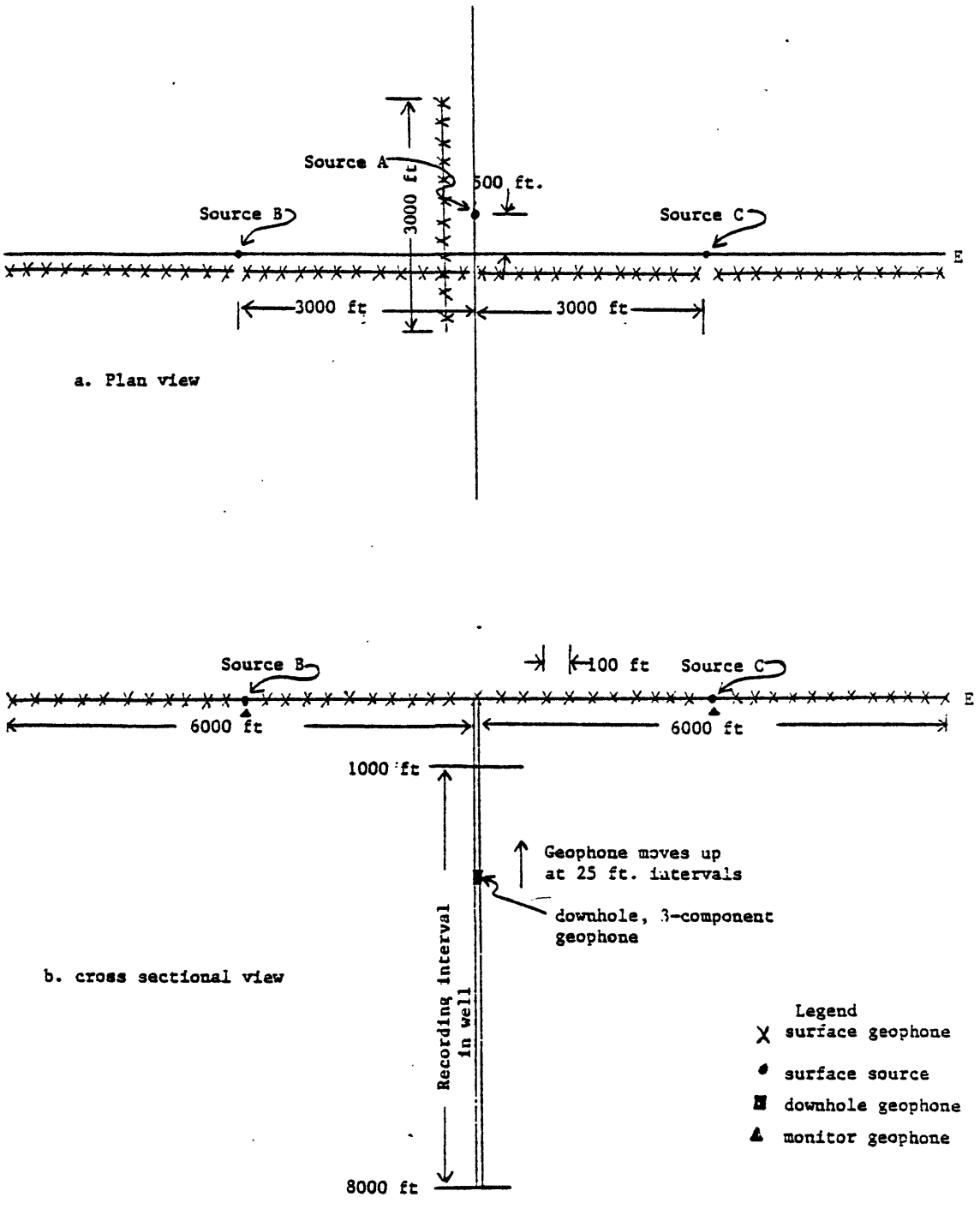

Figure 52.--An example of the conventional VSP field configuration with surface geophones in order to map the lateral extent of the lenticular sand bodies at MWX well site.

VSP data. The main purpose of recording the surface source gathers is to investigate the feasibility of detecting and delineating lenticular-type sand bodies by a downward continuation of source gathers observed on the surface at the MWX well site. If the downward-continued source gathers provide some pertinent information about the spatial extent of a sand body, the future application of this method for similar problems would be great.

The possible processing sequences in delineating lenticular-type sand bodies for the field configuration shown in figure 52 are illustrated in figure 53. The main advantage of processing source gathers with VSP data is that an accurate deconvolution can be accomplished using the downgoing waves measured near the target body by the VSP method.

As mentioned previously, the conventional VSP configuration may not be a practical approach in delineating arbitrarily oriented sand bodies. However, the VSP method C or its slight variation with a conventional VSP method may be a practical approach in delineating lenticular-type sand bodies around a borehole, if some of the problems associated with method C can be solved either by data acquisition techniques or by processing techniques.

SUMMARY AND CONCLUSIONS

The three-dimensional diffraction theory adequately defines the seismic character for a lenticular-type sand body. The overall amplitude variation due to the diffractions from the boundary of a small target is very similar to the interference effect of a thin bed with respect to bed thickness. If 1/4 amplitude criteria are applied in determining the edges of a lenticular-type body, the error in estimating the lateral extent of a body would be in the range of one source wavelength in the case that the source-receiver line is parallel to the axis of the lenticular-type body and the width of the body is in the order of two source wavelengths.

In certain cases, the VSP method is applicable in mapping the lateral extent of a small body around a borehole. As far as the detectability of a small body around a borehole is concerned, a VSP technique has advantages over a conventional surface seismic profiling technique. However, the application of the VSP method to locating the spatial extent of an arbitrarily oriented body has many limitations.

Based on the extensive model study which attempted to delineate the spatial extent of lenticular-type sands at the MWX well site near Rifle, Colorado, the following conclusions can be made:

1. The VSP technique has advantages over the conventional surface seismic method in the detectability of a small lenticular-type sand.
2. Lenticular-type sands in the paludal zone have the highest potential to be delineated seismically.
3. VSP lateral stacking and downward continuation of source or receiver gathers appear to be the appropriate processing techniques in determining the lateral extent of lenticular-type sand bodies.
4. When the approximate orientation of a lenticular-type sand is known, a conventional VSP method may be a viable technique in delineating the spatial extent of a sand.
5. A VSP configuration with a single downhole geophone near the target body and multiple surface sources could have a promising future potential in delineating arbitarily oriented, lenticular-type sands around a borehole.

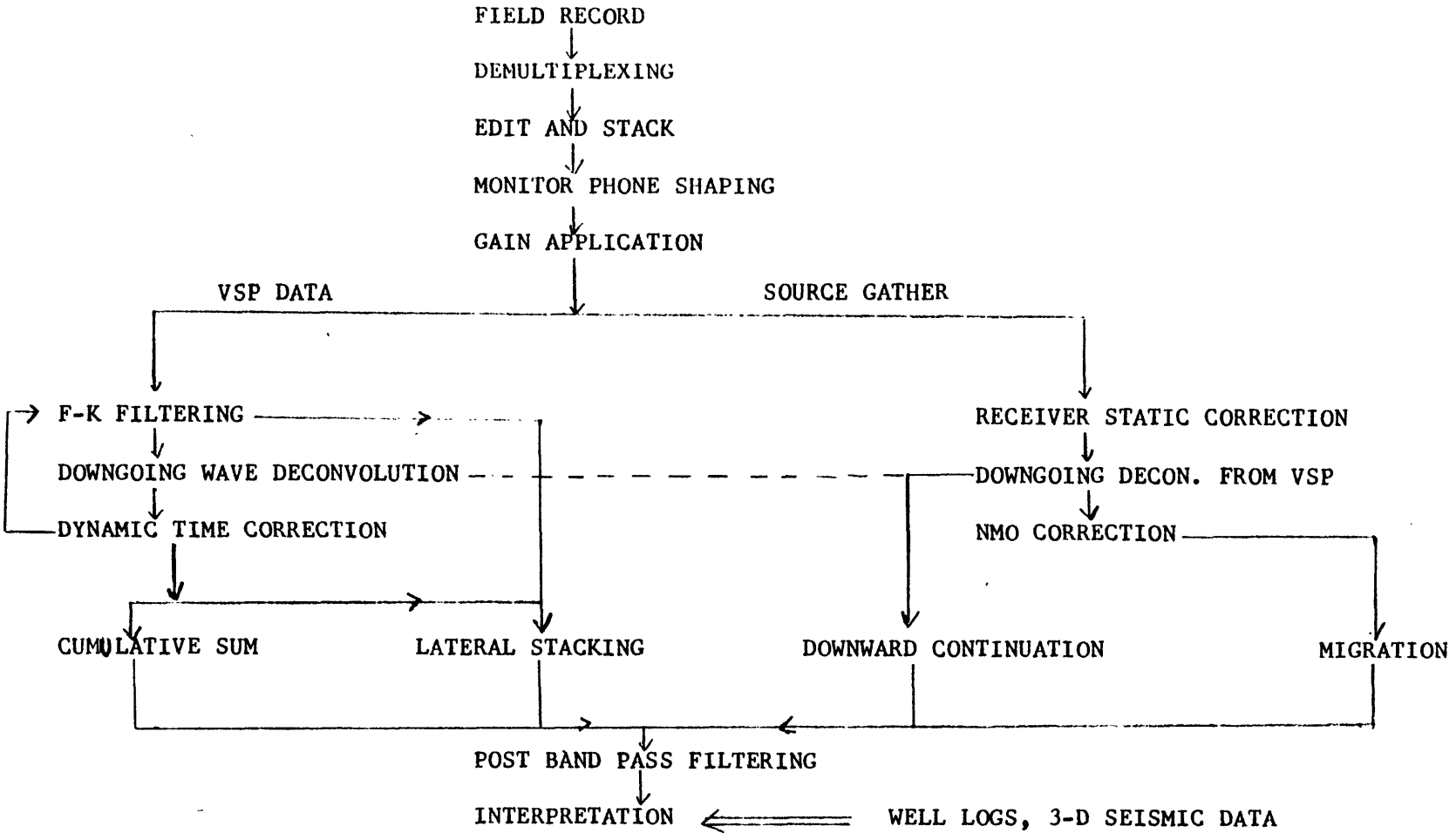

Figure 53.--Processing flow sheet applicable to the data from the field configuration shown in figure 52.

6. A detailed three-dimensional surface seismic method with three-dimensional processing techniques could be an optimum approach for delineating artibrarily oriented small sand bodies, if high-frequency signal can be achieved in the field.

REFERENCES

Balch, A. H., and Lee, M. W., 1982, Some considerations on the use of downhole sources in vertical seismic profiling (abs.): Geophysics, v. 47, no. 7, p. 1117.

Balch, A. H., Lee, M. W., Miller, J. J., and Ryder, R. T., 1982, Use of vertical seismic profiles in seismic investigation of the earth: Geophysics, v. 47, no. 6, p. 906-918.

Berkhout, A. J., 1981, Wave field extrapolation techniques in seismic migration, a tutorial: Geophysics, v. 46, no. 12, p. 1638-1656.

Berryhill, J. R., 1977, Diffraction response for nonzero separation of source and receiver: Geophysics, v. 42, no. 6, p. 1158-1176.

Claerbout, J. F., 1976, Fundamentals of geophysical data processing: with applications to petroleum prospecting: McGraw-Hill Inc., 274 p.

Gal'perin, E. I., 1973, Vertical seismic profiling, in White, J. E., ed.: Society of Exploration Geophysicists Special Publication, no. 12, 270 p.

Hilterman, F. J., 1982, Interpretative lessons from three-dimensional modeling: Geophysics, v. 47, no. 5, p. 784-808.

Lee, M. W., 1983, Vertical seismic profiles at Multi-well Experimental site, Garfield County, Colorado. (In preparation).

Searls, C. A., Lee, M. W., Miller, J. J., Albright, J. N., Fried, Jonathan, and Applegate, J. K., 1983, A coordinated seismic study of the multi-well experiment site: Society of Petroleum Engineers of AIME, SPE/DOE 1983, Symposium on Low Permeability Gas Reservoirs, Preprint no. 11613, 10 p.

Trorey, A. W., 1970, A simple theory for seismic diffraction: Geophysics, v. 35, no. 5, p. 762-784.

_____1977, Diffractions for arbitrary source-receiver locations: Geophysics, v. 42, no. 6, p. 1177-1182.